ADVANCES IN MODELING OF GROUND-SOURCE HEAT PUMP SYSTEMS

By

ANDREW D. CHIASSON

Bachelor of Applied Science
University of Windsor
Windsor, Ontario, Canada
1989

Master of Applied Science
University of Windsor
Windsor, Ontario, Canada
1992

Submitted to the Faculty of the
Graduate College of the
Oklahoma State University
in partial fulfillment of
the requirements for
the degree of
MASTER of SCIENCE
December 1999

ADVANCES IN MODELING OF GROUND-SOURCE HEAT PUMP SYSTEMS

Thesis Approved:

J. D. Spitler

Thesis Adviser

A. F. Emhajan

Wayne B. Powell

Dean of the Graduate College

ACKNOWLEDGEMENTS

This thesis would not have been possible without the contributions of several people. To all of these people, I wish to express my gratitude.

First and foremost, I wish to thank my thesis adviser, Dr. Jeffrey Spitler. His expertise and respected reputation in the thermal sciences field allowed for the funding of many projects and the opportunity for me to gain knowledge and experience in several geothermal topics.

I also wish to thank to Dr. Simon Rees who served as an unofficial co-adviser along the course of this thesis. His expertise in computational methods was quite valuable in helping me to achieve the project goals.

Thanks also to Dr. Marvin Smith who provided input and experimental data regarding the supplemental heat rejecter studies

The review and contribution to this thesis by the committee members, Dr. R. Delahoussaye and Dr. A. Ghajar are appreciated.

Last, but not least, I thank my colleagues in B-10, both here and gone, namely Cenk Yavuzturk and Nagendra Jain, for their ideas and suggestions along the way.

TABLE OF CONTENTS

LIST OF TABLES

LIST OF FIGURES

Figure *Page*

NOMENCLATURE

Symbols

α	=	thermal diffusivity - ft^2/hr (m^2/s);
	=	solar absorptivity (-)
β	=	coefficient of thermal expansion - R^{-1} (K^{-1})
ε	=	emissivity coefficient (-)
γ	=	Euler's constant (0.577215664901)
μ	=	dynamic viscosity - $lb_m/ft\text{-}hr$ (Pa-s)
μ'	=	extinction coefficient - ft^{-1} (m^{-1})
ν	=	kinematic viscosity - ft^2/hr (m^2/s)
θ	=	angle of incidence of sun's rays (radians)
ρ	=	density - lb/ft^3 (kg/m^3)
ρ'	=	reflectance of pond surface (-)
σ	=	Stephan-Boltzmann constant
	=	0.1714 x 10-8 $Btu/hr\text{-}ft^2\text{-}^oR^4$ (5.67×10^{-8} $W/m^2\text{-}K^4$)
τ	=	transmittance of solar radiation (-)
A	=	area - ft^2 (m^2)
c, c_p	=	specific heat capacity - $Btu/lb_m\text{-}^oF$ ($J/kg\text{-}^oC$)
d	=	depth - ft (m)
D	=	diffusion coefficient - ft^2/s (m^2/s)
D^*	=	effective thermal diffusivity - ft^2/s (m^2/s)
ff	=	fouling factor - $ft^2\text{-}^oF/hr\text{-}Btu$ ($m^2\text{-}^oC/W$)
g	=	acceleration due to gravity - ft/s^2 (m/s^2)
h	=	heat or mass transfer coefficient - $Btu/hr\text{-}ft^2\text{-}^oF$ ($W/m^2\text{-}^oC$);
	=	hydraulic head - ft (m)
H	=	borehole depth - ft (m)
i	=	hydraulic gradient - ft/ft (m/m)
I	=	solar radiation flux on horizontal - $Btu/hr\text{-}ft^2$ (W/m^2)
K	=	hydraulic conductivity - ft/s (m/s)
k	=	thermal conductivity - $Btu/hr\text{-}ft\text{-}^oF$ ($W/m\text{-}^oC$)
L	=	characteristic length - ft (m)
ℓ	=	length term described by Eskilson (1987) - ft (m);
	=	distance between nodes or thickness – ft (m)
$\dot{m}$	=	mass flow rate– lb_m/hr (kg/s)
$\dot{m}''$	=	mass flux – $lb_m/hr\text{-}ft^2$ ($kg/s\text{-}m^2$)

Le = Lewis Number (-)
n = porosity (-)
N = quantity (-)
Nu = Nusselt Number (-)
P = perimeter - ft (m);
= pressure - atmospheres
Pe = Peclet number (-)
Pr = Prandtl Number (-)
q = heat transfer rate - Btu/hr (W);
= specific discharge - ft/s (m/s)
q^* = ground thermal load - Btu/hr (W]
q'' = heat flux - Btu/hr-ft^2 (W/m^2)
Q = volumetric flow rate - ft^3/s (m^3/s)
Q^* = heat source/sink term - °F/s (°C/s)
r = radius - ft (m);
= unpolarized solar radiation component (-)
R = retardation coefficient (-);
= thermal resistance - ft^2-°F/hr-Btu (m^2-°C/W)
R^* = ground-water recharge -s^{-1}
Ra = Rayleigh Number (-)
Re = Reynolds Number (-)
S_s = specific storage coefficient - ft^{-1} (m^{-1})
T = temperature - °F (°C)
t = time - s
T_{om} = undisturbed mean temperature of the ground - °F (°C)
U = overall heat transfer coefficient - Btu/hr-ft^2-°F (W/m^2-°C)
V = volume - ft^3 (m^3)
v = average linear groundwater velocity - ft/s (m/s)
= velocity - ft/s (m/s)
V^* = volumetric flow rate - ft^3/s (m^3/s)
w = humidity ratio - lb$_m$ water/lb$_m$ dry air (kg water/kg dry air)
x,z = rectangular coordinates
Δt = time step - s

Subscripts

$\perp$ = perpendicular component
$\parallel$ = parallel component
a = absorbed component of solar radiation
AB = transfer from material A (water) to material B (air)
b = beam radiation;
= borehole
c = convection
circuit = flow circuit or spool
d = diffuse radiation;

	= diffusion
db	= dry bulb
dp	= dew point
eff	= effective
fg	= latent heat of vaporization
fluid	= heat exchange fluid
i	= nodal index;
	= pipe inside
i,j	= coordinate indices
if	= latent heat of fusion
in	= inlet
ℓ	= liquid phase
m,n	= coordinate locations
o	= pipe inside;
	= background or initial
out	= outlet
r	= thermal radiation;
	= refraction
s	= solid phase
surf	= surface
sw,b	= steady-state, borehole wall
t	= current time step:
	= total
t-Δt	= previous time step
w	= water;
	= injected/extracted water
wb	= wet bulb
x,z	= coordinate indices
(x,1)	= coordinate index for a surface node

1. Introduction

1.1. Overview of Ground-Source Heat Pump Systems

Ground-source heat pump (GSHP) systems (also referred to as geothermal heat pump systems, earth energy systems, and GeoExchange systems) have received considerable attention in the recent decades as an alternative energy source for residential and commercial space heating and cooling applications. GSHP applications are one of three categories of geothermal energy resources as defined by ASHRAE (1995). These categories are: (1) high-temperature (>302 °F (>150 °C)) electric power production, (2) intermediate- and low-temperature (<302 °F (<150 °C)) direct-use applications, and (3) GSHP applications (generally <90 °F (<32 °C)). The GSHP applications are distinguished from the others by the fact that they operate at relatively low temperatures.

The term "ground-source heat pump" has become an all-inclusive term to describe a heat pump system that uses the earth, ground water, or surface water as a heat source and/or sink. GSHP systems consist of three loops or cycles as shown in Figure 1-1. The first loop is on the load side and is either an air/water loop or a water/water loop, depending on the application. The second loop is the refrigerant loop inside a water-source heat pump. Thermodynamically, there is no difference between the well-known vapor-compression refrigeration cycle and the heat pump cycle; both systems absorb heat at a low temperature level and reject it to a higher temperature level. The difference between the two systems is that a refrigeration application is only concerned with the low temperature effect produced at the evaporator, while a heat pump may be concerned with

both the cooling effect produced at the evaporator as well as the heating effect produced at the condenser. In these dual-mode GSHP systems, a reversing valve is used to switch between heating and cooling modes by reversing the refrigerant flow direction. The third loop in the system is the ground loop in which water or an antifreeze solution exchanges heat with the refrigerant and the earth.

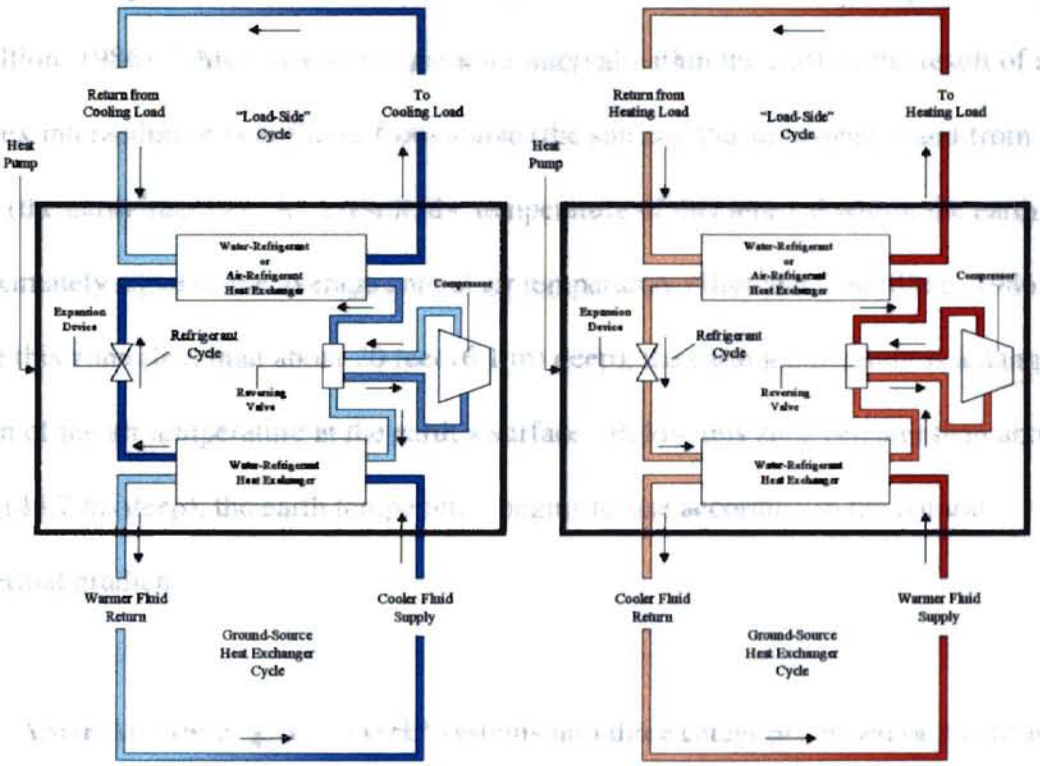

Figure 1-1. Schematic of cycles in a GSHP system in **(a)** cooling mode and **(b)** heating mode.

Efficiencies of GSHP systems are much greater than conventional air-source heat pump systems. A higher COP (coefficient of performance) can be achieved by a GSHP because the source/sink earth temperature is relatively constant compared to air

temperatures. Additionally, heat is absorbed and rejected through water, which is a more desirable heat transfer medium because of its relatively high heat capacity.

GSHP systems rely on the fact that, under normal geothermal gradients of about 0.5 °F/100 ft (30 °C/km) (Grant et al., 1982), the earth temperature is roughly constant in a zone extending from about 20 ft (6.1 m) deep to about 150 ft (45.7 m) deep (Hart and Couvillion, 1986). This constant temperature interval within the earth is the result of a complex interaction of heat fluxes from above (the sun and the atmosphere) and from below (the earth interior). As a result, the temperature of this interval within the earth is approximately equal to the average annual air temperature (Hart and Couvillion, 1986). Above this zone (less than about 20 feet (6.1 m) deep), the earth temperature is a damped version of the air temperature at the earth's surface. Below this zone (greater than about 150 ft (45.7 m) deep), the earth temperature begins to rise according to the natural geothermal gradient.

ASHRAE (1995) groups GSHP systems into three categories based on the heat source/sink used. A fourth category is added here for the sake of completeness. These categories are: (1) ground-water heat pump (GWHP) systems, (2) ground-coupled heat pump (GCHP) systems, (3) surface water heat pump (SWHP) systems, and (4) standing column well (SCW) systems. Each of these is discussed in the following subsections.

1.1.1. Ground-Water Heat Pump Systems

GWHP systems, also referred to as open-loop systems, are the original type of GSHP system. The first GWHP systems were installed in the late 1940s (Kavanaugh and Rafferty, 1997). GWHP systems are not the focus of this thesis, so they will only be briefly described here.

A schematic of a GWHP system is shown in Figure 1-2. In GWHP systems, conventional water wells and well pumps are used to supply ground water to a heat pump or directly to some application. Corrosion protection of the heat pump may be necessary if ground water chemical quality is poor. The "used" ground water is typically discharged to a suitable receptor, such as back to an aquifer, to the unsaturated zone (as shown in Figure 1-2), to a surface-water body, or to a sewer. Design considerations for GWHP systems are fairly-well established; well-drilling technologies and well-testing methods have been well-known for decades. Design considerations include: ground-water availability, ground-water chemical quality, and ground-water disposal method.

The main advantage of GWHP systems is their low cost, simplicity, and small amount of ground area required relative to other GSHP and conventional systems. Disadvantages include limited availability and poor chemical quality of ground water in some regions. With growing environmental concerns over recent decades, many legal issues have arisen over ground water withdrawal and re-injection in some localities.

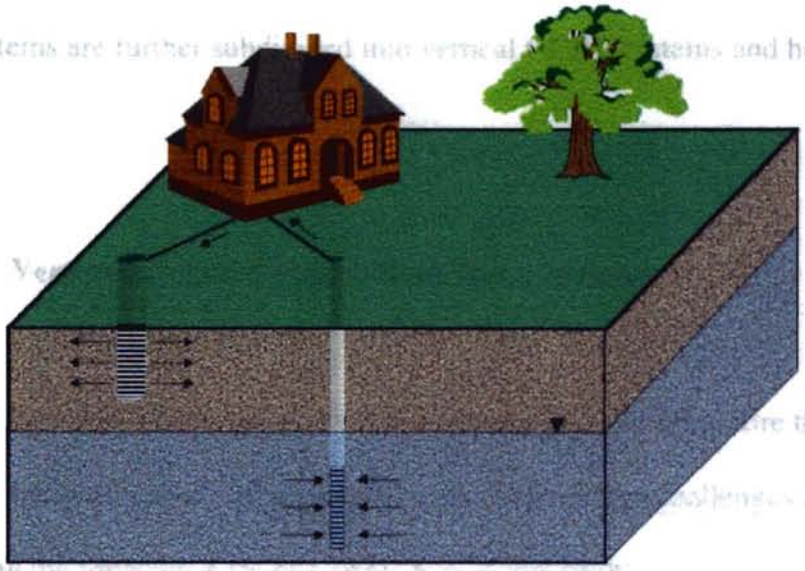

Figure 1-2. A schematic of a ground-water heat pump system.

1.1.2. Ground-Coupled Heat Pump Systems

GCHP systems, also referred to as closed-loop ground-source heat pump systems, were pioneered in the 1970s. Their main advantage over their water-well predecessors is that they eliminate the problems associated with ground water quality and availability and they generally require much less pumping energy than water well systems because there is less elevation head to overcome. GCHP systems can be installed at any location where drilling or earth trenching is feasible.

In GCHP systems, heat rejection/extraction is accomplished by circulating a heat exchange fluid through a piping system buried in the earth. This fluid is either pure water or an antifreeze solution and is typically circulated through high-density polyethylene

(HDPE) pipe installed in vertical boreholes or horizontal trenches as shown in Figure 1-3. Thus, these systems are further subdivided into vertical GCHP systems and horizontal GCHP systems.

1.1.2.1. Vertical Ground-Coupled Heat Pump Systems

Vertical borehole GCHP systems are the primary focus of this entire thesis. Therefore, they are described in some detail here and their design challenges are explained, laying the foundation for the motivation of this study.

In vertical borehole GCHP systems, ground heat exchanger configurations typically consist of one to tens of boreholes each containing a U-shaped pipe through which the heat exchange fluid is circulated. Some Swedish applications use boreholes inclined from the vertical. A number of borehole to borehole plumbing arrangements are possible. Typical U-tubes have a diameter in the range of ¾ in. (19 mm) to 1 ½ in. (38 mm) and each borehole is typically 100 ft (30.5 m) to 300 ft (91.4 m) deep with a diameter ranging from 3 in. (76 mm) to 5 in. (127 mm). The borehole annulus is generally backfilled with a material that prevents contamination of ground water.

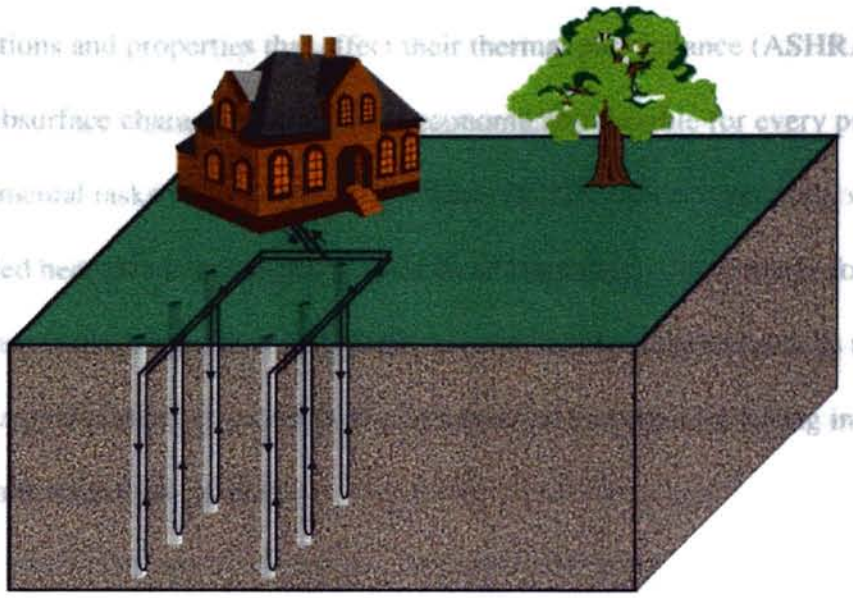

(a)

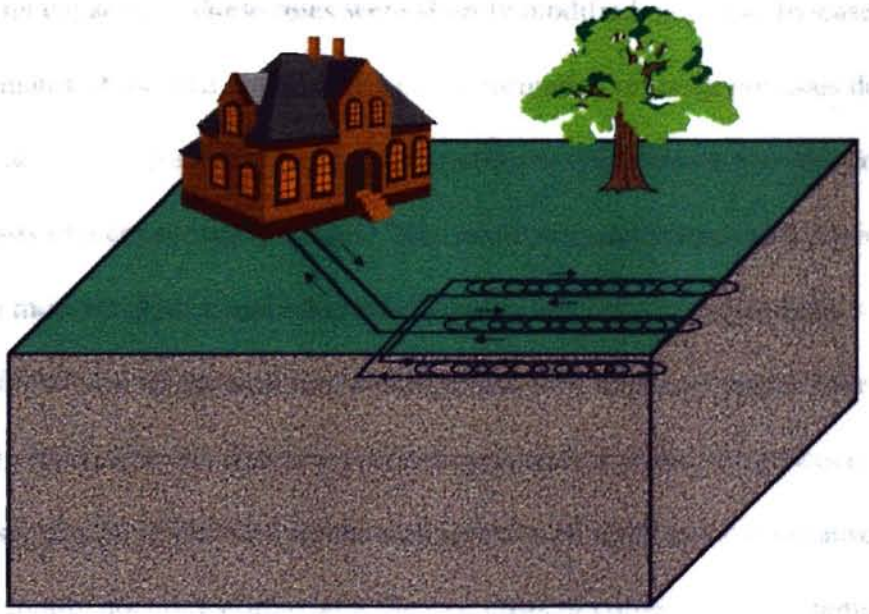

(b)

Figure 1-3. A schematic of **(a)** a vertical borehole ground-coupled heat pump system and **(b)** horizontal ground-coupled heat pump system.

The design of vertical ground heat exchangers is complicated by the variety of geological formations and properties that affect their thermal performance (ASHRAE, 1995). Proper subsurface characterization is not economically feasible for every project. One of the fundamental tasks in the design of a reliable GCHP system is properly sizing the ground-coupled heat exchanger length (i.e. depth of boreholes). Particularly for large systems, an extensive effort is made to design the ground loop heat exchangers so that they are not too large (resulting in too high of a first cost) or too small (resulting in the building's thermal load not being met).

In the early days of GCHP technology, the task of sizing the ground-loop heat exchanger was accomplished using rules of thumb (i.e. 250 feet of bore length per ton of heating or cooling capacity). These rules were slightly modified on a case-by-case basis using some estimates of thermal conductivity of the formation or using previous design experience, but additional costs of more detailed testing or calculations was judged to outweigh the costs of a conservative design. This relatively simple approach proved to be successful in most residential and other small applications, but in larger-scale commercial and institutional applications, some ground-loop heat exchangers failed to meet their design loads after the first few years of operation. Further, the practice of greatly over-designing large GCHP systems was found to be unacceptable because the first costs were simply not competitive with the first costs of conventional systems. Consequently, intensive research regarding methods to optimize ground-loop heat exchanger design has been ongoing for the last decade.

Simple approaches to sizing the ground-loop heat exchanger in larger-scale applications are inadequate mainly because the heat transfer processes in the ground are complicated by thermally interacting boreholes and hourly periodic heat extraction/injection pulses. Annual heat rejection and heat extraction are usually not equal and peak temperatures rise or fall over a number of years. As a result, ground-loop heat exchanger designers need to consider hourly heating and cooling loads of the building and need to perform some simulation of the ground-loop temperatures over the life-cycle of the building. Recent research efforts have produced several methods and computer software programs for this purpose. However, none of the programs consider the effects of ground water flow on ground-loop heat exchanger performance; these effects have not been well understood, perhaps because of the lack of relevant investigations. This is the topic of Chapter 2 of this thesis.

Another challenge in the design of GCHP systems arises from the fact that most commercial and institutional buildings, even in moderate climates, are generally cooling-dominated and therefore reject more heat to the ground than they extract over the annual cycle. This load imbalance may require the heat exchanger length to be significantly greater than the length required if the annual loads were balanced. As a result, the GSHP system may be eliminated from consideration early in the design phase of the project due to excessive first cost. This has given rise to the concept of "supplemental heat rejecters" or so-called "hybrid GSHP systems".

Supplemental heat rejecters have been integrated into building designs to effectively balance the ground loads and therefore reduce the necessary length of the ground-loop heat exchanger. In some applications, the excess heat that would otherwise build up in the ground may be used for domestic hot water heaters, car washes, and pavement heating systems. In cases where the excess heat cannot be used beneficially, conventional cooling towers or shallow ponds can provide a cost-effective means to reduce heat exchanger length.

Design of these supplemental components adds to the challenge of designing the overall hybrid GCHP system because of their highly transient nature. Heat rejection systems are likely to operate more often during the night-time hours or when the building is not in use. Therefore, it is essential that the hourly (or less) behavior of these systems be examined during their design phase. These are the topics of Chapters 3 (shallow ponds) and Chapter 4 (pavement heating systems) of this thesis.

1.1.2.2. Horizontal Ground-Coupled Heat Pump Systems

In horizontal GCHP systems, ground heat exchanger configurations typically consist of a series of parallel pipe arrangements laid out in dug trenches or horizontal boreholes about 3 ft (0.91 m) to 6 ft (1.83 m) deep. A number of piping arrangements are possible. "Slinky" configurations (as shown in Figure 1-3 (b)) are popular and simple to install in trenches and shallow excavations. In horizontal boreholes, straight pipe configurations are installed. Typical pipes have a diameter in the range of ¾ in. (19 mm)

to 1 ½ in. (38 mm) and about 400 ft (121.9 m) to 600 ft (182.9 m) of pipe is installed per ton of heating and cooling capacity.

The thermal characteristics of horizontal GCHP systems are similar to those of vertical ones. The main difference is that horizontal ground-loop heat exchangers are more affected by weather and air temperature fluctuations because of their proximity to the earth's surface. This may result in larger loop temperature fluctuations and therefore lower heat pump efficiencies. Recent research activities have focussed on using these systems as supplemental heat rejecters with vertical borehole GCHP systems. A specific application (i.e. the use of a shallow pavement heating system) is the focus of Chapter 4 of this thesis.

Aside from the invention of the Slinky coil itself and the use of these systems as supplemental heat rejecters, horizontal systems have received much less attention than vertical systems with respect to recent research efforts. This may be due to the fact that vertical systems tend to be preferred in larger applications since much less ground area is required. Also, since horizontal systems are installed at shallow depths, geologic site characterization is relatively easier because soils can be readily seen and sampled. Further, over-conservative designs are not as cost prohibitive as with vertical borehole designs because of the relatively low installation costs of the heat exchanger pipe.

1.1.3. Surface-Water Heat Pump Systems

The third category of GSHP systems is the surface-water heat pump (SWHP) system. A specific application of SWHP systems (i.e. the use of a shallow pond as a supplemental heat rejecter in vertical GCHP systems) is the focus of Chapter 3 of this thesis.

A schematic of a SWHP system is shown in Figure 1-4. The surface-water heat exchanger can be a closed-loop or open-loop type. Typical closed-loop configurations are the Slinky coil type (as shown in Figure 1-4) or the loose bundle coil type. In the closed-loop systems, heat rejection/extraction is accomplished by circulating a heat exchange fluid through HDPE pipe positioned at an adequate depth within a lake, pond, reservoir, or other suitable open channel. Typical pipe diameters range from ¾ in. (19 mm) to 1 ½ in. (38 mm) and a length of 100 feet (30.48 m) to 300 feet (91.44 m) per ton of heating or cooling capacity is recommended by ASHRAE (1995b), depending on the climate. In open-loop systems, water is extracted from the surface-water body through a screened intake area at an adequate depth and is discharged to a suitable receptor.

Heat transfer mechanisms and the thermal characteristics of surface-water bodies are quite different than those of soils and rocks. This subject will be further discussed in Chapter 3 of this thesis. At the present time, design tools for surface-water heat pump systems are in their developmental infancy (Kavanaugh and Rafferty, 1997). However, many successful installations are currently in operation and some guidelines do exist. In

short, the loop design inv

specifying adequate dian

and locating the coil at a

Figure 1-4

1.1.4. Standing Column

The fourth categor

system. These systems ar

recently receiving much at

only briefly discussed here

A schematic of an SCW system is shown in Figure 1-5. This type of GSHP draws water to a heat pump from a standing column of water in a deep well bore and returns the water to the same well. These systems, primarily installed in hard rock areas, use uncased boreholes with typical diameters of about 6 in. (15.24 cm) and depths up to 1500 feet (457.2 m). The uncased borehole allows the heat exchange fluid to be in direct contact with the earth (unlike closed-loop heat exchangers) and allows ground water infiltration over the entire length of the borehole. Properly sited and designed, SCW systems have been shown to have significant installation cost savings over closed-loop GCHP systems. Design guidelines for SCW systems are currently under development.

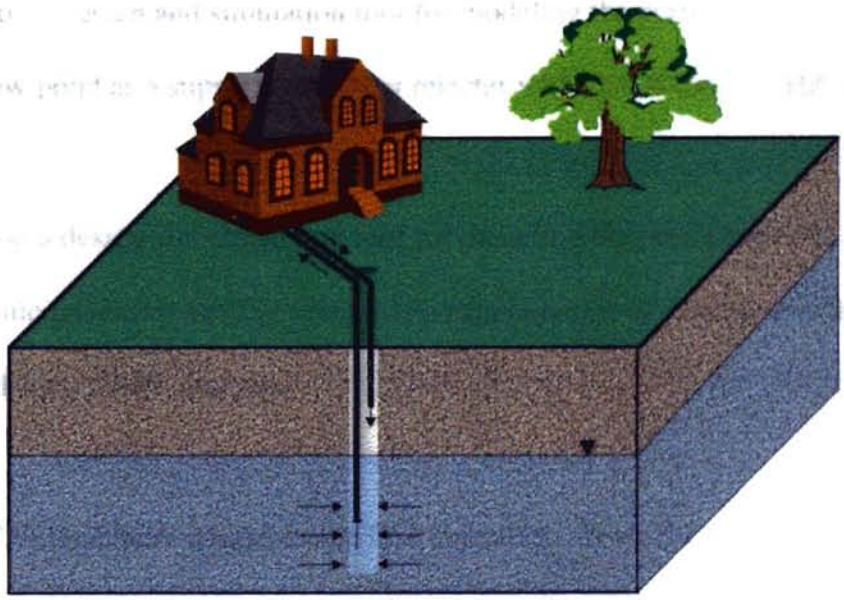

Figure 1-5. A schematic of a standing column well system.

1.2. Thesis Objectives and Scope

This study deals with the modeling of vertical closed-loop and source heat pump systems. The challenges associated with the design were discussed in the previous section. A considerable amount of rese decade has been geared toward optimizing the performance of these ty this study is part of those efforts.

There are three primary objectives of this study. These are to:

(1) examine the effects of ground-water flow on closed-loop G

(2) develop a design and simulation tool for modeling the perfo shallow pond as a supplemental heat rejecter with closed-lo and

(3) develop a design and simulation tool for modeling the perfo hydronic pavement heating system as a supplemental heat re closed-loop GSHP systems.

Chapter 2 of this thesis addresses the first objective. Given the t constraints of finding a suitable site with significant ground water flow, that site, and collecting and analyzing data at the site over a time period computer modeling study was conducted as a preliminary assessment of ground-water flow on closed-loop GSHP systems. Hydraulic and therm soils and rocks were compiled and AQUA3D, a commercially-available

ground-water flow and heat transport model developed by Vatnaskil Consulting Engineers, Inc., Reykjavik, Iceland, was used to simulate the impact of ground-w flow on the average heat exchange fluid temperature in single and multiple bore systems. The impact of ground-water flow on the estimation of soil/rock therma conductivity from in-situ test data was also examined.

Chapter 3 of this thesis addresses the second objective. The development validation of a design and simulation tool for modeling the performance of a shal pond as a supplemental heat rejecter with closed-loop GSHP systems is presentec model has been developed in the TRNSYS modeling environment and can theref coupled to other GSHP system component models for short-time step (hourly or minutely) system analyses. TRNSYS, developed at the University of Wisconsin-Madison, is a widely-used modular transient thermal systems simulation program each system component is described mathematically by a FORTRAN subroutine. simple language, the components are connected together in a manner analogous tc ducting, and wiring in a physical system (Duffie and Beckman, 1991). An examp application of the pond model is also presented.

Chapter 4 of this thesis addresses the third objective. The development an validation of a design and simulation tool for modeling the performance of a hydr pavement heating system as a supplemental heat rejecter with closed-loop GSHP s is presented. This model has also been developed in the TRNSYS modeling envir

for use in short-time step system analyses. An example application of the pavement heating model is also presented.

Finally, Chapter 5 of this thesis summarizes the conclusions of the individual studies.

1.3. The Overall Modeling Approach

Each of the objectives of this thesis deals with the development and/or application of a model. Since the term "model" can be used loosely, some definitions and approaches as applicable to this study are described here.

A "model" is a physical or a mathematical representation of an actual system. This study deals only with mathematical representations of systems. American Society for Testing and Materials (ASTM) defines a mathematical model as "mathematical equations expressing the physical system behavior and including simplifying assumptions". Mathematical models are solved analytically or numerically using manual or computer methods.

The overall modeling approach consists of six stages: (1) define the purpose of the model, (2) develop a conceptual model of the system, (3) develop or define the mathematical model of the system, (4) implement the solution method, (5) validate the model, and (6) apply the model. Each of these is described in the following paragraphs.

The first stage in the modeling approach is to clearly define the purpose and objectives of model. This helps to determine the level of detail and accuracy desired by the model and helps in making decisions regarding the resources needed.

The second stage in the modeling approach is to develop a conceptual model of the system. ASTM defines a conceptual model as "an interpretation or working description of the characteristics and dynamics of the physical system". The purpose of the conceptual model is to describe the system by a set of assumptions and concepts that can be evaluated mathematically.

The third stage in the modeling approach is to develop a mathematical model. In this stage, the conceptual model is translated to mathematical equations that can be solved for the desired unknowns. The solution method and limiting assumptions or simplifications are also identified.

The fourth stage in the modeling approach is to implement the solution method to solve the mathematical equations. With respect to this thesis, this stage involved using computer methods with a combination of commercially-available software and FORTRAN code developed specifically for this study.

The fifth stage in the modeling approach is to validate the model. With respect to this thesis, this stage involved comparing model results, where applicable, to an analytical solution or to experimental data.

The sixth stage in the modeling approach is to finally use the model to analyze the performance and behavior of actual thermal systems.

2. A Preliminary Assessment of the Effects of Ground-Water Flow on Closed-Loop Ground-Source Heat Pump Systems

2.1. Introduction

One of the fundamental tasks in the design of a reliable ground-coupled heat pump system is properly sizing the ground-coupled heat exchanger length (i.e. depth of boreholes). Recent research efforts have produced several methods and commercially-available design software tools for this purpose (Ingersoll, 1954; Kavanaugh, 1984; Eskilson, 1987; IGSHPA, 1991; Spitler et al., 1996; and Kavanaugh and Rafferty, 1997). All of these design tools are based on principles of heat conduction and rely on some estimate of the ground thermal conductivity and volumetric specific heat. These parameters are perhaps the most critical to the system design, yet adequately determining them is often the most difficult task in the design phase.

Methods of determining the thermal properties of the ground have also been the subject of considerable recent research (Eklof and Gehlin, 1996; and Austin et al., 2000). Current methods range from estimating values from published data to conducting laboratory experiments on soil/rock samples to conducting single-borehole, in-situ field tests. In general, thermal property values derived from in-situ field tests are most representative because the values are site-specific and a larger volume of material is evaluated under more realistic conditions than is possible in the laboratory. The typical field procedure in in-situ tests is to measure the temperature response of a fluid flowing through a ground heat exchanger in a single borehole. A schematic of the typical field

apparatus is shown in Figure 2-1. The fluid temperature at regular time intervals and heat added to the fluid stream are recorded over the course of the test.

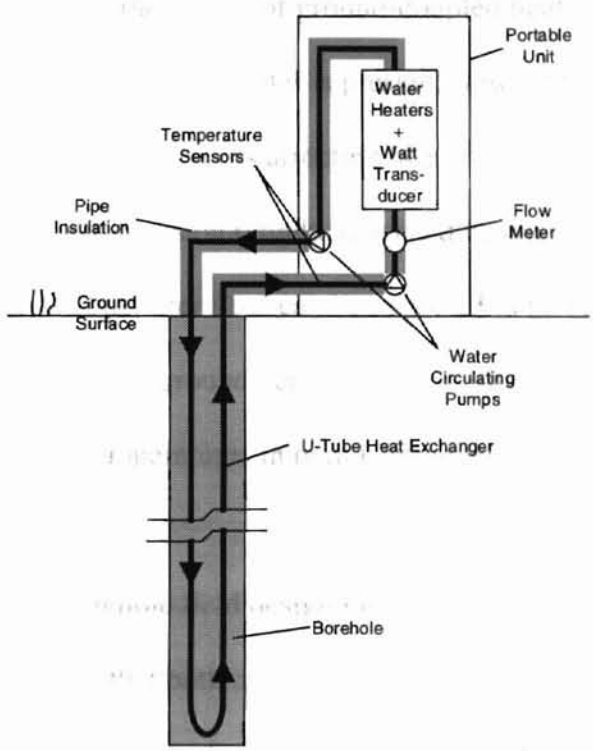

Figure 2-1. Schematic of typical apparatus for in-situ ground thermal conductivity testing.

Determination of thermal conductivity from temperature-time data is an inverse problem. Several analytical and numerical methods exist for interpreting the data set. These methods will not be discussed in detail here, but include the "cylinder-source" analytical solution (Carslaw and Jaeger, 1946), the "line-source" analytical solution (Kelvin, 1882; Ingersoll, 1954), numerical solutions (Mei and Emerson, 1985; Muraya et al., 1996; and Rottmayer et al., 1997), and numerical solutions with parameter estimation

(Shonder and Beck, 1999, Austin et al., 2000). Each of these methods is based on Fourier's Law of heat conduction.

A further complication in the design of ground-coupled heat pump systems is the presence of ground water. Where ground water is present, flow will occur in response to hydraulic gradients and the physical process affecting heat transfer in the ground is inherently a coupled one of heat diffusion (conduction) and heat advection by moving ground water. In general, ground-water flow can be expected to be beneficial to the thermal performance of closed-loop ground heat exchangers since it will have a moderating effect on borehole temperatures in both heating and cooling modes.

Complications in the borehole field design process due to the presence of flowing ground water arise from the fact that both current in-situ conductivity test data interpretation methods and ground-loop heat exchanger design methods are based on models that only consider heat conduction. Therefore, ground-water flow may impact the design process in two ways: (1) thermal conductivities derived from in-situ tests may appear artificially high and (2) borehole fields designed from artificially high thermal conductivity values may be over- or under-designed. An unusually high thermal conductivity value was determined from in-situ test data at a site in Minnesota where significant ground-water flow was believed to occur (Remund, 1998).

The objectives of the work presented in this chapter have been to make a preliminary examination of the effects of ground water flow on both in-situ ground

thermal conductivity measurements and long-term borehole field performance. This has been attempted firstly by examining the range of hydrogeological conditions that might be expected and estimating the order of magnitude of the corresponding ground-water flows. A simple method of examining the importance of heat advection from ground-water flow is then presented.

A finite-element numerical ground-water flow and heat transport model has been used to simulate and observe the effects of ground-water flow on the average fluid temperature in a single U-tube borehole in various geologic materials. The model was used to simulate several in-situ ground thermal conductivity tests, and thermal conductivities were derived from these data using a standard approach. For each test case, the derived thermal conductivities, along with the thermal loads from an actual building, were used to design a hypothetical multi-borehole field by employing conventional design tools and procedures. For different sets of hydrogeological conditions, a numerical model of the whole borehole field was used to simulate its long-term performance. Conclusions are presented on the ability of conventional design procedures to correctly predict the long-term performance of closed-loop ground heat exchangers under different ground-water flow conditions.

2.2. Coupled Ground Water Flow and Heat Transport

2.2.1. Ground-Water Flow

Underground water occurs in two zones: the unsaturated zone and the saturated zone. The term "ground water" refers to water in the saturated zone. The surface separating the saturated zone from the unsaturated zone is known as the "water table". At the water table, water in soil or rock pore spaces is at atmospheric pressure. In the saturated zone (below the water table), pores are fully saturated and water exists at pressures greater than atmospheric. In the unsaturated zone, pores are only partially saturated and the water exists under tension at pressures less than atmospheric. In this paper, we deal only with water in the saturated zone.

Ground water is present nearly everywhere, but it is only available in usable quantities in aquifers. An "aquifer" is defined by Driscoll (1986) as a formation, group of formations, or part of a formation that contains sufficient saturated permeable material to yield economical quantities of water to wells and springs. Aquifers are described as being either confined or unconfined. Unconfined aquifers are bounded at their upper surface by the water table. Confined aquifers are bounded between two layers of lower permeablity materials. In practice, the boreholes of ground-loop heat exchangers may partially penetrate several geologic layers.

The governing equation describing flow through porous media is Darcy's Law:

$$q = -K\frac{dh}{dx} \tag{2-1}$$

where q is the specific discharge (volume flow rate per unit of cross-sectional area), K is the hydraulic conductivity, and h is the hydraulic head. The specific discharge is related to average linear ground water velocity, v, by:

$$v = \frac{q}{n} \tag{2-2}$$

where n is the porosity and is introduced to account for the difference between the unit cross-sectional area and the area of the pore spaces through which the ground water flows (Freeze and Cherry, 1979; Fetter, 1988).

By applying the law of conservation of mass to a control volume and by making use of Darcy's Law (Equation 2-1), an equation defining the hydraulic head distribution can be derived. Transient ground-water flow with constant density can then be expressed in Cartesian tensor notation as:

$$S_s\frac{\partial h}{\partial t} - \frac{\partial}{\partial x_i}\left(\mathrm{K_{ij}}\frac{\partial \mathrm{h}}{\partial x_i}\right) = \mathrm{R}^* \tag{2-3}$$

Since ground water at 110°F (43.3°C) (an extreme temperature limit expected in GSHP applications) has a specific gravity of approximately 0.991, the assumption of constant density flow for low-temperature geothermal applications may be considered valid.

2.2.2. Heat Transport in Ground Water

Heat can be transported through a saturated porous medium by the following three processes:

(1) heat transfer through the solid phase by conduction,

(2) heat transfer through the liquid phase by conduction, and

(3) heat transfer through the liquid phase by advection.

The governing equation describing mass or heat transport in groundwater is a partial differential equation of the advection-dispersion type (Freeze and Cherry, 1979). By applying the law of conservation of energy to a control volume, an equation for heat transport in ground water can be found and can be expressed as:

$$nR\frac{\partial T}{\partial t} + v_i \frac{\partial T}{\partial x_i} - \frac{\partial}{\partial x_i}\left(\mathrm{D_{ij}} \frac{\partial \mathrm{T}}{\partial x_i} \right) = \mathrm{Q}^* \qquad (2\text{-}4)$$

where the velocity, v_i is determined from the solution of Equation 2-3 and T is the temperature of rock/water matrix. It is the second term in Equation 2-4 that represents advection of heat by the ground water and couples Equations 2-3 and 2-4 together. If the ground water velocity is zero, Equation 2-4 reduces to a form of Fourier's Law of heat conduction.

The diffusion coefficient tensor D_{ij} is modeled here as an effective thermal diffusivity given by:

$$D^* = \frac{k_{eff}}{\rho_\ell c_\ell} \tag{2-5}$$

The effective thermal conductivity k_{eff} is a volume-weighted average thermal conductivity of the saturated rock matrix and can be expressed using the porosity as:

$$k_{eff} = nk_\ell + (1-n)k_s \tag{2-6}$$

It is necessary to distinguish between the conductivity and thermal capacity of the water and soil/rock in this way to account for the fact that heat is stored and conducted through both the water and soil/rock, but heat is only advected by the water. Similarly, it is necessary to define a retardation coefficient R accounting for retardation of the thermal plume which results from differences in the liquid and solid volumetric heat capacities:

$$R = \frac{1+(1-n)c_s\rho_s}{n\, c_\ell \rho_\ell} \tag{2-7}$$

2.2.3. Typical Hydraulic and Thermal Property Values for Soils and Rocks

In assessing the significance of ground-water flow to closed loop heat exchanger performance, the question arises as to what locations have significant ground-water flow. Darcy's Law indicates that flow is dependent on both the local hydraulic gradient and the hydraulic conductivity of the geologic material. Heat transfer is dependent on the flow velocity and the thermal properties of the material. It is therefore useful, in making a preliminary assessment of the significance of ground-water flow, to consider the range of naturally-occurring soil and rock properties and possible values of hydraulic gradient.

Naturally-occurring ranges of values of hydraulic and thermal properties of soils and rocks are summarized in Table 2-1. Values of hydraulic gradient are somewhat more site-specific; the United States Environmental Protection Agency (1996) reports a typical range of hydraulic gradient values of 0.0001 to 0.05.

Some specific examples of natural ground water velocities include: 1796 ft/yr (547.5 m/yr) to 7185 ft/yr (2190 m/yr) under a hydraulic gradient of 0.002 to 0.012 in the Snake River Group basalt, Idaho, USA (Lindholm and Vaccaro, 1988); 361 ft/yr (110 m/yr) in the High Plains sand and gravel aquifer, western central USA (Weeks and Gutentag, 1988); and 1.3×10^{-3} ft/yr (4.0×10^{-4} m/yr) to 1.50×10^{-2} ft/yr (4.6×10^{-3} m/yr) in glacial clay soils in Southern Ontario, Canada (Stephenson et al., 1988). Local pumping activities may further increase ground-water flow rates in aquifers.

The thermal properties of soils and rocks are functions of mineral content, porosity, and degree of saturation. Of these, porosity may be considered the most important property simply because of the origin and nature of soils and rocks. Rocks originate under higher heat and pressure environments than soils and consequently generally possess lower porosities. Lower porosities in rocks result in higher contact area between grains and therefore higher thermal conductivities than soils, regardless of mineral content. For saturated materials, increased porosity results in increased heat capacities and therefore lower thermal diffusivities.

TABLE 2-1.

Typical Values of Hydraulic and Thermal Properties of Soils and Rocks

Porous Medium	Hydraulic Properties					Thermal Properties			
	Hydraulic Conductivity* (K) ft/s (m/s)			Porosity* (n) (--)		Velocity** (v) ft/yr (m/yr)	Thermal Conductivity*** (k) Btu/hr-ft-°F (W/m-°C)		Volumetric Heat Capacity*** ($\rho_s c_s$) Btu/ft^3-°F (J/m^3-°C)	
	Range		Geometric Average	Range	Arithmetic Average		Range	Arithmetic Average	Range	Arithmetic Average
Solls										
Gravel	9.84E-04 - 9.84E-02 3.00E-04 - 3.00E-02		9.84E-03 3.00E-03	0.24 - 0.38	0.31	1.00E+04 3.05E+03	0.40 - 0.52 (0.70) - (0.90)	0.46 (0.80)	-- --	2.09E+01 (1.40E+06)
Sand (coarse)	3.0E-06 - 2.0E-02 (9.0E-07) - (6.0E-03)		2.4E-04 (7.3E-05)	0.31 - 0.46	0.385	1.98E+02 (6.01E+01)	0.40 - 0.52 (0.70) - (0.90)	0.46 (0.80)	-- --	2.09E+01 (1.40E+06)
Sand (fine)	6.6E-07 - 6.6E-04 (2.0E-07) - (2.0E-04)		2.1E-05 (6.3E-06)	0.26 - 0.53	0.40	1.66E+01 (5.05E+00)	0.40 - 0.52 (0.70) - (0.90)	0.46 (0.80)	-- --	2.09E+01 (1.40E+06)
Silt	3.3E-09 - 6.6E-05 (1.0E-09) - (2.0E-05)		4.6E-07 (1.4E-07)	0.34 - 0.61	0.475	3.08E-01 (9.40E-02)	0.69 - 1.39 (1.20) - (2.40)	1.04 (1.80)	3.58E+01 - 4.92E+01 (2.40E+06) - (3.30E+06)	4.25E+01 (2.85E+06)
Clay	3.3E-11 - 1.5E-08 (1.0E-11) - (4.7E-09)		7.1E-10 (2.2E-10)	0.34 - 0.60	0.47	4.78E-04 (1.46E-04)	0.49 - 0.64 (0.85) - (1.10)	0.56 (0.98)	4.47E+01 - 5.37E+01 (3.00E+06) - (3.60E+06)	4.92E+01 (3.3E+06)
Rocks										
Limestone, Dolomite	3.3E-09 - 2.0E-05 (1.0E-09) - (6.0E-06)		2.5E-07 (7.7E-08)	0 - 0.20	0.10	8.02E-01 (2.44E-01)	0.87 - 1.91 (1.50) - (3.30)	1.39 (2.40)	3.17E+02 - 8.20E+01 (2.13E+07) - (5.50E+06)	1.99E+02 (1.34E+07)
Karst Limestone	3.3E-06 - 3.3E-02 (1.0E-06) - (1.0E-02)		3.3E-04 (1.0E-04)	0.05 - 0.50	0.275	3.76E+02 (1.15E+02)	1.44 - 2.48 (2.50) - (4.30)	1.96 (3.40)	3.17E+02 - 8.20E+01 (2.13E+07) - (5.50E+06)	1.99E+02 (1.34E+07)
Sandstone	9.8E-10 - 2.0E-05 (3.0E-10) - (6.0E-06)		1.4E-07 (4.2E-08)	0.05 - 0.30	0.18	2.51E-01 (7.65E-02)	1.33 - 3.76 (2.30) - (6.50)	2.54 (4.40)	3.17E+01 - 7.46E+01 (2.13E+06) - (5.00E+06)	5.31E+01 (3.56E+06)
Shale	3.3E-13 - 6.6E-09 (1.0E-13) - (2.0E-09)		4.6E-11 (1.4E-11)	0 - 0.10	0.0525	2.79E-04 (8.50E-05)	0.87 - 2.02 (1.50) - (3.50)	1.44 (2.50)	3.54E+01 - 8.20E+01 (2.38E+06) - (5.50E+06)	5.87E+01 (3.94E+06)
Fractured Igneous and Metamorphic	2.6E-08 - 9.8E-04 (8.0E-09) - (3.0E-04)		5.1E-06 (1.5E-06)	0 - 0.10	0.05	3.21E+01 (9.78E+00)	1.47 - 3.83 (2.50) - (6.60)	2.65 (4.58)	-- --	3.28E+01 (2.20E+06)
Unfractured Igneous and Metamorphic	9.8E-14 - 6.6E-10 (3.0E-13) - (2.0E-10)		8.0E-12 (2.4E-12)	0 - 0.05	0.025	1.01E-04 (3.09E-05)	1.47 - 3.83 (2.50) - (6.60)	2.65 (4.58)	-- --	3.28E+01 (2.20E+06)

Notes: Thermal conductivity values are taken to represent that of materials in the dry condition.

* hydraulic conductivity and porosity data from Domenico and Schwartz (1990).

** v is the average linear ground water velocity based on an assumed gradient of 0.01 ft/ft (m/m).

*** thermal property data from Hellstrom (1991). For sedimentary rocks, Heilstrom lists only c_s. In these cases, a density of 2500 kg/m^3 is assumed.

The porosity of soils and rocks can also be an important controlling influence on hydraulic conductivity (Freeze and Cherry, 1979). Materials with higher porosity generally also have higher hydraulic conductivity. However, this correlation does not hold for fine-grained soils (see Table 2-1.). Porosity and hydraulic conductivity of soils and rocks can be increased by so-called "secondary porosity" which is attributed to solution channels (i.e. in karst limestone) or to fracturing (i.e. in rocks and cohesive soils).

2.2.4. Conduction Versus Convection in Geologic Materials

It has already been noted that it is the presence of advection that distinguishes the heat transfer regime under ground-water flow conditions from that of heat conduction alone. Some assessment of the significance of the flow can be made by considering the order of magnitude of the advection of heat compared to conduction (diffusion).

A dimensionless parameter describing conduction versus convection is the Peclet number (Pe). In this application, the Peclet number expresses the transport of heat by bulk fluid motion to the heat transported by conduction. Domenico and Schwartz (1990) define Pe for heat transport in ground water as:

$$\mathrm{Pe} = \frac{\rho_\ell c_\ell \, q \, L}{k_{eff}} \qquad (2\text{-}8)$$

The term L is defined as some characteristic length dependent on the situation. According to Bear (1972), L can be chosen as any length dimension, so long as it is consistent with other comparisons. In principle, advection becomes significant when Pe

is of order one. The exact value of Pe at which advection becomes significant is slightly dependent on the choice of *L*.

The Peclet number has been used to quantify the relative importance of mechanical (or advective) dispersion versus molecular diffusion in mass transport in ground water. Many studies have been conducted and the data have been summarized by Bear (1972). In short, when the characteristic length was chosen as mean grain size, diffusion is the process controlling mass transport at Peclet numbers less than about 0.4. At Peclet numbers in the range of 0.4 to 5, a transition occurs where mechanical dispersion (or advective dispersion) and diffusion are of the same order of magnitude. Above a Peclet number of about 5, mechanical dispersion (or advective dispersion) dominates. No similar studies conducted for heat transport have been found.

An analysis of the Peclet number using the typical hydraulic and thermal values of soils and rocks presented in Table 2-1 may be used to assess the role of ground water flow in the design of closed-loop ground heat exchangers. The characteristic length could conceivably be chosen as (1) a typical borehole spacing or (2) the length of the borehole field in the direction of flow. The calculated Peclet numbers are listed in Table 2-2 using a typical borehole spacing of 14.8 ft (4.5 m) and assuming the fluid property values of ρ_f, c_f, and k_f as 62.4 lb/ft^3 (1000 kg/m^3), 1.0 Btu/lb-°F (4180 J/kg-°C), and 0.347 Btu/hr-ft-°F (0.60 W/m-°C).

A review of the data presented in Table 2-2 reveals that heat advection by ground water flow is significant process contributing to heat transfer in coarse-grained soils (sands and gravels) and in rocks exhibiting secondary porosities (fracturing and solution channels). When the characteristic length is defined as the borehole spacing, Peclet numbers exceeding 1 exist only for sands, gravels, and karst limestones. It is possible however, that even when the Peclet number is of order one or higher, the effects of the ground-water flow on the temperature response may not be seen within the normal time scale of an in-situ thermal conductivity test. This is one of the reasons for conducting numerical borehole field simulations for the duration of several years.

TABLE 2-2.

Peclet Numbers Corresponding to Typical Values of Hydraulic and Thermal Properties of Soils and Rocks

Porous Medium	Peclet Number *where L = a typical borehole spacing of* 14.8 ft (4.5 m) [--]
Soils	
Gravel	5.72E+02
Sand (coarse)	1.34E+01
Sand (fine)	1.15E+00
Silt	1.28E-02
Clay	3.24E-05
Rocks	
Limestone, Dolomite	5.92E-03
Karst Limestone	5.28E+00
Sandstone	1.77E-03
Shale	1.05E-06
Fractured Igneous and Metamorphic	6.32E-02
Unfractured Igneous and Metamorphic	1.00E-07

2.2.5. Numerical Ground-Water Flow and Heat Transport Models

In assessing the effects of ground-water flow on U-tube heat exchanger performance, one is mainly interested in the temperature of the heat exchange fluid. Therefore, modeling of the U-tubes in some detail is important in this problem. The heat exchange fluid temperature is affected by the transient building thermal loads in addition to the heat transfer in the porous medium around the borehole. Consequently, this problem is characterized by an irregular model domain with time-varying boundary conditions and is best handled by a numerical model.

Numerous commercially-available and public domain numerical software codes exist for modeling mass and/or heat transport in ground water. Of these, the following 8 were selected for a more detailed review for potential application to this project:

- ***3DFEMFAT (3-Dimensional Finite Element Method Flow and Transport)*** by G. Yeh, Pennsylvania State University. This code was developed to simulate mass transport in variably-saturated porous media. Density-dependent flow can also be simulated.

- ***AQUA3D*** by Vatnaskil Consulting Engineers, Reykjavik, Iceland. This code is also a three-dimensional, finite-element code. It was developed mainly for simulation of mass-transport problems but allows easy adaptation of boundary conditions to model heat transport without density-dependent ground-water flow.

- ***FEFLOW (Finite Element FLOW)*** by WASY Institute for Water Resources Planning and Systems Research, Ltd., Berlin, Germany. This code is also a three-dimensional, finite-element code. It is capable of simulating both mass and heat transport in variable-density ground-water flow systems.

- ***Flowpath II*** by Waterloo Hydrologic, Inc. (WHI), Waterloo, Ontario. This code is a two-dimensional finite difference code. It was developed originally for simulation of ground-water flow problems only; contaminant-transport simulation capabilities, mainly in the horizontal plane, have been recently added.

- ***HST3D (Heat and Solute Transport in 3 Dimensions)*** by USGS, Denver, Colorado. This code is a three-dimensional finite-difference code. It is capable of simulating mass and heat transport in variable-density ground-water flow systems. It was developed mainly for simulating problems involving waste injection into aquifers.

- ***MT3D^{96} (Mass Transport in 3 Dimensions)*** by S.S. Papadopulos & Associates, Inc., Bethesda, Maryland. This code is also a three-dimensional finite-difference code. It solves the mass transport equation only and requires a solution to the ground-water flow equation from another code. It was developed for simulating contaminant-transport problems in ground water.

- ***SUTRA (Saturated-Unsaturated TRAnsport)*** by United States Geological Survey (USGS), Denver, Colorado. This code is a two-dimensional finite-element code. It is capable of simulating mass or energy transport in variably-saturated, variable-density ground-water flow systems. It was mainly developed as a cross-sectional model for simulating salt-water intrusion into fresh-water aquifers.

- ***SWIFT (Sandia Waste Isolation Flow and Transport)*** by HSI GeoTrans, Sterling, Virginia. This code is a three-dimensional finite-difference code. It is capable of simulating mass and heat transport in variable-density ground-water flow systems in porous or fractured media. It was developed mainly for simulating problems involving deep-well radioactive waste injection into geologic repositories.

In the code selection process, particular attention was paid to the following items: (1) the type of boundary conditions handled by the code, (2) the solution scheme employed by the code, (3) verification of the code, and (4) cost. Each of these points is described in more detail below.

The type of boundary conditions handled by the code was perhaps the most important consideration in the code selection process. For simulation of periodic heat extraction or heat rejection to the ground, the selected code needed to be capable of handling time-varying, heat flux boundary conditions. Further, since a relatively large number of time-varying data were to be used as input, the selected code needed to be capable of reading time-varying conditions from an external file.

The software codes that were reviewed for this project employ either finite-difference methods (FDM) of finite-element methods (FEM) to solve the partial differential equations describing heat/mass transport in ground water (Equations 2-3 and 2-4). The solution scheme was considered important for two main reasons. First, FEM offers an advantage over FDM in the ability to represent complex or irregular geometries (i.e. circular U-tubes in a rectangular domain). Second, there has been controversy in the literature over advantages of FEM over FDM in solving the advection-dispersion equation (Equation 2-4). In general, experience has shown the FEM to be generally superior to FDM in solution stability (Wang and Anderson (1982) and Mercer and Faust (1986)). Consequently, codes employing an FEM solution scheme were preferred.

Documented verification of the code was an important consideration since it often requires years to find and fix bugs in these types of software programs. All of the 8 codes listed above have been originally developed in the 1980s and many validation examples exist.

The cost of the code was also a main consideration in the selection process since the project had an allocated budget for software.

2.3. The Numerical Model

2.3.1. Model Description

The computer code selected for this study was AQUA3D. It is a commercially-available software package originally developed in 1983 by Vatnaskil Consulting Engineers of Reykjavik, Iceland. The partial differential Equations 2-3 and 2-4 are discretized spatially by a Galerkin finite element method using triangular elements with linear weighting functions (Vatnaskil, 1998). The temporal term of the equations is dealt with by first order backward differencing in time. AQUA3D does not allow for the explicit representation of the heat transport equation, but provides a general form of the mass transport equation (Equation 2-4). Temperatures were in fact calculated by suitable choice of the coefficients of the mass transport equation and corresponding adaptation of the boundary conditions.

The finite element ground-water flow and mass/heat transport model was used in this study as the primary means of assessing the effects of ground-water flow on closed-loop heat exchangers. Use of a numerical model allows a wide range of conditions to be examined and is the only practical means of modeling a whole borehole field. In each test case, a uni-directional flow field was imposed over the whole numerical domain. As the flow was assumed to be fully-saturated and within homogeneous geologic material, it was only necessary to use a two-dimensional model.

2.3.2. The Finite Element Mesh

Finite element meshes for a single borehole geometry, and for a complete borehole field geometry have been constructed using triangular elements. Nodal spacing was kept relatively fine around the pipe walls where the steepest temperature gradients were expected. The mesh for the single borehole geometry was constructed within a square domain and consisted of 465 nodes, as shown in Figure 2-2.

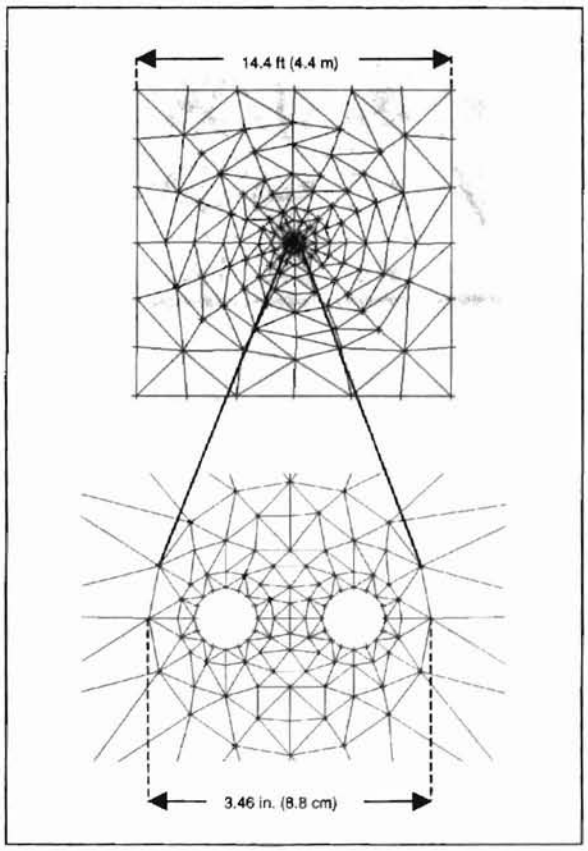

Figure 2-2. Finite element mesh representing a single borehole.

A mesh for a four-by-four configuration borehole field was constructed by using the single borehole mesh (Figure 2-2) as the basis for the mesh at each borehole and by expanding the mesh in the direction of ground-water flow as shown in Figure 2-3. This mesh consisted of 4532 nodes.

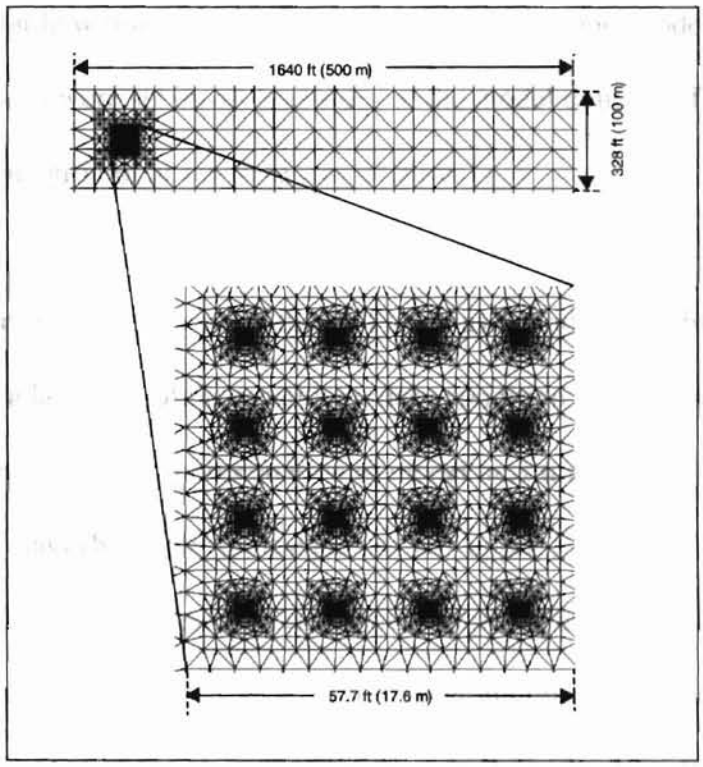

Figure 2-3. Finite element mesh representing a 16 borehole field.

2.3.3. Boundary Conditions

Two sets of boundary conditions are required: one set for the flow model and one set for the transport model.

In the flow model, first-type or fixed-value (Dirichlet) boundary conditions were set on the left-hand and right-hand boundaries in order to impose a fixed hydraulic gradient across the domain. Second-type or fixed-gradient (Neumann) boundary conditions were set on the upper and lower boundaries of the flow domain and were specified as zero flux. This work assumes that no ground-water recharge takes place across the water table within the model domain. In the transport model, Dirichlet boundary conditions were set on all four sides of the model domain. These conditions represent fixed background or far-field temperatures.

In order to impose the ground thermal loads as boundary conditions at the U-tube pipe walls, some adaptation of the usual boundary condition was required. This arises from the use of the mass transport equation to model heat transport. First, a zero flux condition for the mass (heat) transport equation was applied at each of the sixteen nodes forming each pipe wall. The required heat flux is imposed using a source term in the ground-water flow equation at these nodes (representing injection of the heating/cooling water). The flow injected, V^*, was set negligibly small (3.53×10^{-19} ft^3/s [1.0×10^{-20} m^3/s]) so as not to disturb the ground-water flow field. The temperature of this injection flow, T_w was set to achieve the required heat input (the ground thermal load), so that,

$$T_w \approx \frac{q^*}{\rho_\ell c_\ell V^*} \tag{2-9}$$

The values of ρ_ℓ and c_ℓ are taken as constants of 62.4 lb/ft^3 (1000 kg/m^3) and 1.0 Btu/lb-°F (4180 J/kg-°C). The average temperature of the heat exchange fluid in each borehole is taken as the average of the nodal temperatures of the 32 nodes defining the U-tube pipe

in each borehole. Where single borehole cases were simulated, the heat input per pipe node, q^*, was set at a fixed value representative of in-situ thermal conductivity test conditions. Where the whole borehole field was modeled, q^* was determined from the time-varying building loads.

2.3.4. Validation of the Numerical Model

In order to check the accuracy of the AQUA3D model and the implementation of the boundary conditions, an appropriate analytical solution was sought. Numerous analytical solutions have been developed for the advection-dispersion equation (Equation 2-4). However, these are mostly specific to pollutant-transport problems (T is replaced by solute concentration in Equation 2-4) involving point or line sources with uniform concentration in time. Fetter (1988) and Bear (1972) summarize solutions for boundary and initial conditions describing situations that are commonly found in nature. The literature gives little to no attention to analytical solutions describing the explicit transport of heat in ground water.

The most appropriate analytical solution found was that described by Eskilson (1987) for steady-state heat extraction from a borehole in a ground-water flow field. However, Eskilson's solution contains some approximations.

Eskilson (1987) describes the steady-state temperature at the borehole wall ($T_{sw,b}$) as:

$$T_{sw,b} = T_{om} + \frac{q^{'}}{H}\left\{\frac{1}{2\pi k_s}\left[\ln\left(\frac{H}{2r_b}\right) - P_w\left(\frac{H}{\ell}\right)\right]\right\} \qquad (2\text{-}10)$$

The logarithmic term gives the steady-state resistance and $P_w\left(\frac{H}{\ell}\right)$ is a correction term accounting for ground-water flow which is approximated as:

$$P_w\left(\frac{H}{\ell}\right) = \ln\frac{H}{2\ell} + \gamma - \frac{1}{2}\ln(3) \qquad (2\text{-}11)$$

for ℓ defined as:

$$\ell = \frac{2k_s}{\rho_\ell c_\ell q} \qquad \text{where} \quad \ell >> r_b \qquad (2\text{-}12)$$

Comparisons of the steady-state temperature at the wall of a pipe were made using both the AQUA3D and the Eskilson (1987) solution. The following data were used as inputs: a pipe diameter of 0.787 in. (2 cm) (i.e. a single leg of a typical U-tube), a pipe depth of 250 ft (76.2 m), soil thermal property values of sand from Table 2-1, water properties as described above, a far-field temperature of 63°F (17.2°C), and a heat flux of 8530 Btu/hr (2500 W). The temperature predicted by AQUA3D at steady-state time and Eskilson's (1987) solution were 101.4°F (38.54°C) and 99.59°F (37.55°C), respectively. In terms of temperature increase above the far-field temperature, the percent difference in error between the two solutions is 4.9%. This error was considered to be acceptable.

2.4. Results And Discussion

2.4.1. Single-Borehole Simulations

The numerical model was initially used to determine average borehole temperatures for a range of soil and rock types over a two-year simulation time. The objective was to examine trends in heat exchanger performance with increasing Peclet number. The hydraulic and thermal property inputs are those listed in Table 2-1 and a hydraulic gradient of 0.01 was assumed. A constant heat flux of 8530 Btu/hr (2500 W) was applied on a U-tube in a 250 ft (76.2 m) deep borehole. The initial temperature and first-type boundary conditions were set at 63°F (17.2°C). The model domain is that shown in Figure 2-2. A simulation time of two years with a time step of 5 days was used for these simulations. For comparison purposes, simulations were made for each case but with zero ground-water flow.

Plots of average borehole fluid temperature versus time for three example geologic materials are shown in Figure 2-4. A review of these plots reveals that a "typical" ground water flow rate in a coarse sand dramatically lowers the average borehole fluid temperature when compared to the zero-flow case. After a one-year period, the average fluid temperature in the borehole is approximately 15°F (8.3°C) lower than the average fluid temperature in the borehole where no ground-water flow was simulated, and appears to have reached a steady state. A small reduction in peak temperature is shown for the case of fine sand. However, "typical" ground water flow

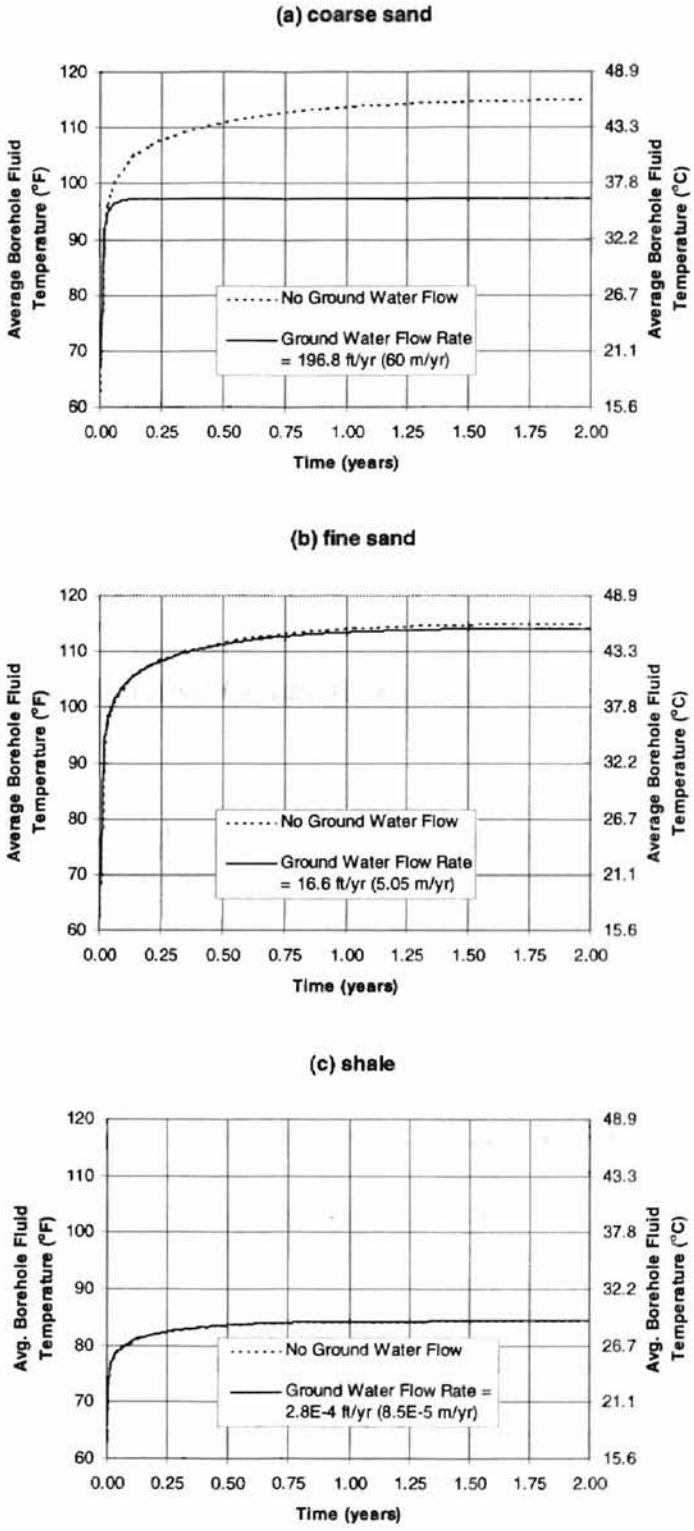

Figure 2-4. Average borehole fluid temperature vs. time for (**a**) coarse sand, (**b**) fine sand, and (**c**) shale.

rates in rocks such as granites, limestones, dolomites, and shales were found to have a negligible effect on the average borehole fluid temperature.

The trends shown in these results are in agreement with the previous Peclet number analysis. At Peclet numbers of order one or higher, advection of heat by flowing ground water is a significant process contributing to heat transfer in the ground. At Peclet numbers of order less than one, conduction is the dominant heat transfer process and enhancement to the heat exchanger performance is negligible.

2.4.2. Simulated In-Situ Thermal Conductivity Tests

The second objective of the single-borehole simulations was to determine the effects of ground-water flow (in a material where ground-water flow is expected to be significant) on the interpretation of data from in-situ ground thermal conductivity tests. The previous results showed the effects of ground-water flow to be most significant in the cases of gravel and coarse sand. Accordingly, the simulated in-situ thermal conductivity test calculations have been based on coarse sand properties.

As previously discussed, in-situ thermal conductivity tests involve the application of a steady heat flux to a test borehole along with the measurement of the temperature response of the circulating water. These data are used either with an analytical model or with a numerical model and parameter estimation technique to arrive at a value of thermal conductivity of the soil/ rock formation. Here, the borehole temperature response

is calculated for a range of ground-water flows using the AQUA3D model. These data have been analyzed in exactly the same way as if the data had been measured in-situ. Hence, 'effective' thermal conductivities have been estimated for different flow conditions.

In-situ test conditions were modeled by applying a constant heat flux of 8530 Btu/hr (2500 W) on a U-tube in a 250 ft (76.2 m) deep borehole. The simulation time periods were 50 hours and one week, corresponding to typical durations of in-situ ground thermal conductivity tests. The model time step was 2.5 minutes. The initial temperature and first-type boundary conditions were set at 63°F (17.2°C) and the model domain is that shown in Figure 2-2. Model input hydraulic and thermal property values are those listed in Table 2-1 for a coarse sand, except the ground water flow velocity was varied from a "typical" value of 196.8 ft/yr (60 m/yr) to a more extreme value of 1968.5 ft/yr (600 m/yr) by adjusting the hydraulic conductivity value. Twelve cases were simulated as listed in Table 2-3.

Resulting temperature responses for the 12 cases are plotted in Figure 2-5. A review of Figure 2-5 shows that ground water flow in a coarse sand significantly impacts the average borehole fluid temperature over the time scales of an in-situ ground thermal conductivity test. Two noteworthy conclusions can be drawn from these simulations: (1) as ground water velocity increases, the time to reach steady-state conditions decreases and (2) as ground water velocity increases, the steady-state temperature decreases. Also, the deviation from the zero-flow condition can be seen to be dependent on the duration of

the test; temperatures are further reduced with increasing duration. Hence, the duration of the test could be expected to have an influence on the estimated thermal conductivity derived from an in-situ test.

TABLE 2-3
Case Summary of Simulated In-Situ Ground Thermal Conductivity Tests

Case	Simulation Time Period	Ground Water Flow Velocity
1	50 hours	No Ground Water Flow
2	50 hours	196.8 ft/yr (60 m/yr)
3	50 hours	393.7 ft/yr (120 m/yr)
4	50 hours	787.4 ft/yr (240 m/yr)
5	50 hours	1574.8 ft/yr (480 m/yr)
6	50 hours	1968.5 ft/yr (600 m/yr)
7	1 week	No Ground Water Flow
8	1 week	196.8 ft/yr (60 m/yr)
9	1 week	393.7 ft/yr (120 m/yr)
10	1 week	787.4 ft/yr (240 m/yr)
11	1 week	1574.8 ft/yr (480 m/yr)
12	1 week	1968.5 ft/yr (600 m/yr)

The effective thermal conductivity values predicted by the Austin et al. (2000) model are plotted against the corresponding ground-water flow velocity for each of the two in-situ test simulation times (50 hours and 1 week) in Figure 2-6. The actual values are listed by case number in Table 2-4. A review of these results shows that as ground water flow velocity increases, the predicted effective thermal conductivity values from a conduction-based model are significantly different, depending on the duration of the simulated test. These values are "effective" values since they include the effects of ground water advection. However, at this stage of the design process, it is not clear if the

50-hour data set or the 1-week data set produces more representative values, or if either data set produces representative values at all.

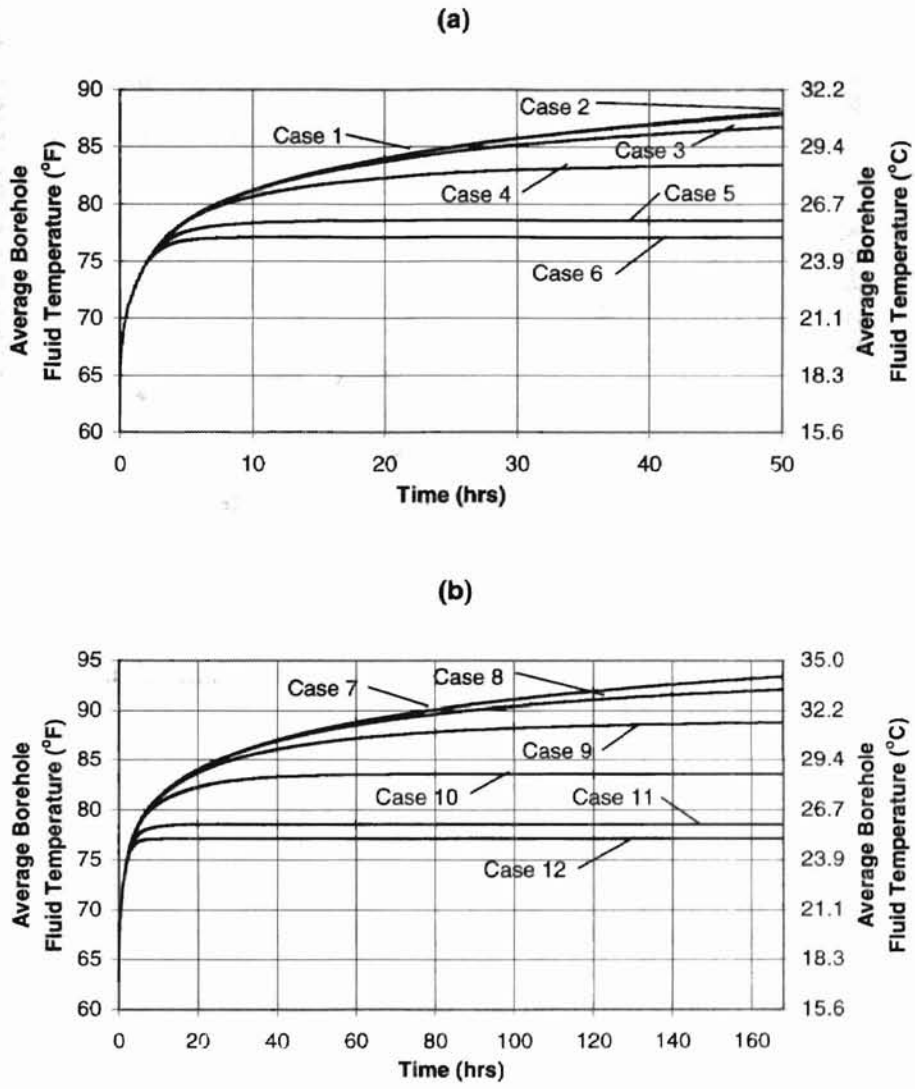

Figure 2-5. Average borehole fluid temperatures for the 12 simulated in-situ ground thermal conductivity test cases in a coarse sand with ground water velocities ranging from 0 to 1968 ft/yr (600 m/yr) for (**a**) 50 hours and (**b**) one week.

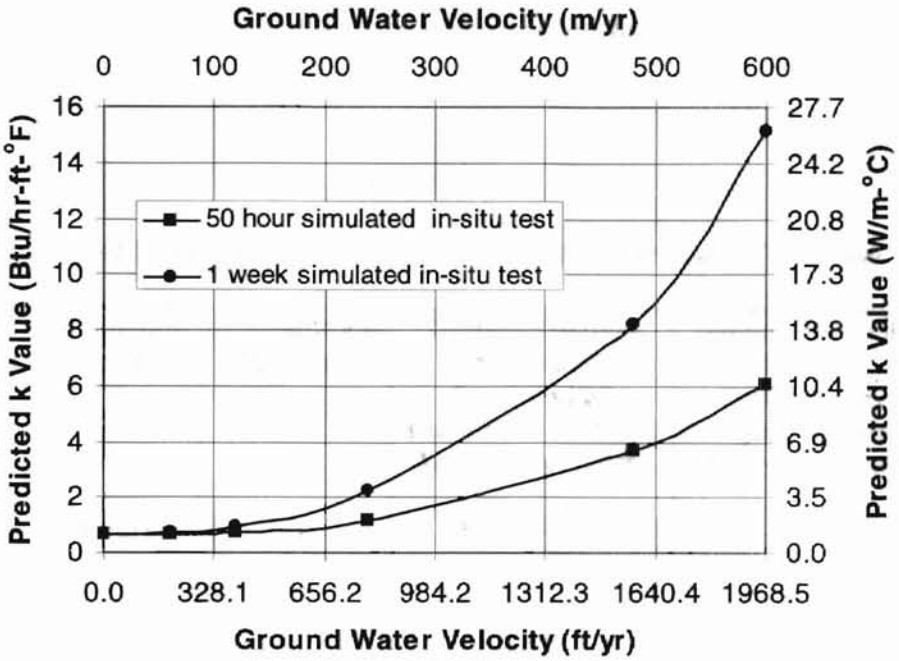

Figure 2-6. Predicted effective ground thermal conductivity values versus ground-water flow velocity for 50-hour and 1-week simulated in-situ thermal conductivity tests.

2.4.3. Borehole Field Simulations

In order to investigate the effects of ground-water flow on borehole field performance and system design procedures further, the predicted ground thermal conductivities were used to design a borehole field for a test building. The test building was an actual building located in north-central Oklahoma. This building is a single-story office building with 8 thermal zones and has a predominant demand for cooling. The hourly building loads were determined for one year using building energy simulation software (BLAST, 1986). The building loads were then converted to ground loads under

the assumption that all heat pumps in the system have a constant coefficient of performance of 4.0. The ground loads for this building are shown in Figure 2-7.

TABLE 2-4

Summary of Borehole Field Design Parameters for Each Test Case

Case Number	Simulation Duration (hours)	Ground-Water Flow Rate ft/yr (m/yr)	Ground Thermal Conductivity Predicted by Numerical Model of Austin et al. (2000) Btu/hr-ft-°F (W/m-°C)	Design Borehole Depth Predicted by Design Software of Spitler et al. (1996) ft (m)
1	50	0	0.643 (1.11)	239.98 (73.15)
2	50	196.85 (60.00)	0.650 (1.12)	238.56 (72.71)
3	50	393.70 (120.00)	0.731 (1.26)	224.10 (68.31)
4	50	787.40 (240.00)	1.146 (1.98)	171.56 (52.29)
5	50	1574.80 (480.00)	3.657 (6.33)	87.24 (26.59)
6	50	1968.50 (600.00)	6.074 (10.51)	61.58 (18.77)
7	168	0	0.625 (1.08)	243.86 (74.33)
8	168	196.85 (60.00)	0.691 (1.20)	230.86 (70.37)
9	168	393.70 (120.00)	0.962 (1.66)	191.58 (58.39)
10	168	787.40 (240.00)	2.250 (3.89)	115.91 (35.33)
11	168	1574.80 (480.00)	8.229 (14.24)	48.02 (14.64)
12	168	1968.50 (600.00)	15.107 (26.14)	26.90 (8.20)

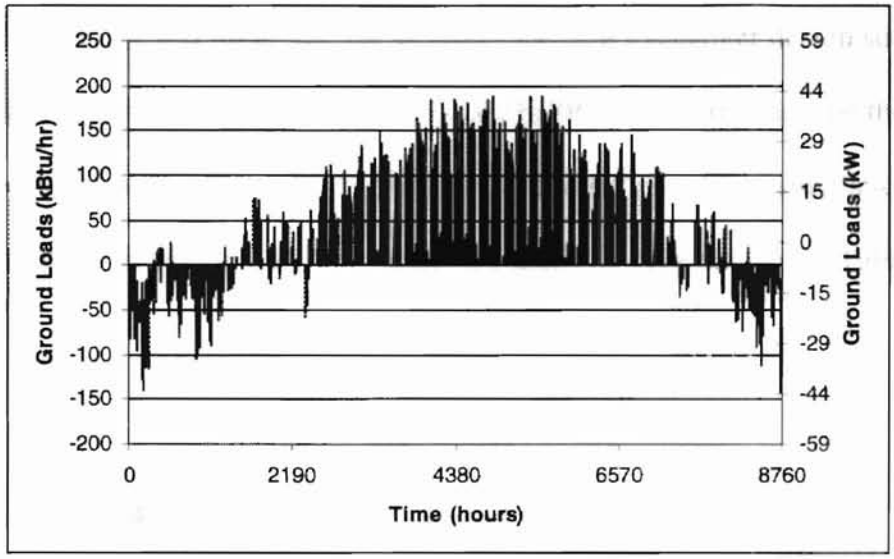

Figure 2-7. Hourly ground loads for the test building. Heating load is shown negative, representing heat extracted from the ground; cooling load is shown positive, representing heat rejected to the ground.

Borehole field designs were produced for each of the twelve test cases. This was done with GLHEPRO, a commercially-available ground-loop heat exchanger design software tool developed by Spitler et al. (1996). A 16 borehole field (four-by four boreholes in a square pattern) was deemed adequate for the test building ground loads (Figure 2-7). The monthly loads and peak hourly loads are generally input in the design software. For this study, no peak hourly loads were specified for the sake of the computational time required for the subsequent borehole field simulations (see discussion below). Peak design entering fluid temperatures to the heat pump were specified at 90°F (32.2°C) maximum and 35°F (1.7°C) minimum. The borehole depths were sized for 20-years of operation.

For each test case, the corresponding effective thermal conductivity shown in Figure 2-6 and Table 2-4 was input into the ground-loop heat exchanger design software (GLHEPRO). The borehole depths predicted by GLHEPRO are plotted against the corresponding ground water flow velocity for each of the two in-situ test simulation times (50 hours and 1 week) in Figure 2-8. The values are listed by case number in Table 2-4.

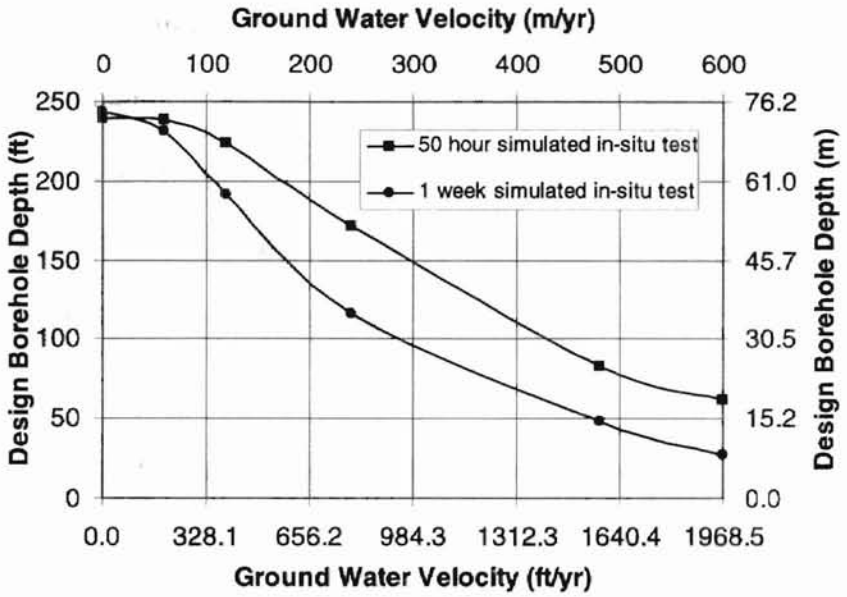

Figure 2-8. Design borehole depths versus ground-water flow velocity for 50-hour and 1-week simulated in-situ thermal conductivity tests.

AQUA3D was further used to simulate the long-term performance of each borehole field designed from the simulated in-situ ground thermal conductivity test cases. The model domain was that previously described for the multi-borehole field simulations shown in Figure 2-3. The simulation time for all cases was 10 years and the model time step was 5 days. The simulated heat flux at the internal boundary nodes defining the U-tube pipes was a time-varying source corresponding to the monthly ground loads for the

test building. Hydraulic and thermal property inputs for each borehole field case number is the same as the corresponding single-borehole case number, except for the borehole depths, which are those listed in Table 2-4. Each 10-year simulation required approximately 60 hours of computation time on a personal computer with a 233 megahertz pentium II processor.

Annual maximum and minimum peak temperatures are plotted for each case in Figure 2-9. Examination of the cases with no ground-water flow (cases 1 and 7) shows annual rises in peak temperature typical of cooling-dominated buildings. After the second year, all of the cases with ground-water flow show no changes in minimum and maximum temperatures from year to year.

Some notable differences can be seen between the borehole field designs based on 50-hour test data compared to one week test data. This is shown by cases 5 and 6 which represent thermal conductivity values determined from a 50-hour test at ground water flow velocities of 1574.8 ft/yr (480 m/yr) and 1968.5 ft/yr (600 m/yr), respectively, and by cases 11 and 12 which are for the same flow rates but based on thermal conductivity values determined from one-week test data. The thermal conductivity values determined in cases 11 and 12 are unrealistically high and consequently the design borehole depths are too shallow; the result is that the maximum peak temperature of the simulated borehole field in both cases exceeds the maximum design temperature during the first year. This implies that for in-situ test cases where the average borehole fluid temperature reaches steady-state in a relatively short time (as demonstrated by case 4/10, case 5/11,

and case 6/12 in Figure 2-5), increasing the duration of the in-situ test produces decreased confidence in the accuracy of the effective thermal conductivity value determined from the test.

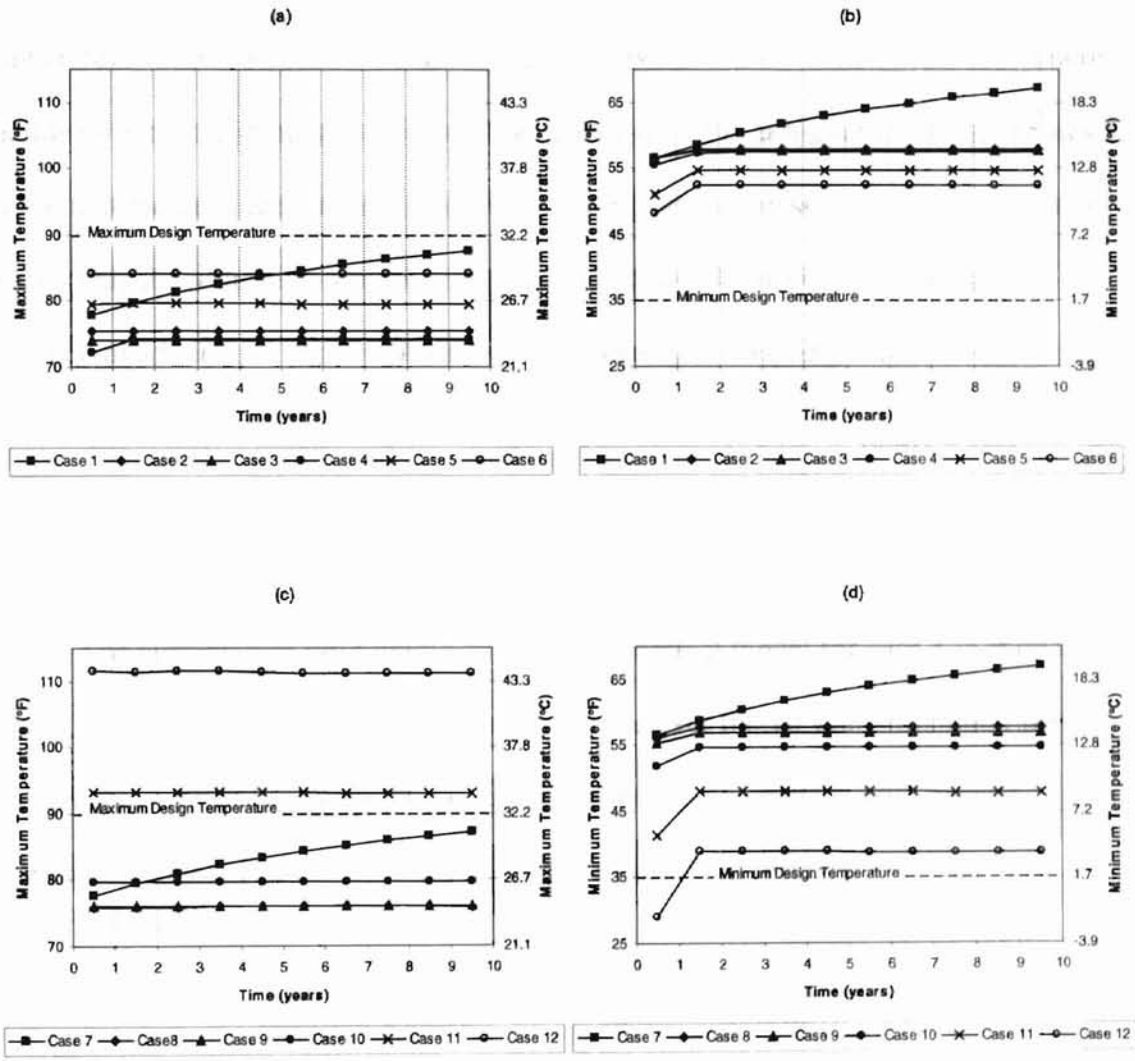

Figure 2-9. Annual maximum (**a**) and (**c**) and minimum (**b**) and (**d**) average borehole fluid temperatures for the 16 borehole field simulations.

Except for cases 11 and 12, the annual maximum and minimum temperatures fell within the design conditions. Having followed conventional design procedures, it is interesting to note from Figure 2-9 (a) that it is the cases where the ground-water flow is moderate (cases 2, 3, and 4) that are most over-designed. These cases have maximum peak temperatures of about 74°F (23.3°C), some 16°F (8.9°C) below the maximum design temperature. Considerable drilling cost savings could be seen in cases like this where shallower borehole depths could have been adequate. It is at higher flow rates (cases 5 and 6) that the peak temperature was closest to the original design condition after ten years. This illustrates the non-linearity introduced into the design problem by the presence of advection. It also illustrates the difficulty in adapting conventional design methods to accurately size closed-loop ground heat exchangers in cases with significant ground-water flow.

The temperature field predicted by the numerical model for case 8 is shown in Figure 2-10 in the form of a series of contour plots over the 10 year simulation period. The data are plotted for the end of September, when the average annual ground temperatures are the greatest (i.e. at the end of the cooling season).

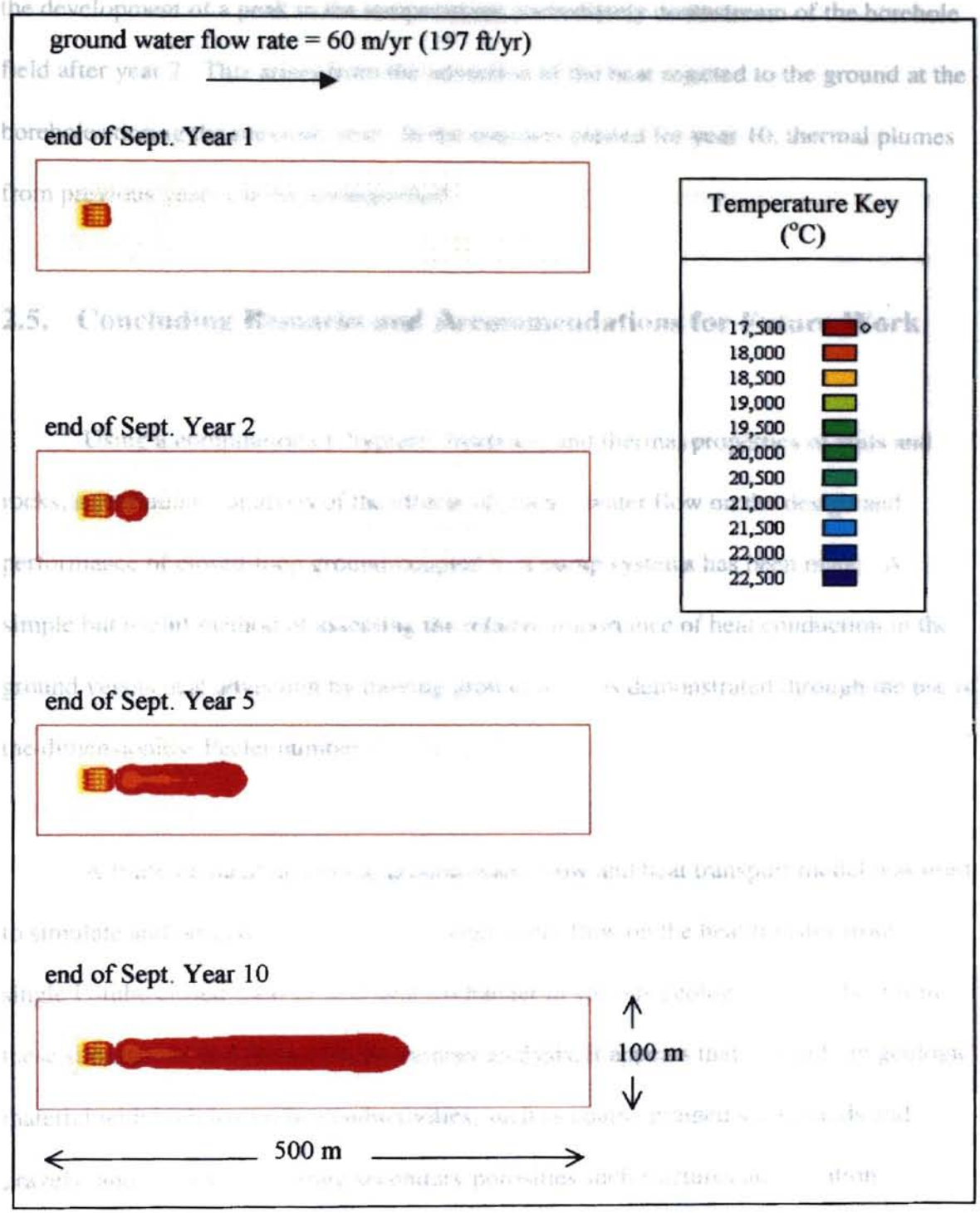

Figure 2-10. Temperature contours for Case 8 for the end of September of years 1, 2, 5, and 10.

A further feature that is shown in the predicted temperature field (Figure 2-10) is the development of a peak in the temperatures immediately downstream of the borehole field after year 2. This arises from the advection of the heat rejected to the ground at the boreholes during the previous year. In the contours plotted for year 10, thermal plumes from previous years can be distinguished.

2.5. Concluding Remarks and Recommendations for Future Work

Using a compilation of "typical" hydraulic and thermal properties of soils and rocks, a preliminary analysis of the effects of ground-water flow on the design and performance of closed-loop ground-coupled heat pump systems has been made. A simple but useful method of assessing the relative importance of heat conduction in the ground versus heat advection by moving ground water is demonstrated through the use of the dimensionless Peclet number.

A finite-element numerical ground-water flow and heat transport model was used to simulate and observe the effects of ground-water flow on the heat transfer from a single U-tube closed-loop ground heat exchanger in various geologic materials. From these simulations and from a Peclet number analysis, it appears that it is only in geologic material with high hydraulic conductivities, such as coarse-grained soils (sands and gravels) and in rocks exhibiting secondary porosities such fractures and solution channels, that ground-water flow could be expected to have a significant effect on closed-loop heat exchanger performance.

The effect of ground-water flow on in-situ thermal conductivity test results has been examined by numerically simulating test conditions around a single borehole under different flow conditions. These data were analyzed as if it came from real in-situ sources to arrive at effective thermal conductivity values. As expected, in all cases of ground-water flow, these values were artificially high. Results from one week test data have been shown to be no more reliable than data from 50-hour tests.

The finite-element numerical ground water flow and heat transport model was also used to simulate the 10-year performance of borehole fields designed from application of conventional design procedures using the derived thermal conductivity data. For coarse-grained sands, the presence of moderate ground-water flows had the effect of removing the year-by-year increase in ground temperature found in systems where there is no ground-water flow. The borehole fields designed using conventional methods and the derived effective thermal conductivities were generally over-designed. However, in some cases at very high ground-water flow rates, temperatures were found to rise above the design criteria.

From this preliminary assessment of the effects of ground-water flow, it appears difficult to adapt results from current design and in-situ measurement methods to fully account for ground-water flow conditions. Over the last decade, considerable progress has been made in developing both in-situ test methods and design procedures for borehole field design for situations where there is no ground-water flow. Research would

be required in a number of areas before the same progress could be made to deal with the situations of ground-water flow. These include:

- Identification of suitable numerical and/or analytical models that include ground-water flow and could be used to analyze in-situ test data.
- Experimental investigation of potential in-situ test data analysis methods at sites with significant ground-water flow.
- Identification of suitable design methods, or adaptations to existing methods, that could be used for closed-loop ground heat exchanger design.
- Development of design guidelines and software tools that could be used by practicing engineers for in-situ testing and system design tasks in situations of significant ground-water flow.

3. A Model for Simulating the Performance of a Shallow Pond as a Supplemental Heat Rejecter with Closed-Loop Ground-Source Heat Pump Systems

3.1. Introduction

Commercial buildings and institutions are generally cooling-dominated, and therefore reject more heat than they extract over the annual cycle. In order to adequately dissipate the imbalanced annual loads, the required ground-loop heat exchanger lengths are significantly greater than the required length if the annual loads were balanced. Consequently, under these circumstances, ground-source heat pump systems may be eliminated from consideration during the feasibility study phase of the HVAC design process because of excessive first cost.

To effectively balance the ground loads and reduce the necessary size of the ground loop heat exchanger, supplemental components can be integrated into the ground-loop heat exchanger design. GSHP systems that incorporate some type of supplemental heat rejecter are commonly referred to as hybrid GSHP systems. In some applications, the excess heat that would otherwise build up in the ground may be used for domestic hot water heaters, car washes, and pavement heating systems. In cases where the excess heat cannot be used beneficially, shallow ponds can provide a cost-effective means to balance the thermal loading to the ground and reduce heat exchanger length.

The objective of the work presented in this chapter has been to develop a design and simulation tool for modeling the performance of a shallow pond that can be usefully

and cost-effectively integrated into a ground-source heat pump system as a supplemental heat rejecter. The pond model has been developed in the TRNSYS modeling environment (SEL, 1997) and can be coupled to other GSHP system component models for short-time step (hourly or minutely) system analyses. The model has been validated by comparing simulation results to experimental data. As an example of the model's applicability, GSHP system simulation results are presented for a commercial building located in Tulsa, Oklahoma with a hypothetical closed-loop GSHP system with and without a shallow pond supplemental heat rejecter.

3.2. Heat Transfer In Ponds

3.2.1. General Overview

Pertinent concepts of heat transfer in ponds and lakes have been summarized by many sources. Dake and Harleman (1969) conducted studies of thermal stratification in lakes and addressed the overall thermal energy distribution in lakes. ASHRAE (1995), ASHRAE (1995b), and Kavanaugh and Rafferty (1997) describe heat transfer in lakes in relation to their use as heat sources and sinks.

Solar energy is identified as the main heating mechanism for ponds and lakes. The main cooling mechanism is evaporation. Thermal radiation can also account for a significant amount of cooling during night hours. Convective heating or cooling to the atmosphere is less significant. Natural convection of water due to buoyancy effects is the primary mechanism for heat transfer within a surface water body. Conduction heat

transfer to the ground is generally a relatively insignificant process, except in cases where the water surface is frozen.

Shallow ponds are generally thermally unstratified. Natural stratification of deeper ponds and lakes is due to buoyancy forces and to the fact that water is at its greatest density at 39.2°F (4°C). Therefore, over the annual cycle, water in deeper ponds will completely over-turn. Thermal stratification in ponds is also dictated by inflow and outflow rates or ground water seepage rates. If inflow and outflow rates are high enough, the pond will not stratify. Consequently, thermal stratification occurs only in ponds and lakes that are relatively deep, generally greater than 20 - 30 ft (6.1 - 9.1 m), with low inflow rates. The relevant heat transfer mechanisms occurring within shallow ponds are illustrated in Figure 3-1.

3.2.2. Existing Pond and Lake Models

Several mathematical and computer models have been developed for simulation of lakes used as heat sinks/sources and for solar ponds.

Raphael (1962) developed a numerical model for determining the temperature of surface water bodies as heat sinks for power plants. Thermal stratification of the water body was not considered. Input data to the model included weather data and inflow and outflow data for the water body. Raphael reported that the model successfully predicted the temperature changes in a river used as a heat sink for a power plant.

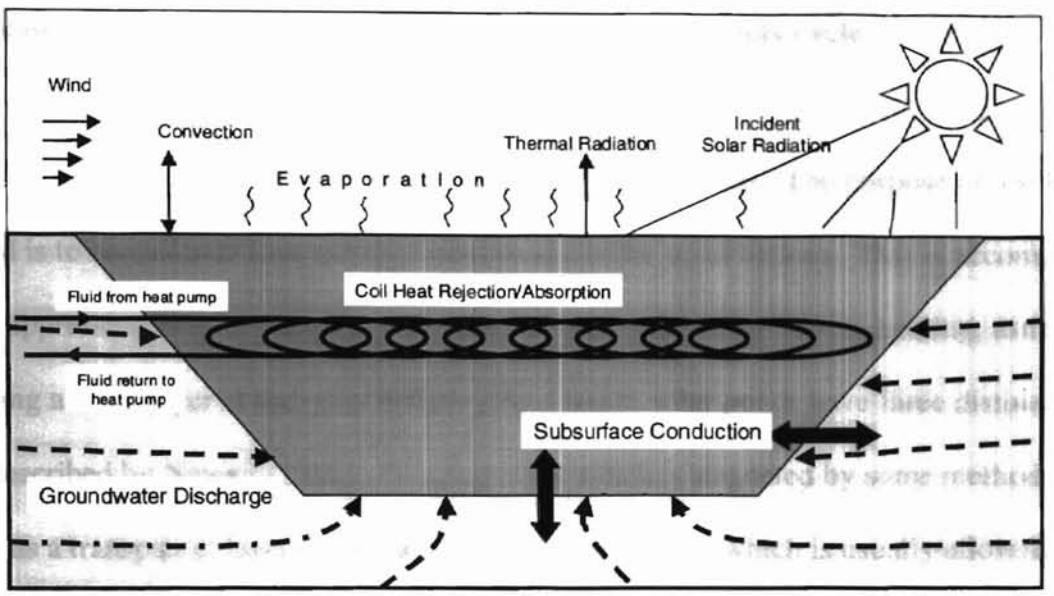

Figure 3-1. Heat transfer mechanisms in shallow ponds.

Jobson (1973) developed a mathematical model for water bodies used as heat sinks for power plants. Thermal stratification of the water body was not considered. The results of that work showed that the heat transfer at the water/air interface is highly dependent on the natural water temperature and the wind speed..

Cantrell and Wepfer (1984) developed a numerical model for evaluating the potential of shallow ponds for dissipating heat from buildings. The model takes weather data and building cooling load data as inputs and computes the steady-state pond temperature using an energy balance method. Thermal stratification of the pond was not considered. The model showed that a 3-acre (12,141 m^2), 10-feet (3.048 m) deep pond in

Cleveland, Ohio could reject 1000 tons (3516 kW) of thermal energy with a maximum increase in pond temperature of about 5°F (2.78°C) over a daily cycle.

Rubin et al. (1984) developed a model for solar ponds. The purpose of a solar pond is to concentrate heat energy from the sun at the pond bottom. This is accomplished by suppressing natural convection within the pond induced by bottom heating, usually by adding a brine layer at the pond bottom. As a result, solar ponds have three distinct zones as described by Newell (1984): (1) a top layer which is stagnated by some method and acts as a transparent layer of insulation, (2) a middle layer which is usually allowed to be mixed by natural convection, and (3) a lower layer where solar energy is collected. The model of Rubin et al. (1984) applied an implicit finite difference scheme to solve a one-dimensional heat balance equation on a solar pond. Large-scale convective currents in the pond were assumed to be negligible while small-scale convective currents were handled by allowing the coefficient of heat diffusion to vary through the pond depth. Solar radiation was modeled as an exponentially decaying function through the pond depth. The model successfully predicted seasonal variations in solar pond temperatures.

Srinivasan and Guha (1987) developed a model similar to the model of Rubin et al. (1984) for solar ponds. The Srinivasan and Guha (1987) model consisted of three coupled differential equations, each describing a thermal zone within the solar pond. Solar radiation in each zone is computed as a function of depth. The model also successfully predicted seasonal variations in solar pond temperatures with various heat extraction rates.

Pezent and Kavanaugh (1990) developed a model for lakes used as heat sources or sinks with water-source heat pumps. The model essentially combined the models of Srinivasan and Guha (1987) to handle stratified cases and of Raphael (1962) to handle unstratified cases. As such, thermal stratification of a lake could be handled in the summer months, when lakes are generally most stratified, and neglected in the winter months, when lakes are generally unstratified. The model is driven by monthly average bin weather data and handles both heat extraction and heat rejection. With no heat extraction or rejection, the model favorably predicted a lake temperature profile in Alabama. The temperatures within the upper zone of the lake (the epilimnion) and the lower zone of the lake (the hypolimnion) were predicted to within 4°F (2.22°C) and approximately 1°F (0.55°C), respectively. However, the model had some difficulty in matching the intermediate zone (the thermocline), perhaps due to the fact that this zone possesses moving boundaries (unlike the boundaries of a solar pond which are more distinct). As concluded by Pezent and Kavanaugh (1990), a numerical method is necessary to more accurately predict the thermocline profile.

The model presented in this paper is based on the assumption that thermal gradients in shallow ponds are negligible, especially during times of heat rejection. This model is developed in the TRNSYS modeling environment and can be coupled to other component models for larger system simulations. Further, this model allows the pond performance to be simulated on hourly or minutely time scales.

3.3. Experimental Methods

3.3.1. Pond Description and Data Collection

Pond construction and data collection for this study have been conducted by researchers affiliated with the Division of Engineering Technology at the Oklahoma State University.

Two ponds were constructed on a test site at the north end of the campus. The ponds are rectangular with a plan area of 40 ft (12.19 m) by 3 ft (0.91 m). Each pond was constructed with vertical sidewalls with one of the ponds being 2 feet (0.61 m) deep and the other being 3.5 ft (1.07 m) deep. The walls and the bottom of each pond were constructed of reinforced concrete, approximately 8 in. (20.3 cm) thick.

Heat was rejected to each pond by circulating heated water through a "slinky" heat exchanger (a pipe coiled in a circular fashion such that each loop overlaps the adjacent loop) installed in each pond. Each slinky pipe was made of high-density polyethylene plastic and is 500 feet (152.40 m) long with a nominal diameter of ¾ in. (0.019 m). The pipe was coiled such that the resulting slinky heat exchanger was 40 ft (12.19 m) long with a diameter of 3 ft (0.91 m) and a 10-in. (0.254 m) pitch (the separation distance between the apex of each successive loop). In the 2-ft (0.61-m) deep pond, the slinky heat exchanger was positioned horizontally within the pond at a depth of approximately 10 in. (0.254 m). In the 3.5-ft (1.07-m) deep pond, the slinky heat

exchanger was positioned vertically within the pond along the center-line of the long axis of the pond.

The temperature of the pond water was measured by thermistors positioned at four locations within the pond: (1) near the pond surface at the center of the slinky, (2) below the slinky at its center, (3) near the pond surface at the end opposite from the supply end, and (4) below the slinky at the end of the pond opposite from the supply end. Slinky supply and return water temperatures were measured by thermistors embedded in the slinky header. Each system also included a flow meter, a water heating element, and a watt transducer. All sensor information was recorded by the data acquisition system at time intervals of 6 minutes.

The tests were controlled to maintain a set supply water temperature by heating the supply water if the temperature fell below a set point. Two set point temperatures were used in this study: 90°F (32.2°C) in the summer season and 75°F (23.9°C) in the winter season.

3.3.2. Weather Instrumentation and Data Collection

Weather data for this study were obtained from the Oklahoma Mesonet (**meso**scale **net**work), which is a weather station network consisting of weather monitoring sites scattered throughout Oklahoma. Depending on the weather parameter, data are recorded at time intervals ranging from 3 seconds to 30 seconds and averaged over 5-minute observation intervals.

Weather data at 15-minute intervals for the Stillwater monitoring station were acquired for the time periods of interest for this study. The Stillwater station is located approximately 1 mile from the test pond site. Data for the following parameters were obtained: wind speed, wind direction, air temperature, relative humidity, and solar radiation. Further details of the weather station network may be found in Elliott et al. (1994).

3.4. Model Development

3.4.1. Governing Equations

The governing equation of the model is an overall energy balance on the pond using the lumped capacitance (or lumped parameter) approach:

$$q_{in} - q_{out} = V\rho c_p \frac{dT}{dt} \tag{3-1}$$

where q_{in} is the heat transfer to the pond, q_{out} is the heat transfer from the pond, V is the pond volume, ρ is the density of the pond water, c_p is the specific heat capacity of the pond water, and $\frac{dT}{dt}$ is the rate of change of temperature of the pond water. This approach assumes that temperature gradients within the water body are negligible. Considering the heat transfer mechanisms shown in Figure 3-1, Equation 3-1 can be expressed to describe the rate of change in average pond temperature as:

$$\frac{dT}{dt} = \frac{q_{solar} + q_{thermal} + q_{convection} + q_{ground} + q_{groundwater} + q_{evaporation} + q_{fluid}}{V\rho c_p} \quad (3\text{-}2)$$

where, q_{solar} is the solar radiation heat gain to the pond, $q_{thermal}$ is the thermal radiation heat transfer at the pond surface, $q_{convection}$ is the convection heat transfer at the pond surface, q_{ground} is the heat transfer to/from the ground in contact with the pond, $q_{groundwater}$ is the heat transfer due to groundwater inflow or outflow, $q_{evaporation}$ is the heat/mass transfer due to evaporation at the pond surface, and q_{fluid} is the total heat transfer to/from the heat exchange fluid flowing in all spools or coils in the pond. Each of the heat transfer terms used in the above equation is defined below.

3.4.1.1. Solar Radiation Heat Gain

Solar radiation heat gain (q_{solar}) is the net solar radiation absorbed by the pond. It is assumed that all solar radiation incident on the pond surface becomes heat gain except for the portion reflected at the surface.

To determine the reflected component of solar radiation, the angle of incidence (θ) of the sun's rays is first computed at each time step from correlations given by Spencer (1971), Duffie and Beckman (1991), and ASHRAE (1997). The angle of refraction (θ_r) of the sun's rays at the pond surface is given by Snell's Law. The reflectance (ρ') is computed from:

$$\rho' = \tau_a - \tau \quad (3\text{-}3)$$

where $\tau$is the transmittance of solar radiation by the pond surface and the subscript 'a' refers to the absorbed component. These are computed after Duffie and Beckman (1991) as:

$$\tau_a = e^{\frac{-\mu' d}{\cos\theta_r}} \tag{3-4}$$

and

$$\tau = \frac{1}{2}\left(\frac{1-r_{\parallel}}{1+r_{\parallel}} + \frac{1-r_{\perp}}{1+r_{\perp}}\right) e^{\frac{-\mu' d}{\cos\theta_r}} \tag{3-5}$$

where μ' is the extinction coefficient for water, d is the pond depth, $r_{\parallel}$ represents the parallel component of unpolarized radiation, and $r_{\perp}$ represents the perpendicular component of unpolarized radiation which are computed after Duffie and Beckman (1991) as:

$$r_{\parallel} = \frac{\tan^2(\theta_r - \theta)}{\tan^2(\theta_r + \theta)} \tag{3-6}$$

$$r_{\perp} = \frac{\sin^2(\theta_r - \theta)}{\sin^2(\theta_r + \theta)} \tag{3-7}$$

Finally, the amount of solar radiation absorbed by the pond (q_{solar}) is expressed as:

$$q_{solar} = I(1-\rho')A_{pond} \tag{3-8}$$

where I is the solar radiation flux incident on the pond surface (here, the total reflectance is approximated by the beam reflectance) and A_{pond} is the area of the pond surface. The

model also accepts solar radiation in the form of beam (I_b) and diffuse (I_d) components, in which case I is computed from:

$$I = I_b \cos\theta + I_d \tag{3-9}$$

3.4.1.2. Thermal Radiation Heat Transfer

This heat transfer mechanism accounts for heat transfer at the pond surface due to thermal or long-wave radiation. This model uses a linearized radiation coefficient (h_r) defined as:

$$h_r = 4\varepsilon\sigma\left(\frac{T_{pond} + T_{sky}}{2}\right)^3 \tag{3-10}$$

where ε is the emissivity coefficient of the pond water, σ is the Stefan-Boltzmann constant, T_{pond} is the pond temperature in absolute units, and T_{sky} is the sky temperature in absolute units. T_{sky} is computed from relationship given by Bliss (1961) which relates sky temperature to the dew point temperature (T_{dp}) and the dry bulb temperature (T_{db}):

$$T_{sky} = T_{db}\left(0.8 + \frac{T_{dp}}{250}\right)^{\frac{1}{4}} \tag{3-11}$$

where all temperatures are in absolute units. The model uses the TRNSYS psychrometric subroutine to compute T_{dp} if it is unknown. T_{dp} is computed from either of the following pairs of state properties: (1) dry bulb temperature (T_{db}) and wet bulb temperature (T_{wb}) or (2) T_{db} and relative humidity. The thermal radiation heat transfer ($q_{thermal}$) is then computed by:

$$q_{thermal} = h_r A_{pond} (T_{sky} - T_{pond}) \tag{3-12}$$

3.4.1.3. Convection Heat Transfer at the Pond Surface

This mechanism accounts for heat transfer at the pond surface due to free and forced convection. Several empirical formulations exist for determining the convection coefficient for different geometries. For a pond surface, correlations for a horizontal flat plate are the most applicable.

In free convection heat transfer, the Nusselt Number (Nu) is often correlated to the Rayleigh Number (Ra), which describes the relative magnitude of the buoyancy and viscous forces in the fluid:

$$\mathrm{Ra} = \frac{g\beta(\Delta T)L^3}{\nu\alpha} \tag{3-13}$$

where g is the acceleration due to gravity, α is the thermal diffusivity of air, β is the volumetric thermal expansion coefficient of air, ν is the kinematic viscosity of air, ΔT refers to the temperature difference between the pond and the air, and L is the characteristic length. The thermal properties α, β, and ν are all evaluated at the film temperature which can be approximated as the average of the air and pond temperatures. In the model, the thermal properties of air are computed at each time step using correlations given by Irvine and Liley (1984). For horizontal flat plates, the characteristic length (L) can be defined as the ratio of the area (A) to the perimeter (P) (Incropera and DeWitt, 1996):

$$L = \frac{A}{P} \tag{3-14}$$

In external free convection flows over a horizontal flat plate, the critical Rayleigh Number is about 10^7. Therefore, two empirical relations for the Nusselt number are used in the model as described by Incropera and DeWitt (1996) for free convection from the upper surface of a heated plate or the lower surface of a cooled plate:

$$\mathrm{Nu} = 0.54\mathrm{Ra}^{\frac{1}{4}} \qquad (10^4 < \mathrm{Ra} < 10^7 - \text{laminar flow}) \tag{3-15a}$$

and

$$\mathrm{Nu} = 0.15\mathrm{Ra}^{\frac{1}{3}} \qquad (10^7 > \mathrm{Ra} > 10^{11} - \text{turbulent flow}) \tag{3-15b}$$

The convection coefficient (h_c) for free convection can then be determined from:

$$h_c = \frac{\mathrm{Nu}\ k}{L} \tag{3-16}$$

where k is the thermal conductivity of air evaluated at the film temperature as with the other thermal properties described above and L is the characteristic length described by Equation 3-14.

In forced convection heat transfer, Nu is a function of the Reynolds (Re) and Prandtl (Pr) Numbers. The Reynolds number is described as:

$$\mathrm{Re} = \frac{vL}{\nu} \tag{3-17}$$

where v is the wind speed, ν is the kinematic viscosity of air, and the characteristic length (L) is now defined by the length dimension over which the wind blows and is determined from the pond orientation (degrees from north) and wind direction. The Prandtl Number is defined as:

$$\mathrm{Pr} = \frac{c_p \mu}{k} \tag{3-18}$$

where c_p is the specific heat capacity of air, μ is the dynamic viscosity of air, and k is the thermal conductivity of air, all evaluated at the air film temperature.

For external forced convection over a flat plate (i.e. the pond surface), the critical Reynolds Number is approximately 10^5 (Incropera and DeWitt, 1996). Therefore, two empirical relations for the Nusselt number are used in the model as described by Incropera and DeWitt (1996) for forced convection over a flat plate:

$$\mathrm{Nu} = 0.664\,\mathrm{Re}^{\frac{1}{2}}\,\mathrm{Pr}^{\frac{1}{3}} \quad \text{(laminar flow regime)} \tag{3-19a}$$

and

$$\mathrm{Nu} = 0.037\,\mathrm{Re}^{\frac{4}{5}}\,\mathrm{Pr}^{\frac{1}{3}} \quad \text{(mixed and turbulent flow)} \tag{3-19b}$$

The convection coefficient (h_c) for forced convection can then be determined by Equation 3-16 with the characteristic length value described by Equation 3-14 for a horizontal flat plate.

Finally, the convection heat transfer at the pond surface ($q_{convection}$) is computed by:

$$q_{convection} = h_c A_{pond} (T_{air} - T_{pond}) \tag{3-20}$$

where T_{air} is the ambient air temperature and h_c is taken as the maximum of the free convection coefficient and the forced convection coefficient. This practice of choosing the larger of the free and forced convection coefficients is recommended by Duffie and Beckman (1991) and McAdams (1954) and is used in the absence of additional experimental evidence regarding combined free and forced convection.

3.4.1.4. Heat Transfer to the Ground

This heat transfer mechanism accounts for heat conduction to/from the soil or rock in contact with the sides and the bottom of the pond. This mechanism of heat transfer is highly site-specific and complex and depends on many factors such as soil/rock thermal properties, climatic factors, pond geometry, and thermal loading history. In this model, a semi-empirical approach developed by Hull et al. (1984) was chosen to determine heat losses/gains from the bottom and sides of the pond. Hull et al. (1984) used a three-dimensional numerical code to compute steady-state ground heat losses from solar ponds of varying sizes, geometries, and sidewall insulation types.

Hull et al. (1984) expresses ground heat losses from any pond as a function of the pond area, pond perimeter, the ground thermal conductivity (k_{ground}), and the distance

from the pond bottom to a constant temperature sink. For practical purposes, the constant temperature sink can be taken as the groundwater table (Kishore and Joshi, 1984). For a rectangular pond with vertical side walls, a heat transfer coefficient for ground heat transfer (U_{ground}) can be computed from:

$$U_{ground} = 0.999\left(\frac{k_{ground}}{d_{groundwater} - d_{pond}}\right) + 1.37\left(\frac{k_{ground} P_{pond}}{A_{pond}}\right) \tag{3-21}$$

where k_{ground} is the thermal conductivity of the ground, $d_{groundwater}$ is the depth to the water table or the constant source/sink from the ground surface, d_{pond} is the pond depth, and P_{pond} is the pond perimeter. The conduction heat transfer between the ground and the pond is then given by:

$$q_{ground} = U_{ground} A_{pond} (T_{groundwater} - T_{pond}) \tag{3-22}$$

It is recognized that the above conduction heat transfer model is a relatively simple representation of the true transient behavior of heat transfer in the ground. However, ground heat conduction is a relatively minor process affecting the overall heat transfer within the pond as compared to other processes.

3.4.1.5. Heat Transfer Due to Ground Water Seepage

This heat transfer mechanism accounts for inflows and outflows of ground water to the pond. Although ground water contributions may not be expected in shallow heat rejecter ponds, this heat transfer mechanism can be used to account for other inflows and outflows, such as make-up water or rain water.

The volumetric groundwater flow rate (Q) is computed by Darcy's Law:

$$Q = Ki(P_{pond}(d_{pond} - d_{groundwater}) + A_{pond}) \tag{3-23}$$

where K is the hydraulic conductivity of the soil/rock surrounding the pond and i is the hydraulic gradient. The heat transfer contribution from ground water ($q_{groundwater}$) is then given by:

$$q_{groundwater} = Q\rho c_p (T_{groundwater} - T_{pond}) \tag{3-24}$$

where ρ and c_p represent the density and specific heat capacity of ground water. These properties of ground water are computed from relationships given in the Handbook of Chemistry and Physics (CRC, 1980).

3.1.4.6. Heat Transfer Due to Evaporation

This heat transfer mechanism is the most important one contributing to pond cooling. This model uses the j-factor analogy to compute the mass transfer of evaporating water ($\dot{m}''_w$) at the pond surface:

$$\dot{m}''_w = h_d (w_{air} - w_{surf}) \tag{3-25}$$

where h_d is the mass transfer coefficient, w_{air} is the humidity ratio of the ambient air, and w_{surf} represents the humidity ratio of saturated air at the pond surface. The w_{surf} term is

computed using the TRNSYS psychrometric subroutine by setting T_{db} and T_{wb} equal to the pond temperature. The w_{air} term may also be computed using the TRNSYS psychrometric subroutine depending on what two state properties of the air are known. The model accepts the following pairs of state properties for the calculation of w_{air} if it is unknown: (1) T_{db} and T_{wb}, (2) T_{db} and relative humidity or (3) T_{db} and T_{dp}. The mass transfer coefficient (h_d) is defined using the Chilton-Colburn analogy as:

$$h_d = \frac{h_c}{c_p \mathrm{Le}^{\frac{2}{3}}} \tag{3-26}$$

where h_c is the convection coefficient defined previously, c_p is the specific heat capacity of the air evaluated at the pond-air film temperature, and Le is the Lewis number. Le is computed as:

$$\mathrm{Le} = \frac{\alpha}{D_{AB}} \tag{3-27}$$

where α is the thermal diffusivity of the air evaluated at the pond-air film temperature and D_{AB} represents the binary diffusion coefficient. The thermal properties (α and c_p) of air are computed at each time step using correlations given by Irvine and Liley (1984). D_{AB} is computed after Mills (1995) who references Marrero and Mason (1972):

$$D_{AB} = \frac{1.87x10^{-10}T^{2.072}}{P_{air}} \qquad (280\mathrm{K} < \mathrm{T} < 450\mathrm{K}) \tag{3-28}$$

where T refers to the pond-air film temperature in absolute units and P_{air} is the atmospheric pressure in atmospheres.

The heat transfer due to evaporation ($q_{evaporation}$) is then computed by:

$$q_{evaporation} = h_{fg} A_{pond} \dot{m}''_{w} \tag{3-29}$$

where h_{fg} is the latent heat of vaporization and is computed at each time step from the relationship given by Irvine and Liley (1984).

3.4.1.7. Heat Transfer Due to the Heat Exchange Fluid

Heat transfer due to the heat exchange fluid represents the pond thermal load. This model has been developed to account for water or antifreeze as the heat exchange fluid. The thermal properties of the fluid are computed at each time step from correlations given in the Handbook of Chemistry and Physics (CRC, 1980) for water and from correlations given by Wadivkar (1997) for an antifreeze solution. The thermal properties are computed at the average fluid temperature (T_{fluid}). This temperature is computed as the average of the inlet and outlet temperatures at the given time step. Since the outlet temperature at any current time step is not known, the previous converged value is used as an initial guess and calculation of T_{fluid} is iterative. Solution of the pond temperature is also an iterative procedure as discussed below.

The heat transfer due to the heat exchange fluid (q_{fluid}) is computed by:

$$q_{fluid} = UA_{pipe}(T_{fluid} - T_{pond})(N_{circuit}) \tag{3-30}$$

where UA_{pipe} is the overall heat transfer coefficient for the pipe expressed in terms of inside pipe area and $N_{circuit}$ refers to the number of flow circuits (i.e. the number of spools) installed in the pond. Thus, Equation 3-30 is based on the assumption that one spool is one flow circuit and that the flow rate is divided evenly between the circuits in a parallel arrangement. The term UA_{pipe} is expressed in terms of the inside pipe area as:

$$UA_{pipe} = \frac{2\pi r_i L_{spool}}{\Sigma R_t} \tag{3-31}$$

where r_i is the inner pipe radius, L_{spool} is the length of one spool or circuit, and ΣR_t represents the composite thermal resistance which is defined by the following resistance network:

$$\Sigma R_t = R_i + R_{pipe} + R_o + ff \tag{3-32}$$

where R_i is the thermal resistance due to fluid flow through the pipe, R_{pipe} is the pipe thermal resistance, R_o is the thermal resistance at external pipe surface, and ff represents a fouling factor at both the inner and outer pipe walls. The resistance terms are defined as follows (in terms of inner pipe radius):

$$R_i = \frac{1}{h_i}, \tag{3-33}$$

$$R_{pipe} = \frac{r_i}{k_{pipe}} \ln\left(\frac{r_o}{r_i}\right) \tag{3-34}$$

and

$$R_o = \frac{r_i}{r_o}\left(\frac{1}{h_o}\right) \tag{3-35}$$

where h_i is the convection coefficient due to fluid flow through the pipe, k_{pipe} is the thermal conductivity of the pipe material, h_o is the convection coefficient at the outer surface of the pipe, and r_i and r_o are the inner and outer radii of the pipe, respectively.

The above convection coefficients are determined using correlations for the Nusselt number in flow through a horizontal cylinder, since no specific correlations exist for a slinky coil. A constant heat flux at the pipe surface is assumed.

In convection heat transfer due to internal flow, Nu is a function of the Reynolds and Prandtl numbers. Determination of Re is described in Equation 3-17. For this case, v represents the mass flow rate of the heat exchange fluid, ν represents the kinematic viscosity of the heat exchange fluid, and the characteristic length (L) is the inner pipe diameter. A Reynolds number of 2000 is assumed to be critical. For laminar, fully-developed flow in the pipe (Re<2000), the Nusselt Number is a constant equal to 4.36 (Incropera and DeWitt, 1996, Equation 8-53). For turbulent flow, the Dittus-Boelter relation is used to compute the Nusselt Number:

$$\mathrm{Nu}_i = 0.023\,\mathrm{Re}^{\frac{4}{5}}\,\mathrm{Pr}^{x} \tag{3-36}$$

where Pr is defined by Equation 3-18 for μ, c_p, and k representing the thermal properties of the heat exchange fluid evaluated at its average temperature. The value of the exponent x in Equation 3-36 is dependent upon whether the entering fluid is being heated or cooled; x is equal to 0.3 if the entering fluid is greater than the pond temperature and x is equal to 0.4 if the entering fluid is less than the pond temperature. The inside pipe convection coefficient can then be determined by using Equation 3-16 where Nu is Nu_i, k is the thermal conductivity of the heat transfer fluid, and L is the characteristic length which is defined in this case as the inner diameter of the pipe (Incropera and DeWitt, 1996).

In free convection at the external pipe surface, the Nusselt Number is a function of the Rayleigh Number. Ra is computed using Equation 3-13 where α, β, and ν represent the thermal diffusivity of water, the volumetric thermal expansion coefficient of water, and the kinematic viscosity of water, respectively, all evaluated at the pipe film temperature, which is approximated as the average of the pipe surface and pond temperatures at the given time step. The term ΔT refers to the temperature difference between the pipe surface and the pond temperatures. Nu for free convection from a horizontal cylinder is defined as (Churchill and Chu (1975)):

$$\mathrm{Nu}_o = \left(0.60 + \frac{0.387\mathrm{Ra}^{\frac{1}{6}}}{\left(1 + (0.559/\mathrm{Pr})^{\frac{9}{16}}\right)^{\frac{8}{27}}} \right)^2 \qquad (3\text{-}37)$$

where Pr is defined by Equation 3-18 for μ, c_p, and k representing the thermal properties of the pond water evaluated at the pipe film temperature. Now the external pipe convection coefficient can be determined by using Equation 3-16 where Nu is Nu_o, k is the thermal conductivity of the pond water evaluated at the pipe film temperature, and L is the characteristic length which is defined now as the outer pipe diameter.

The outlet fluid temperature (T_{out}) is computed from an overall energy balance on the pipe:

$$T_{out} = T_{fluid} - \frac{q_{circuit}}{2\dot{m}c_p} \tag{3-38}$$

where $\dot{m}$ is the mass flow rate of the heat exchange fluid per flow circuit, c_p is the specific heat capacity of the heat exchange fluid, and $q_{circuit}$ is the heat rejected/extracted by one flow circuit. This outlet temperature is used to compute the average fluid temperature at the next iteration as described above.

3.4.1.8. Solving the Overall Energy Balance Equation

The differential equation describing the overall energy balance on the pond (Equation 3-2) is rearranged in the form:

$$\frac{dT}{dt} = x_1 T + x_2 \tag{3-39}$$

where T represents the pond temperature, x_1 contains all terms of Equation 3-2 that multiply T, and x_2 contains all terms of Equation 3-2 that are independent of T.

Equation 3-39 is a linear first-order ordinary differential equation which is solved at each time step using the exponential function as an integrating factor. The solution is given by the TRNSYS differential equation solver subroutine as:

$$T_t = \left(T_{t-\Delta t} + \frac{x_1}{x_2} \right) e^{x_1 \Delta t} - \frac{x_1}{x_2} \tag{3-40}$$

where T_t is the average pond temperature at the new time step and $T_{t-\Delta t}$ is the average pond temperature at the previous time step.

Many of the quantities in the heat transfer equations described above require that the average pond temperature at the current time step be known. Thus, the actual pond temperature is arrived at iteratively. A convergence criterion for the pond temperature of 1.8×10^{-5}°F (1×10^{-5}°C) is used.

3.4.2. Computer Implementation

Thc component configuration for the pond model is shown in Figure 3-2. A companion model was also developed which manipulates any weather data needed for the pond model. The weather component model makes use of the TRNSYS psychrometric subroutine to compute moist air properties given two known state properties. The two

state properties are dry bulb temperature and one of wet bulb temperature, relative humidity, or dew point temperature. The weather component model also computes the sky temperature, the solar radiation on a horizontal surface, and the solar incidence angle. A computer algorithm is shown in Figure 3-3 in the form of a flow chart.

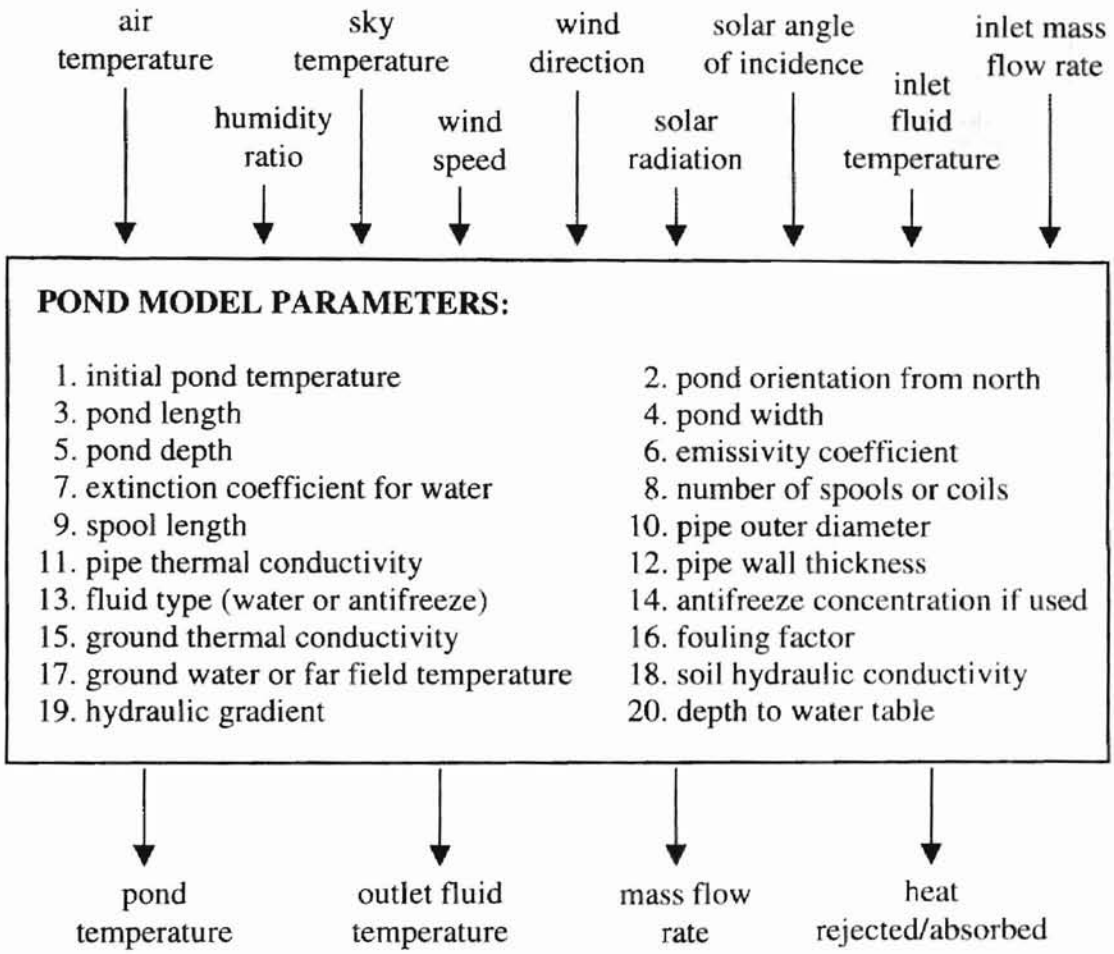

Figure 3-2. Pond model component configuration.

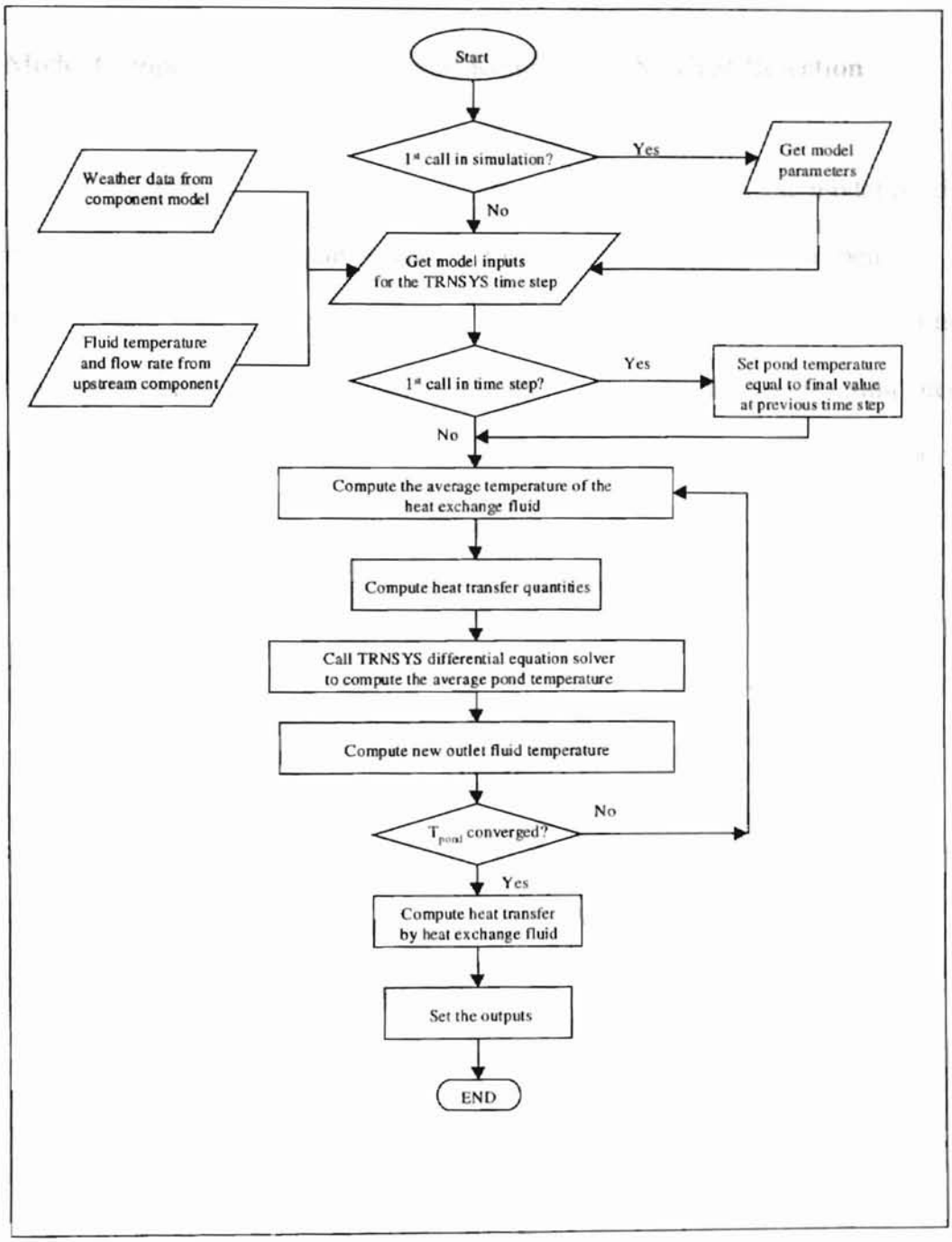

Figure 3-3. Pond model computer algorithm.

3.5. Results and Discussion

3.5.1. Model Comparison to Experimental Results with No Heat Rejection

The first step in the model verification process was to compare the model pond temperatures to measured pond temperatures during times when no heat was being rejected to the ponds. This comparison allowed a validity check of the simulation of the several environmental heat transfer mechanisms occurring within the ponds. Simulated and actual pond average hourly temperatures are shown in Figure 3-4 for an 8-day period in July 1998 when no heat was rejected to the ponds. Therefore, in these cases, the model is driven by weather data input only.

A review of the plots in Figure 3-4 shows that the model temperatures compare favorably to the measured pond temperatures. The simulated temperatures are within 3°F (1.67 °C) of the observed temperatures throughout the test period. The difference between the average simulated pond temperature and the average observed pond temperature for the entire test period is 1.93°F (1.07°C) for the 2-feet deep pond and 1.55°F (0.86°C) for the 3.5-feet deep pond. Shallow ground water was not encountered at the site and therefore ground water contributions were not considered. Fouling of the heat exchanger pipe was also not considered.

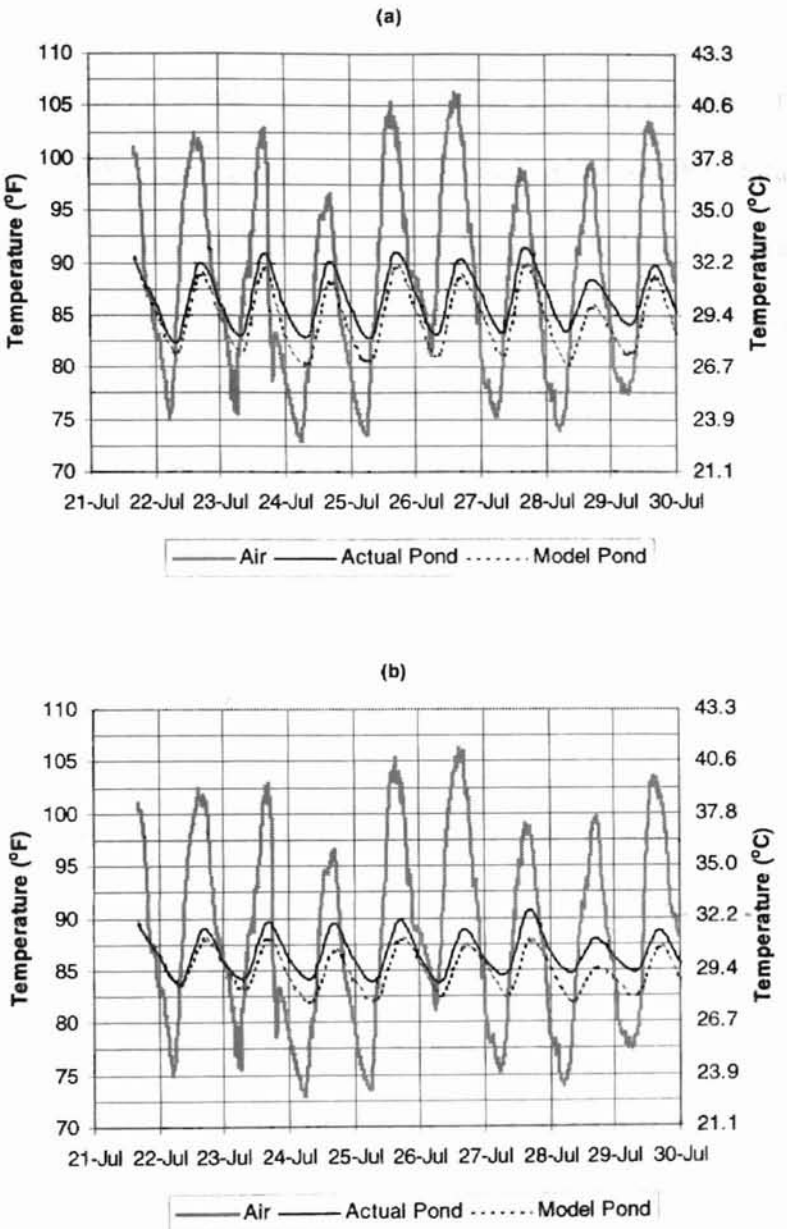

Figure 3-4. Comparison of observed and simulated average pond temperatures with no heat rejection in the (**a**) 2-feet (0.61 m) deep pond and (**b**) 3.5-feet (1.07 m) deep pond.

3.5.2. Model Comparison to Experimental Results with Heat Rejection

Heat rejection to the ponds was simulated over a 25-day period from November 12 to December 7, 1998. Input data to the model consisted of weather data as described previously in addition to measured slinky heat exchanger supply water temperatures and flow rates on 6-minutely time intervals. The model performance was evaluated by comparing (1) the simulated to the observed return temperature of the heat exchange fluid and (2) the simulated cumulative heat rejected to the ponds to the measured water heating element and pump power input. These comparisons are shown in Figures 3-5 and 3-6 respectively. As with the previous comparisons, ground water contributions and fouling of the heat exchanger pipe were not considered.

A review of the temperature plots in Figure 3-5 shows that model fluid return temperatures compare favorably to the observed fluid return temperatures. The average observed and modeled fluid return temperatures over the test period in the 2-feet (0.61-meter) deep pond were 70.5°F (21.4°C) and 70.2°F (21.2°C), respectively, and in the 3.5-feet (1.07-meter) deep pond were 69.2°F (20.7°C) and 70.4°F (21.3°C), respectively. The deeper pond has slightly larger differences between modeled and observed fluid return temperatures. The error is small, however, and is probably acceptable for purposes of simulating hybrid GSHP systems; even a 2°F (1.11°C) error in return fluid temperature from the pond will cause only a slight difference in modeled heat pump performance.

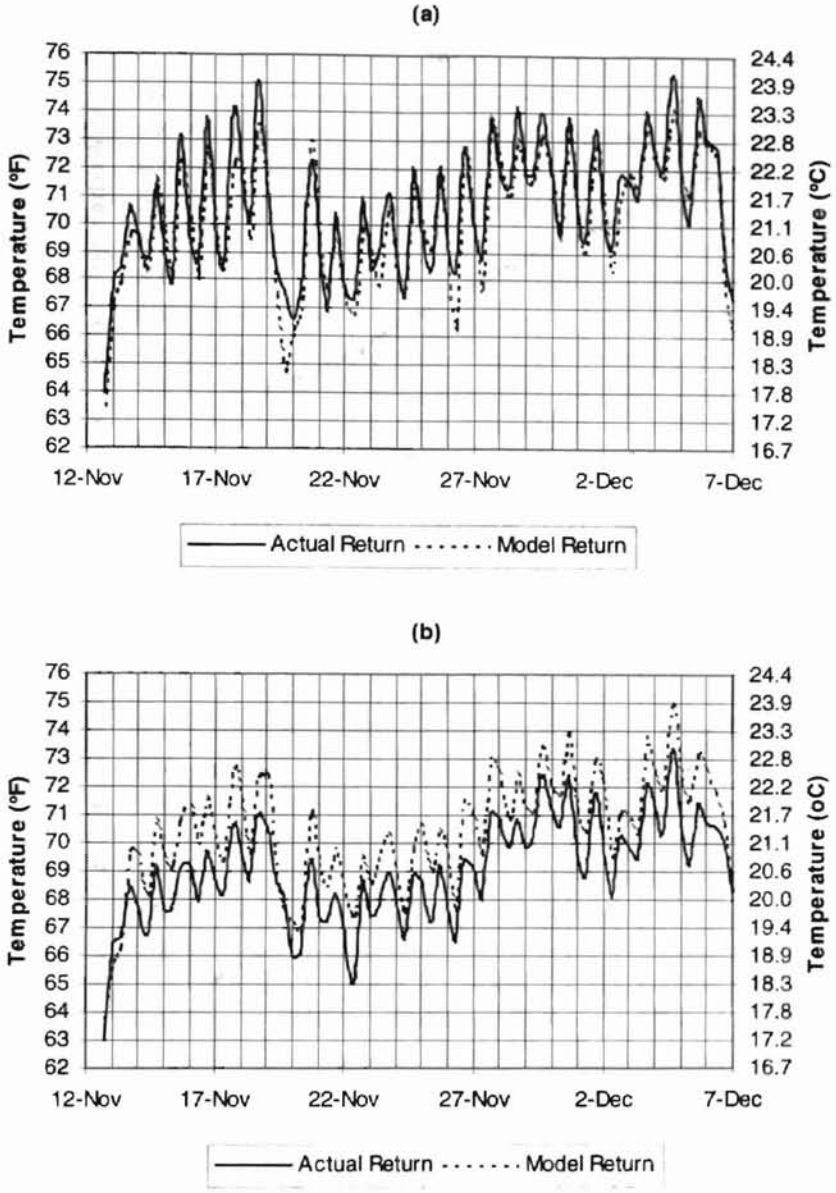

Figure 3-5. Comparison of observed and simulated heat exchange fluid return temperatures for the (**a**) 2-feet (0.61-m) deep pond and (**b**) 3.5-feet (1.07-m) deep pond.

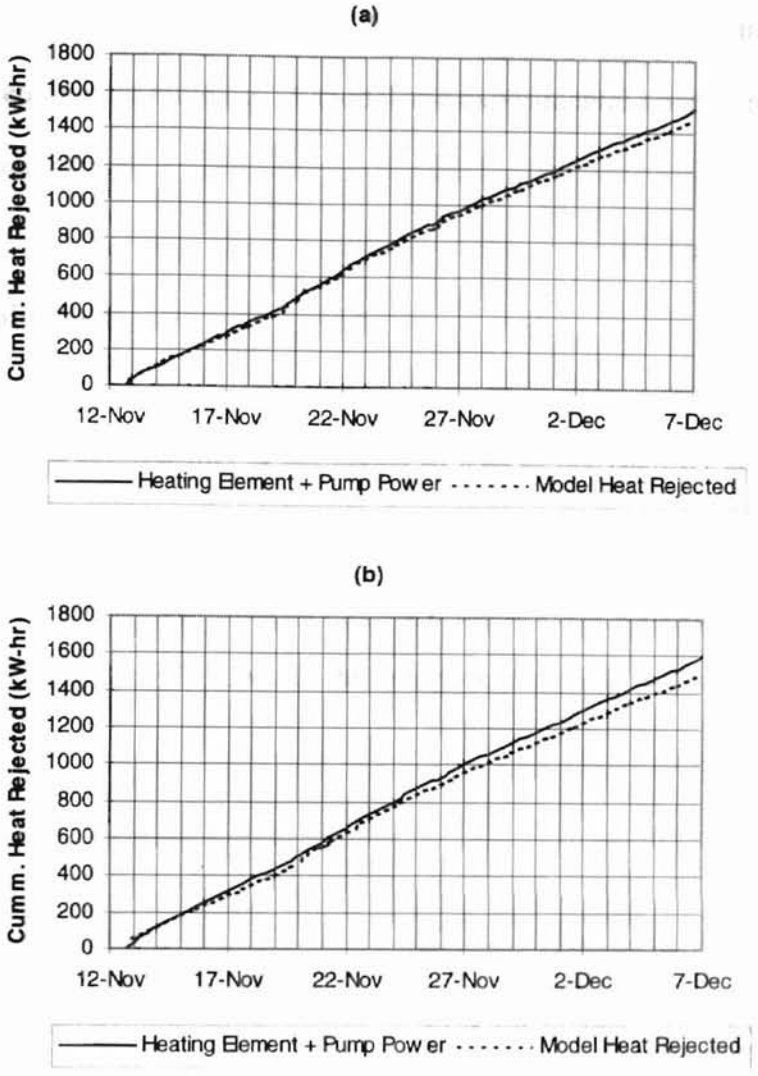

Figure 3-6. Comparison of observed and simulated heat rejected to the (**a**) 2-feet (0.61-m) deep pond and (**b**) 3.5-feet (1.07-m) deep pond.

A review of the plots in Figure 3-6 shows that the model cumulative heat rejected compares well to the measured heating element and pump power input. At the end of the 25-day test period, the percent difference between the cumulative simulated heat rejected and the cumulative measured heat rejected is –2.95 % for the 2-feet deep (0.61-meter)

pond and -5.20 % for the 3.5-feet (1.07-meter) deep pond. These discrepancies may be due partly to heat losses from the pond supply/return pipes to the ground and to the atmosphere in the equipment building. A model and experimental uncertainty analysis is presented in Appendix A.

3.5.3. Model Application

To illustrate the applicability of the model as well as the viability of using shallow ponds as supplemental heat rejecters in GSHP systems, a model of a hypothetical GSHP system was constructed in the TRNSYS modeling environment. A simplified system schematic is shown in Figure 3-7. Each of the component models is described briefly below.

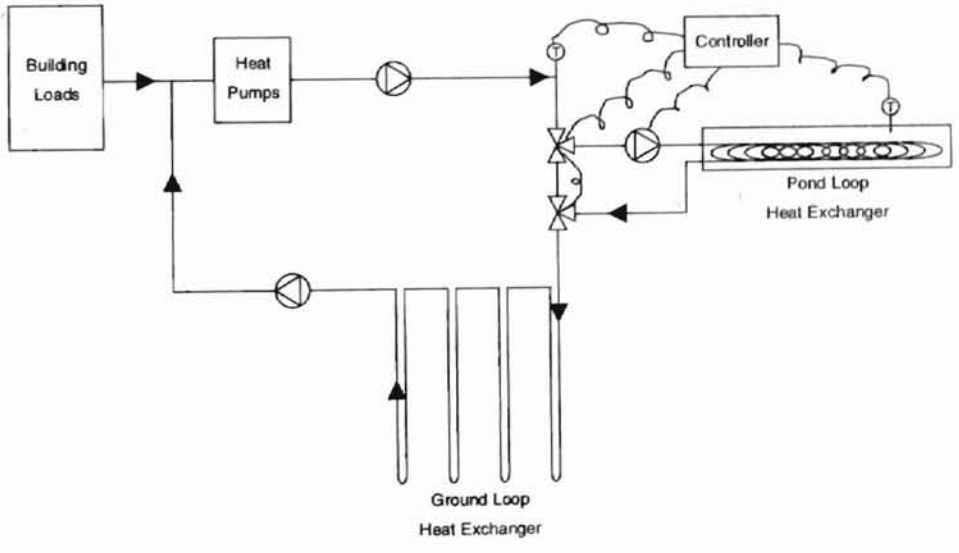

Figure 3-7. System schematic for the example model of a GSHP system with a shallow pond supplemental heat rejecter.

The building is not modeled explicitly in this application. The hourly building thermal loads are pre-computed using a proprietary building energy analysis program and are read from a file and passed to the heat pump subroutines. The building is an actual four-story, 45,000-ft^2 (4181-m^2) office building located in Tulsa, Oklahoma and is highly cooling dominated. The building thermal loads are shown in Figure 3-8.

A simple water-to-air heat pump model was developed for this and other GSHP system simulations. Inputs to the model include sensible and latent building loads, entering fluid temperature, and fluid mass flow rate. The model uses quadratic curve-fit equations to manufacturer's catalog data to compute the heat of rejection in cooling mode, heat of absorption in heating mode, and the heat pump power consumption. Outputs provided by the model include exiting fluid temperature, power consumption, and fluid mass flow rate. In this application, one heat pump component model handles the heating load and a second heat pump component model handles the cooling load.

The ground-loop heat exchanger model used in this application is that described by Yavuzturk and Spitler (1999) which is based partly on the work of Eskilson (1987) who developed "long time-step" (monthly) response factors for vertical ground-coupled U-tube heat exchangers. The model of Yavuzturk and Spitler (1999) extends the work of Eskilson (1987) to hourly or less ("short-time step") time intervals. The development of the short time-step response factors are based on an analytically validated, transient two-dimensional implicit finite volume model (Yavuzturk et al., 1999) that simulates the heat transfer over a vertical U-tube ground heat exchanger. In this application, the modeled borehole field consisted of one hundred 250-feet (76.2-m) deep boreholes arranged in a

10 by 10 square pattern. The total system flow was rate 270 gpm (61.36 m^3/hr). Representative thermal properties of sedimentary rock were chosen.

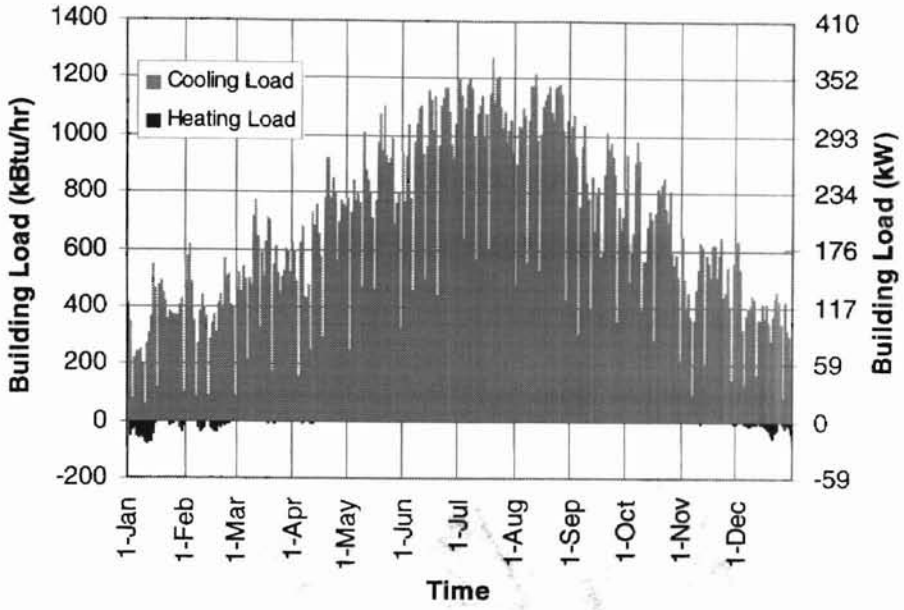

Figure 3-8. Building thermal loads for the example building in Tulsa, OK. Cooling loads are shown as positive values, indicating heat to be rejected to the GSHP system; heating loads are shown as negative values, indicating heat to be extracted from the GSHP system.

Models for ancillary components such as pumps, t-pieces, flow diverters, and the differential controller are described by SEL (1997). The control strategy used to activate the circulating pump to the pond was chosen somewhat arbitrarily by using the temperature difference between the pond and the exiting fluid temperature from the heat pumps. When this temperature difference exceeds 9°F (5°C), the circulating pump to the pond is energized and heat will be rejected to the pond. During these times of heat rejection to the pond, flow is diverted to the pond such that each heat exchanger coil in the pond receives 4 gpm (0.909 m^3/hr) of water. The properties of each heat exchanger

coil in the example model are the same as those described in the experimental procedure. Hourly input weather data for the pond model were taken from a typical meteorological year (TMY) record for Tulsa, Oklahoma.

The model was run for two cases for a duration of 3 years with a time step of one hour. The first case was the GSHP system with no pond and the second case was the GSHP system with the pond. Hourly heat pump entering water temperatures are shown in Figure 3-9 for both cases.

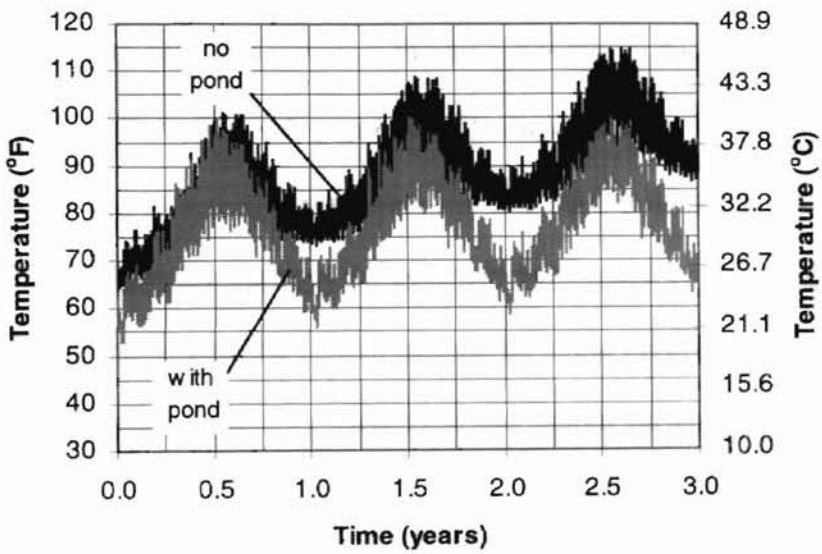

Figure 3-9. Entering heat pump water temperatures for the example GSHP system simulation with no pond and with a 2-feet (0.6096-m) deep, 6000-ft^2 (557.4 m^2) pond.

A review of the data presented in Figure 3-9 shows the advantages of using a pond supplemental heat rejecter. Assuming that a maximum heat pump entering water temperature of 100°F (37.78°C) is desirable, the system without the pond would fail during the second year of operation. In fact, based on the results of a ground-loop heat

exchanger sizing program (Spitler et al., 1996), the boreholes of a 10 by 10 square pattern would need to be approximately 400 feet (121.9 m) deep to accommodate the cooling-dominated loads of this building for 20 years of operation. Such a system would likely be eliminated from consideration early on in the design phase because of excessive first cost.

Using the TRNSYS model as a design tool, the size of the pond supplemental heat rejecter was determined under the assumption that the 10 by 10 borehole field could not be feasibly deeper than 250 feet (76.2 m). The heat pump entering water temperatures for the GSHP system with the pond shown in Figure 3-9 were produced by simulating a 2-feet (0.61-m) deep, 6000 ft^2 557 (m^2) pond with 50 slinky heat exchanger coils. A summary of pond performance is given in Table 3-1. By adding the pond supplemental heat rejecter in this example, the depth of the borehole field could be decreased by approximately 35%. A more detailed system simulation could involve system life-cycle operating cost analyses, control strategy variations, and design variable optimization.

Table 3-1. Summary of Pond Performance for Example GSHP System Simulation

Year	Hours ON	Average Pond Temperature		Heat Pump Maximum Entering Fluid Temperature		Heat Rejected	
		(°F)	(°C)	(°F)	(°C)	(kBtu)	(MJ)
1	3937	74.79	23.77	99.95	37.75	1,618,224	1,706,903
2	4873	76.37	24.65	100.29	37.94	2,160,080	2,278,452
3	5324	77.52	25.29	100.18	37.88	2,498,961	2,635,904

3.6. Concluding Remarks and Recommendations for Future Work

A design and simulation tool for modeling the performance of a shallow pond as a supplemental heat rejecter in ground-source heat pump systems has been developed. The model has been developed in the TRNSYS modeling environment (SEL, 1997) and can be coupled to other GSHP system component models for short-time step (hourly or minutely) system analyses. The model has been validated by comparing simulation results to experimental data.

The model accounts for several natural heat transfer mechanisms within a surface water body plus convective heat transfer due to a closed-loop heat exchanger coil. The heat transfer fluid is assumed to be carried by a series of pipes in the form of bundle spools or "slinky" coils. Environmental heat transfer mechanisms that are simulated by the model include solar radiation heat gain, heat and mass transfer due to evaporation, convection heat transfer to the atmosphere, thermal or long-wave radiation heat transfer, conduction heat transfer to the surrounding soil or fill material, and ground water discharge contributions. The solution scheme involves a lumped-capacitance approach and the resulting first-order differential equation describing the overall energy balance on the pond is solved numerically. Some outputs provided by the model include average pond temperature, exiting fluid temperature, and heat rejected to the pond.

An example application has been presented to demonstrate the use of the model as well as the viability of the use of shallow ponds as supplemental heat rejecters in GSHP

systems. Through this example, it is shown that the size of ground-loop heat exchangers can be significantly decreased by incorporating a shallow pond into the GSHP system.

The potential exists for significantly increasing the performance of shallow ponds used as supplemental heat rejecters in GSHP systems. Further research is suggested in the following areas:

- Optimization of the design procedure and control strategy. Hybrid ground source heat pump systems have many degrees of freedom; there are tradeoffs between the reduction in size of the ground loop heat exchanger, the size of the pond, and the control strategy. To more fully understand this, additional research using the simulation techniques developed in this paper is needed. This research would also take into account the economic costs and benefits, which we have not investigated.
- Additional validation of the model, using data from a working system, would be useful.
- Extension of the model to cover deep ponds for situations where an existing pond or lake is available.
- The use of spray fountains and other aeration devices in the pond to enhance pond cooling.
- The impact of pipe configuration within the pond on the overall system performance.

4. A Model for Simulating the Performance of a Pavement Heating System as a Supplemental Heat Rejecter with Closed-Loop Ground-Source Heat Pump Systems

4.1. Introduction

The reasons for using supplemental heat rejecters in vertical borehole GSHP systems have been described in Section 3.1. Several combinations of so-called "hybrid GSHP systems" are possible. Chapter 3 has dealt with using a shallow pond as supplemental heat rejecter. This chapter deals with using a hydronic pavement heating system as a supplemental heat rejecter. With additional heating equipment where applicable, these types of systems can also provide a useful and cost-effective method for pavement de-icing.

The objective of the work presented in this chapter has been to develop a design and simulation tool for modeling the performance of a hydronic pavement heating system that can be usefully and cost-effectively integrated into a ground-source heat pump system as a supplemental heat rejecter. The pavement heating model has been developed in the TRNSYS modeling environment (SEL, 1997) and can therefore be coupled to other GSHP system component models for short-time step (hourly or minutely) system analyses. The model has been validated by comparing simulation results to experimental data. As an example of the model's applicability, GSHP system simulation results are presented for a commercial building located in Tulsa, Oklahoma with a hypothetical closed-loop GSHP system with and without a pavement supplemental heat rejecter.

4.2. Heat Transfer in Pavement Slabs

Hydronically-heated pavement systems are commonly one of two types of configurations: (1) "serpentine" configuration (Figure 4-1) or (2) "slinky" configuration (Figure 4-2).

The serpentine configuration is that commonly used in snow-melting systems. The pipes are embedded in the pavement material and are placed on even centers and connected with U-shaped tubing. In the slinky configuration, a pipe is coiled in a circular fashion such that each loop overlaps the adjacent loop. The slinky is typically installed in fill material near the base of the pavement slab.

Pertinent concepts of heat transfer in pavement slabs have been addressed for snow melting applications by many sources including Adlam (1950), Chapman (1952), Kilkis (1994), ASHRAE (1995), and Ramsey et al. (1999). Heat transfer mechanisms acting upon the pavement slab are shown schematically in Figure 4-3. Heat transfer within the slab itself is by conduction. Internal sources of heat are due to convection from flow of the heat transfer fluid through the pipes. Heat fluxes at the pavement surface are due to a number of environmental interactions and include convection, solar radiation, thermal (long-wave) radiation, sensible heat transfer from precipitation, and latent heat transfer from melting snow and evaporating water. On the bottom and sides of the slab, heat fluxes are due to conduction to the ground and may or may not be

significant as compared to the top surface heat fluxes. If the slab bottom is exposed, as in the case of a bridge or parking deck, heat transfer from the bottom surface is by convection and radiation to the surroundings.

4.3. Experimental Methods

4.3.1. Test Slab Description and Data Collection

Two hydronically-heated concrete slabs have been constructed on a test site at the Oklahoma State University and used for this study. Each is discussed in the following subsections.

4.3.1.1. Bridge Deck Test Section

The first test slab was constructed resembling a concrete bridge deck. Construction details are given by Liao and Hogue (1996). The test slab is rectangular with a plan area of 10 ft (3.05 m) by 3 ft (0.91 m) and a thickness of 8 in. (0.2032 m). The slab has been constructed on a steel frame and insulated on all four sides to minimize edge losses. Heat was rejected to the slab by circulating a heated fluid through a pipe system installed in a serpentine configuration. The pipes are made of polybutylene with a nominal diameter of ¾-inch (0.01905-m) and were embedded at a depth of 2.5 in. (0.0635 m) from the slab surface on 6.5-inch (0.1651-m) centers.

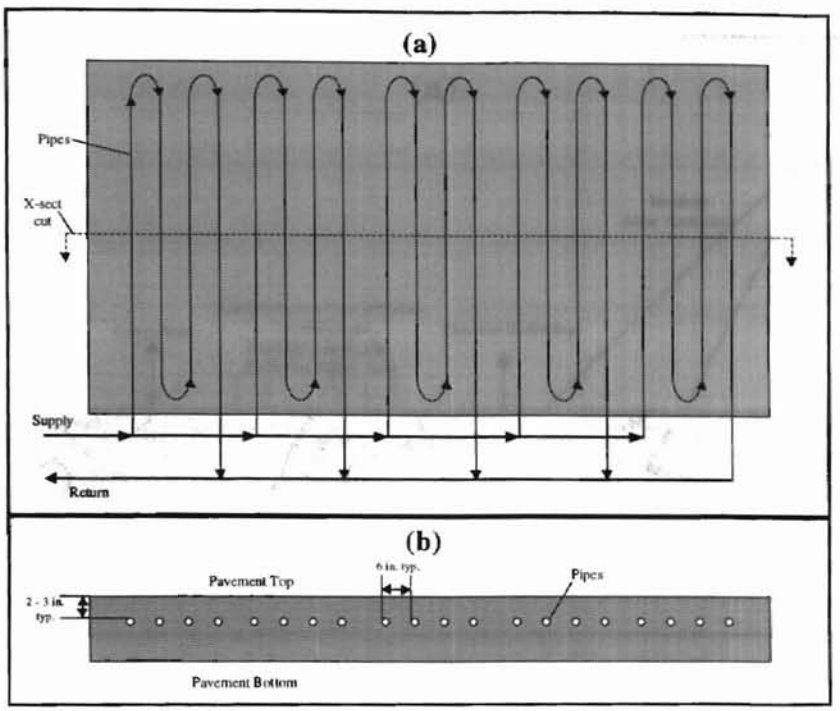

Figure 4-1. Serpentine pipe configuration in a hydronically-heated pavement slab in (**a**) plan view and (**b**) cross-sectional view.

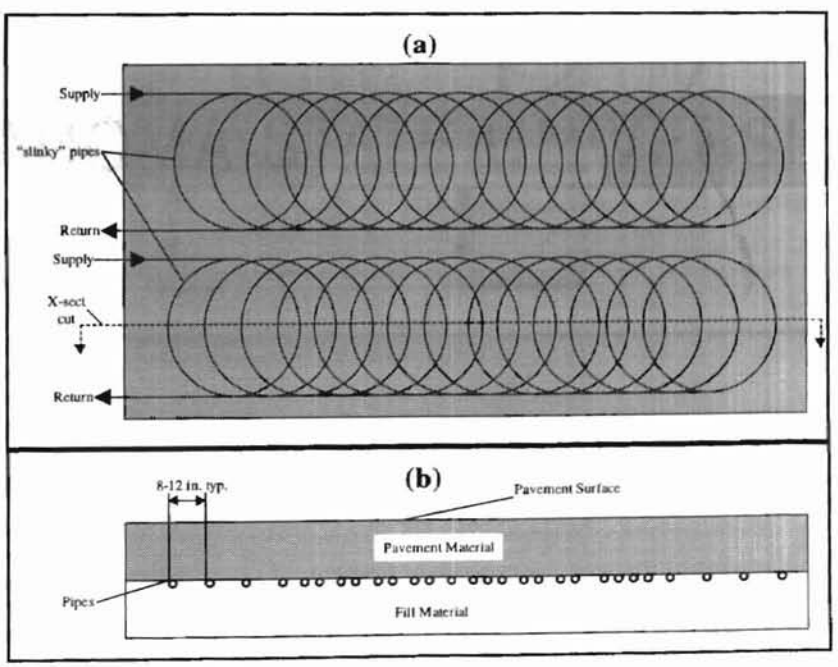

Figure 4-2. Slinky pipe configuration in a hydronically-heated pavement slab in (**a**) plan view and (**b**) cross-sectional view along the slinky center-line.

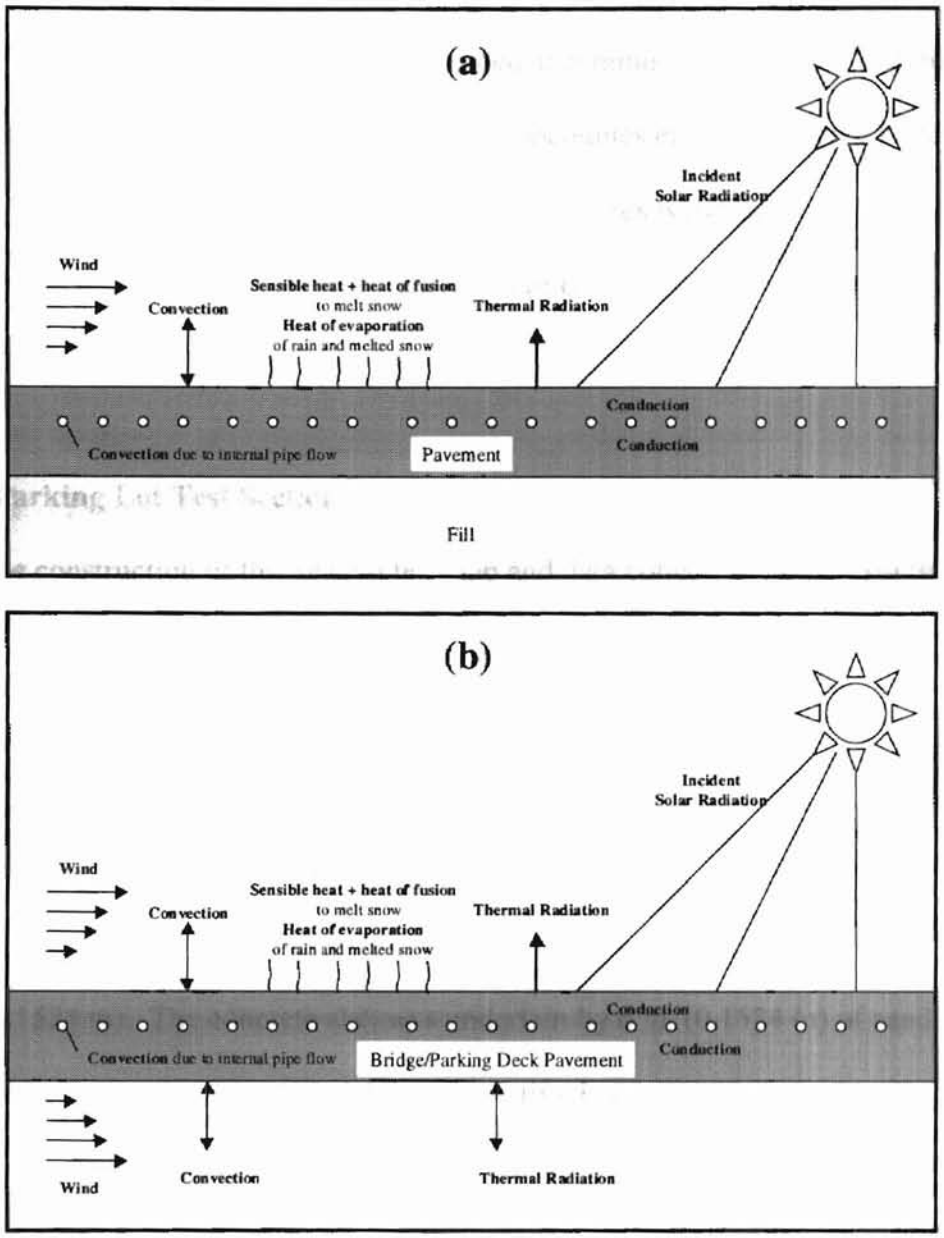

Figure 4-3. Heat transfer mechanisms in hydronically-heated pavement slabs with (**a**) no bottom exposure to the atmosphere and (**b**) bottom exposure to the atmosphere.

Data used in this portion of the study were collected by Wadivkar (1997). An antifreeze heat exchange fluid was circulated through the bridge deck coupled to a closed-loop ground-source heat pump system over several night-time periods during the

winter of 1996. The bridge deck fluid supply and return temperatures, the fluid flow rate, and the bridge surface temperature were recorded at 5-minutely intervals. The bridge surface temperature was measured using 28 thermocouples embedded in the concrete surface and the bridge fluid supply and return temperatures were measured using thermocouples embedded in the pipes. Icing conditions on the concrete surface were also noted during the Wadivkar (1997) study.

4.3.1.2. Parking Lot Test Section

The construction of this second test slab and data collection for this study have been conducted by researchers affiliated with the Division of Engineering Technology at the Oklahoma State University.

This test slab was constructed resembling a parking lot or concrete sidewalk. This test slab is rectangular with a plan area of 40 ft (12.19 m) by 4 ft (1.22 m) and a thickness of 6 in. (0.1524 m). The concrete slab was underlain by 6 in. (0.1524 m) of sand fill material. Heat was rejected to the slab by circulating heated water through a slinky heat exchanger installed at the concrete/sand fill interface. The slinky pipe is made of HDPE plastic and is 500 feet (152.40 m) long with a nominal diameter of ¾ in. (0.01905 m). The pipe was coiled such that the resulting slinky heat exchanger is 40 ft (12.19 m) long with a diameter of 3 ft (0.91 m) and a 10-in. (0.254 m) pitch (the separation distance between the apex of each successive loop).

The temperature of the concrete surface was measured by two thermistors embedded in the concrete at a depth of approximately ¼ in. (0.0064 m) from the surface.

One thermistor was placed near the slinky center between two pipes of the slinky and the other was placed near the end of the slinky above a pipe. Slinky supply and return water temperatures were measured by thermistors embedded in the slinky header. The remainder of the heat rejection system included a flow meter, a water heating element, and a watt transducer. All sensor information was recorded at time intervals of 6 minutes.

The tests are controlled to maintain a set water temperature by heating the water if the temperature falls below a set point. Two set point temperatures were used in this study: 90°F (32.2°C) in the summer season and 75°F (23.9°C) in the winter season.

4.3.2. Weather Instrumentation and Data Collection

Weather data for this study were obtained from the Oklahoma Mesonet (**meso**scale **net**work), which is a weather station network consisting of weather monitoring sites scattered throughout Oklahoma. Depending on the weather parameter, data are recorded at time intervals ranging from 3 seconds to 30 seconds and averaged over 5-minute observation intervals.

Weather data at 15-minute intervals for the Stillwater monitoring station were acquired for the time periods of interest for this study. The Stillwater station is located approximately 1 mile from the test site. Data for the following parameters were obtained: wind speed, wind direction, air temperature, relative humidity, and solar radiation. Further details of the weather station network may be found in Elliott et al. (1994).

4.4. Model Development

4.4.1. Governing Equations

Transient heat transfer in the pavement slab is represented in the model in two-dimensional (2-D) cross-section using the cartesian coordinate system. The 2-D approach is reasonable if the cross-section is taken through the mid-section of the slab along the major direction of fluid flow in the pipe system. The transient 2-D heat conduction equation can be expressed as:

$$\frac{\partial^2 T}{\partial x^2} + \frac{\partial^2 T}{\partial z^2} = \frac{1}{\alpha}\frac{\partial T}{\partial t} \tag{4-1}$$

This equation has been discretized using an explicit finite difference method. The typical geometry and notation of the finite difference cells in the x-z cartesian coordinate plane are shown in Figure 4-4.

The nodal equations are formulated using a node-centered, energy balance approach. The resulting general form of the explicit finite difference equation is:

$$\sum_{i=1}^{4} q''_i{}^{(t-\Delta t)} A = V\rho c_p \left(\frac{T_{(m,n)}{}^{t} - T_{(m,n)}{}^{(t-\Delta t)}}{\Delta t} \right) \tag{4-2}$$

where, $q_i^{\prime\prime(t-\Delta t)}$ is the heat flux across the cell face i at the previous time step, A is the cell face area (assuming a unit depth), V is the cell volume (assuming a unit depth), ρ is the

average density of the cell material, c_p is the average specific heat capacity of the cell material, $T_{(m,n)}^{t}$ is the nodal temperature at the current time step, $T_{(m,n)}^{t-\Delta t}$ is the nodal temperature at the previous time step, and Δt is the time step. The heat flux, q'', for conduction into node *(m,n)* during a given time step is given by Fourier's Law in discrete form as:

$$q''_{i\rightarrow(m,n)} = k\frac{(T_i - T_{(m,n)})}{\ell} \tag{4-3}$$

where subscript *i* denotes a neighboring node (from 1 to 4), *k* is the average thermal conductivity of the material between nodes *i* and *(m,n)*, and ℓ is the distance between nodes *i* and *(m,n)*.

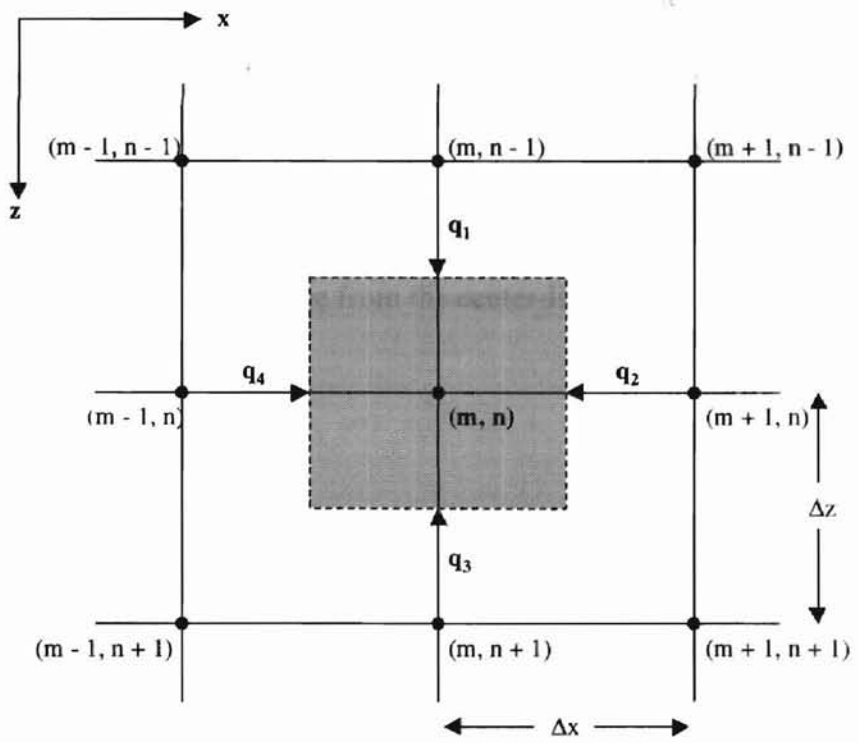

Figure 4-4. Finite difference cell geometry and notation.

The size of the time step is limited by the need to maintain stability. In this fully explicit method, the stability criterion for two-dimensional problems is given by:

$$\frac{\alpha \Delta t}{\ell^2} \leq \frac{1}{4} \tag{4-4}$$

where α is the thermal diffusivity of the material within the cell and ℓ is the nodal spacing.

4.4.2. The Finite Difference Grid

The finite difference grid used in the model is shown in Figure 4-5. A uniform square nodal spacing equal to the pipe radius has been used. Because of symmetry and small temperature differences between adjacent pipe, and neglecting edge effects, the model domain was reduced to a width equivalent to one-half of the pipe spacing as shown in Figure 4-5. In the z direction, the domain corresponds to the top of the slab and bottom of the slab or the base of the underlying fill material. In the x direction, the domain corresponds to a distance from the center-line of a pipe to half the distance to the adjacent pipe.

4.4.3. Boundary Conditions

The boundaries of the model domain are treated as flux-type (Neumann) conditions as shown in Figure 4-5. The temperature at each boundary node is given by

the energy balance equation (Equation 4-2), where q_i'' represents the appropriate external flux and conduction flux from adjacent nodes.

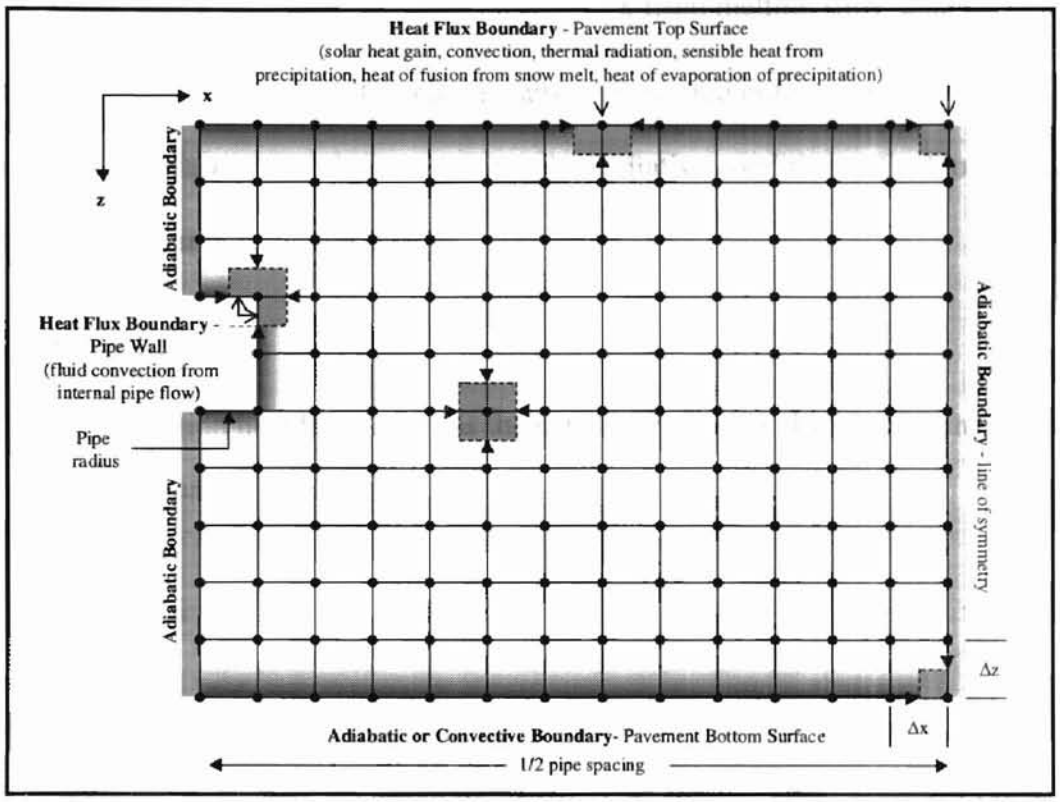

Figure 4-5. The model domain showing the finite-difference grid and boundary conditions. Shaded squares show example control volumes for different types of grid node geometries.

Lines of symmetry on the left- and right-hand boundaries are, by definition, zero-flux conditions. Heat flux at the pipe surface nodes represents convection from the heat transfer fluid. Heat flux at each top surface node ($q''_{(m,1)}$) is given by:

$$q''_{(m,1)} = q''_{solar} + q''_{thermal} + q''_{convection} + q''_{rain,snow-sensible} + q''_{rain,snow-latent} \qquad (4\text{-}5)$$

where q''_{solar} is the solar radiation heat flux, $q''_{thermal}$ is the thermal radiation heat flux, $q''_{convection}$ is the convection heat flux, $q''_{rain,snow-sensible}$ is the sensible heat flux from falling rain and snow, and $q''_{rain,snow-latent}$ is the latent heat flux from melting snow and evaporating/condensing water. The bottom surface is treated either as an insulated surface or as a surface exposed to convective plus radiative conditions. Each of the heat flux terms is further described below.

4.4.3.1. Solar Radiation Heat Flux

Solar radiation heat flux (q''_{solar}) is the net solar radiation absorbed by the pavement surface and is given by:

$$q''_{solar} = \alpha I \tag{4-6}$$

where I is the solar radiation incident on the pavement surface and α is the absorptivity coefficient for the pavement material. The absorptivity coefficient is corrected for solar incidence angle (θ) dependence using an empirical correlation given by Duffie and Beckman (1991). The model also accepts solar radiation in the form of beam (I_b) and diffuse (I_d) components, in which case I is computed from:

$$I = I_b \cos\theta + I_d \tag{4-7}$$

The angle of incidence (θ) of the sun's rays is computed at each time step from correlations given by Spencer (1971), Duffie and Beckman (1991), and ASHRAE (1997).

4.4.3.2. Thermal Radiation Heat Flux

This heat transfer mechanism accounts for heat flux at the pavement top surface and bottom surface (if exposed) due to thermal or long-wave radiation. This model uses a linearized radiation coefficient (h_r) defined as:

$$h_r = 4\varepsilon\sigma\left(\frac{T_{(m,n)} + T_2}{2}\right)^3 \tag{4-8}$$

where ε is the emissivity coefficient of the pavement material, σ is the Stefan-Boltzmann constant, $T_{(m,n)}$ is the surface node temperature in absolute units, and T_2 represents the sky temperature in absolute units. T_{sky} is computed from the relationship given by Bliss (1961). If the bottom of the slab is exposed, Equation 4-8 is also used to determine h_r for the bottom surface, where T_2 represents the ground temperature in absolute units, which is approximated as the air temperature. The thermal radiation heat flux at each node ($q''_{thermal}$) is then computed by:

$$q''_{thermal} = h_r(T_2 - T_{(m,n)}) \tag{4-9}$$

4.4.3.3. Convection Heat Flux at the Pavement Surfaces

This mechanism accounts for heat transfer at the pavement top and bottom surfaces due to free and forced convection. The convection coefficient (h_c) is a function of the Nusselt Number (Nu). Several empirical formulations exist for determining the convection coefficient for different geometries. For a pavement surface, correlations for

a horizontal flat plate are the most applicable and therefore the convection coefficient (h_c) is determined as described in Section 3.4.1.3.

In free convection heat transfer, Nu is a function of the Rayleigh Number (Ra). Ra is determined as described by Equation 3-13 where ΔT refers to the temperature difference between the pavement surface at node (m,n) and the air, L is the characteristic length described for horizontal flat plates as the ratio of the area to the perimeter (Incropera and DeWitt, 1996), and the thermal properties α, β, and ν are evaluated at the film temperature, which can be approximated as the average of the air and the pavement surface temperature at node (m,n). In external free convection flows over a horizontal flat plate, the critical Rayleigh Number is about 10^7. Therefore, two empirical relations for the Nusselt number are used in this model as described by Incropera and DeWitt (1996) for free convection from the upper surface of a heated plate or the lower surface of a cooled plate (Equations 3-15a and 3-15b). The convection coefficient (h_c) for free convection can then be determined from Equation 3-16 where k is the thermal conductivity of air evaluated at the film temperature and L is the characteristic length described above.

In forced convection heat transfer, Nu is usually correlated to the Reynolds (Re) and Prandtl (Pr) Numbers. For external forced convection over a flat plate (i.e. the pavement surface), the critical Reynolds Number is approximately 10^5. Therefore, two empirical relations for the Nusselt number are used in the model as described by Incropera and DeWitt (1996) for forced convection over a flat plate (Equations 3-19a and

3-19b). The convection coefficient (h_c) for forced convection can then be determined by Equation 3-16 with the characteristic length value described as the ratio of the length (parallel to the wind direction) to the perimeter.

Finally, the convection heat flux at each pavement surface node ($q''_{convection}$) is computed by:

$$q''_{convection} = h_c (T_{air} - T_{(m,n)}) \tag{4-10}$$

where T_{air} is the dry-bulb air temperature and h_c is taken as the maximum of the free convection coefficient and the forced convection coefficient. This practice of choosing the larger of the free and forced convection coefficients is recommended by Duffie and Beckman (1991) and McAdams (1954) and is used in the absence of additional experimental evidence regarding combined free and forced convection.

4.4.3.4. Heat Flux Due to Rain and Snow

This heat transfer mechanism includes both sensible and latent effects. This model uses a simple mass/energy balance on water at the pavement surface to account for heat and mass transfer. The thermal properties of water are computed from correlations given in the Handbook of Chemistry and Physics (CRC, 1980).

The sensible heat flux due to falling rain or snow at each pavement surface node ($q''_{rain,snow}$) is given by:

$$q''_{rain,snow} = \dot{m}''_{rain,snow}\, c_p (T_{air} - T_{(m,1)}) \tag{4-11}$$

where $\dot{m}''_{rain,snow}$ is the rainfall or snowfall rate in water equivalent mass per unit time per unit area and c_p is the specific heat capacity of water at the air temperature.

Latent heat transfer is considered only if the air temperature or the slab surface temperature is above 33°F (0.55°C). Accumulation of rain is not considered; rainfall is assumed to drain instantaneously from the pavement surface, forming a thin film from which evaporation occurs.

This model uses the j-factor analogy to compute the mass flux of evaporating water at each pavement surface node ($\dot{m}''_w$):

$$\dot{m}''_w = h_d (w_{air} - w_{(m,1)}) \tag{4-12}$$

where h_d is the mass transfer coefficient, w_{air} is the humidity ratio of the ambient air, and $w_{(m,1)}$ represents the humidity ratio of saturated air at the surface node. The mass transfer coefficient (h_d) is defined using the Chilton-Colburn analogy defined previously by Equation 3-26 where h_c is the convection coefficient defined above, c_p is the specific heat capacity of the air evaluated at the pavement node - air film temperature, and Le is the Lewis number described by Equation 3-27 where α and D_{AB} are each evaluated at the pavement node - air film temperature. The heat flux due to evaporation ($q''_{evaporation}$) is then given by:

$$q''_{evaporation} = h_{fg}\dot{m}''_{w} \tag{4-13}$$

where h_{fg} is the latent heat of vaporization and is computed from the relationship given by Irvine and Liley (1984).

The heat flux due to melting snow and ice is determined using a mass balance on freezing precipitation that has accumulated at the pavement surface. The accumulation of ice at the beginning of each time step is determined from the sum of the rainfall rate and the snowfall rate if the air temperature or the slab surface temperature is below 33°F (0.55°C). Although snow is a porous medium, it is treated in the model as an equivalent ice layer. Sublimation of ice is not considered. The mass flux of water due to melting ice ($\dot{m}''_{icemelt}$) at the pavement surface is then given by:

$$\dot{m}''_{icemelt} = \frac{q''_{solar} + q''_{thermal} + q''_{convection} + q''_{rain,snow-sensible} + q''_{evaporation} + q''_{conduction,ice}}{h_{if}} \tag{4-14}$$

where $q''_{conduction,ice}$ is the conduction heat flux from the pavement surface into the ice layer and h_{if} is the latent heat of fusion of water. The other heat flux terms have been defined previously. If the ice thickness is greater than zero, the heat flux into each pavement surface node ($q''_{(m,1)}$) is given by:

$$q''_{(m,1)} = -\dot{m}''_{icemelt}\, h_{if} \tag{4-15}$$

The thickness of the ice layer at the end of the time step ($\ell_{ice,new}$) is computed by:

$$\ell_{ice,new} = \ell_{ice,old} - \left(\frac{\dot{m}''_{w} + \dot{m}''_{icemelt}}{\rho_{ice}} \right) \Delta t \tag{4-16}$$

4.4.3.5. Heat Transfer Due to the Heat Exchange Fluid

Heat transfer due to the heat exchange fluid is represented by heat flux at the pipe surface nodes. This model has been developed to account for water or antifreeze as the heat exchange fluid. The thermal properties of the fluid are computed at each time step from correlations given in the Handbook of Chemistry and Physics (CRC, 1980) for water and from correlations given by Wadivkar (1997) for an antifreeze solution. The thermal properties are computed at the average fluid temperature (T_{fluid}). This temperature is computed as the average of the inlet and outlet temperatures at the given time step. Since the outlet temperature at any current time step is not known, the previous converged value is used as an initial guess and calculation of T_{fluid} is iterative.

The heat flux due to the heat exchange fluid (q''_{fluid}) is computed per flow circuit by:

$$q''_{fluid} = U_{pipe}(T_{fluid} - T_{(m,n)}) \tag{4-17}$$

where U_{pipe} is the overall heat transfer coefficient for the pipe and is expressed as:

$$U_{pipe} = \frac{1}{\frac{1}{h_{pipe}} + \frac{\ell}{k_{pipe}}} \tag{4-18}$$

where h_{pipe} is the convection coefficient due to fluid flow through the pipe, k_{pipe} is the thermal conductivity of the pipe material, and ℓ_{pipe} is the wall thickness of the pipe.

The convection coefficient due to fluid flow in the pipe is determined using correlations for the Nusselt Number in flow through a horizontal cylinder. A constant heat flux at the pipe surface is assumed. For laminar flow in the pipe (Re<2000), the Nusselt Number is a constant equal to 4.36 (Incropera and DeWitt, 1996, Equation 8-53). For turbulent flow, the Dittus-Boelter relation is used to compute the Nusselt Number as described by Equation 3-36. The value of the exponent x in Equation 3-36 is dependent upon whether the entering fluid is being heated or cooled; x is equal to 0.3 if the entering fluid is greater than the slab temperature and x is equal to 0.4 if the entering fluid is less than the slab temperature. The convection coefficient (h_{fluid}) is given by Equation 3-16 where k is the thermal conductivity of the heat transfer fluid and the characteristic length (L) is defined as the inner diameter of the pipe.

The outlet fluid temperature (T_{out}) is computed from an overall energy balance on the pipe flow circuit:

$$T_{out} = T_{fluid} - \frac{q''_{fluid} A_{pipe}}{2\dot{m}c_p} \tag{4-19}$$

where A is the inside surface area of the pipe per flow circuit, $\dot{m}$ is the mass flow rate of the heat exchange fluid per flow circuit, and c_p is the specific heat capacity of the heat exchange fluid. This outlet temperature is used to compute the average fluid temperature at the next iteration as described above.

The total heat transfer due to the fluid flow ($q_{transfer,fluid}$) is given by:

$$q_{transfer,fluid} = \dot{m} c_p (T_{in} - T_{out}) N_{circuit} \quad (4\text{-}20)$$

where $N_{circuit}$ is the number of flow circuits.

4.4.4. Computer Implementation

The component configuration for the pavement heating model is shown in Figure 4-6. A companion model was also developed which manipulates any weather data needed for the pavement heating model. The weather component model makes use of the TRNSYS psychrometric subroutine to compute moist air properties given two known state properties. The two state properties are dry bulb temperature and one of wet bulb temperature, relative humidity, or dew point temperature. The weather component model also computes the sky temperature, the solar radiation on a horizontal surface, and the solar incidence angle. A computer algorithm is shown in Figure 4-7 in the form of a flow chart.

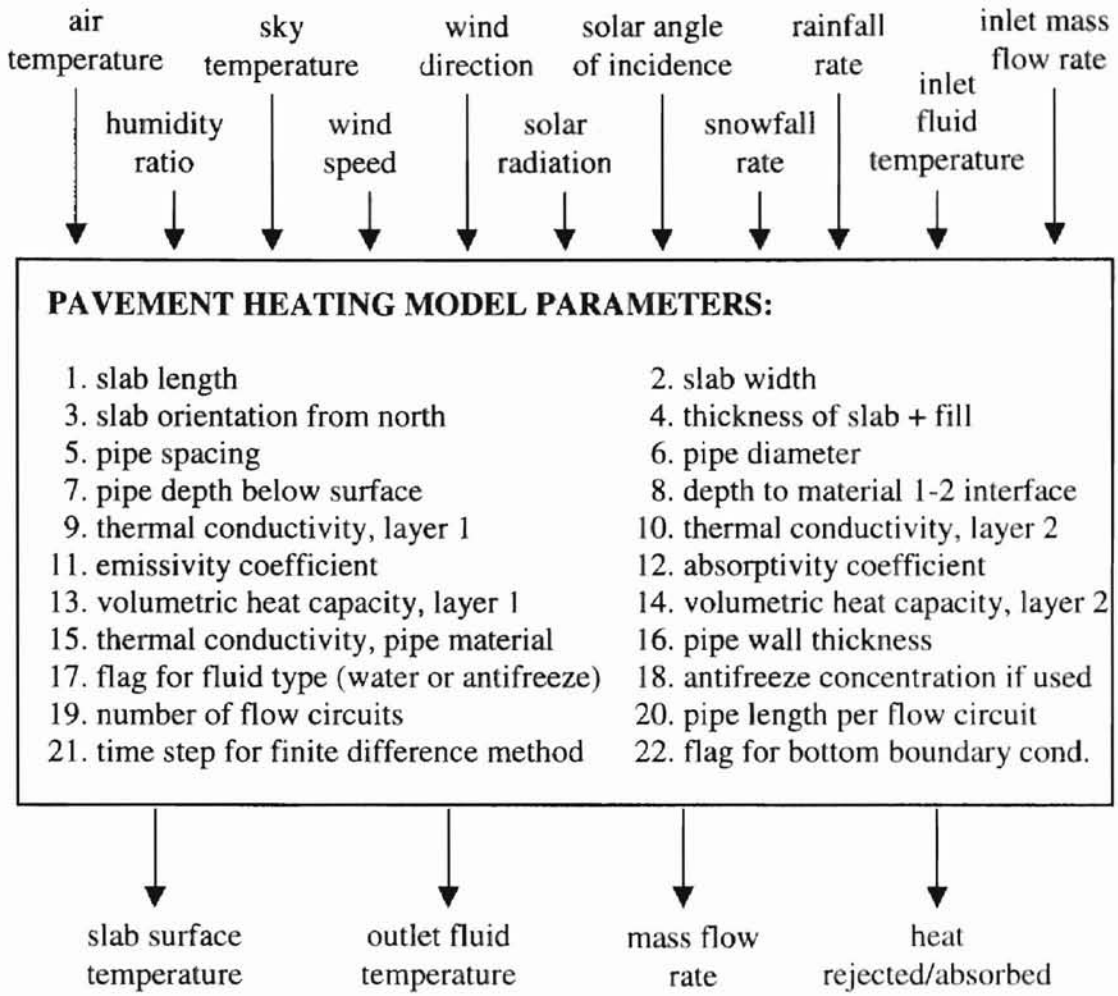

Figure 4-6. Pavement heating model component configuration.

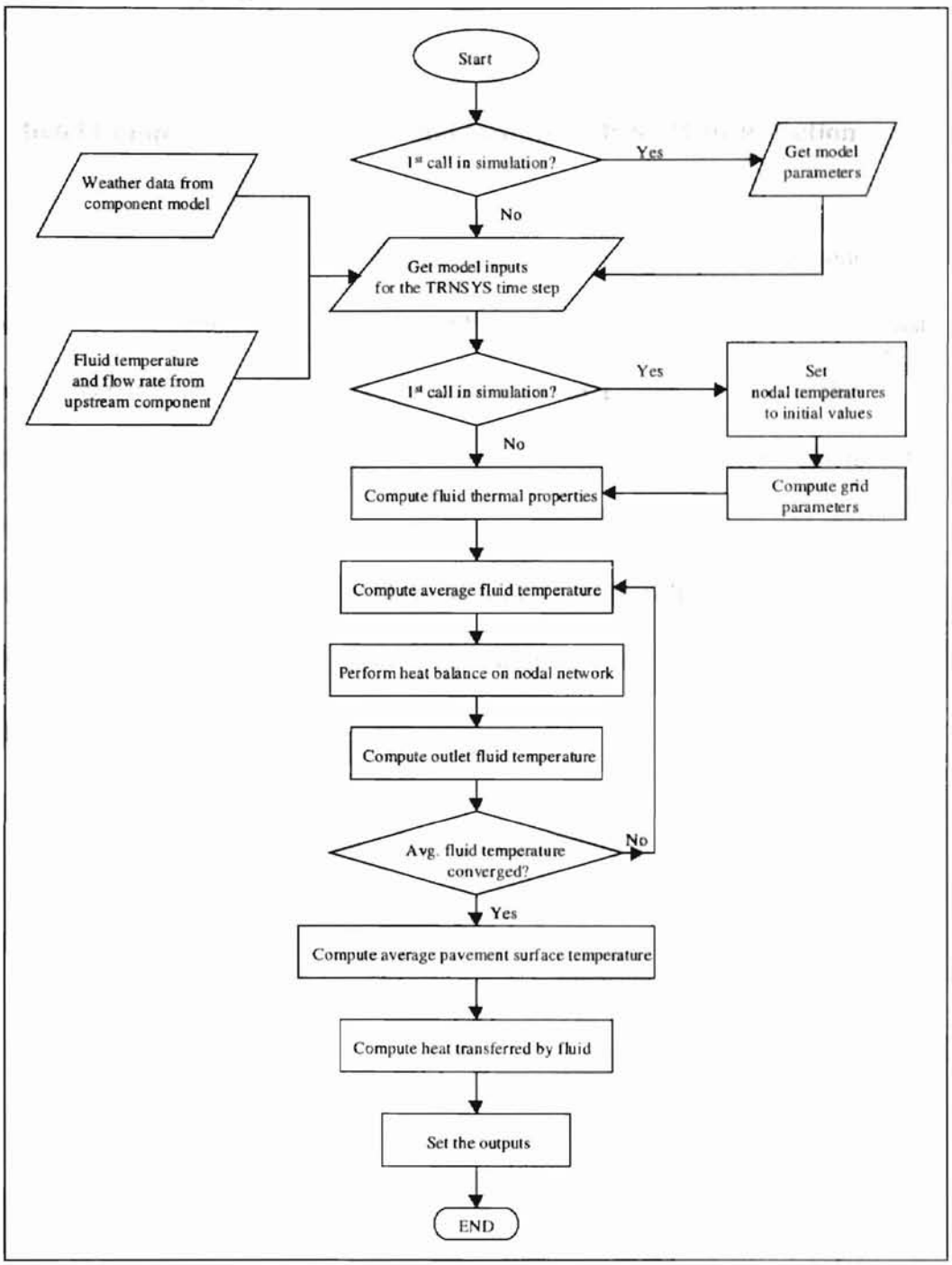

Figure 4-7. Pavement heating model computer algorithm.

4.5. Results and Discussion

4.5.1. Model Comparison to Experimental Results with No Heat Rejection

The first step in the model verification process was to compare the model pavement slab temperatures to measured slab temperatures during times when no heat was being rejected to the slab. This comparison allowed a validity check of the simulation of the several environmental heat transfer mechanisms occurring within the pavement. Simulated and actual pavement average hourly temperatures are shown for the parking lot test section in Figure 4-8 for an 8-day period in July 1998 when no heat was rejected to the pavement. Therefore, in this case, the model is driven by weather data input only.

A review of the plot in Figure 4-8 shows that the model slab surface temperatures compare favorably to the measured slab surface temperatures. The simulated peak daily and nightly temperatures are generally lower than the measured values. These discrepancies are generally within 3°F (1.67°C) .

4.5.2. Model Comparison to Experimental Results with Heat Rejection

Heat rejection to the bridge-deck test section was simulated for the nights of March 7-8, 1996 and March 24-25, 1996. During the night of March 7-8, 1996, a thin layer of ice had formed on the bridge deck prior to the heat rejection test. Heat rejection to the parking lot test section was simulated over a 36-day period from November 12 to

December 18, 1998. Input data to the model consisted of weather data as described previously in addition to measured slab heat exchanger supply water temperatures and flow rates on 5- minutely time intervals for the bridge deck field tests and 6-minutely time intervals for the parking lot field tests.

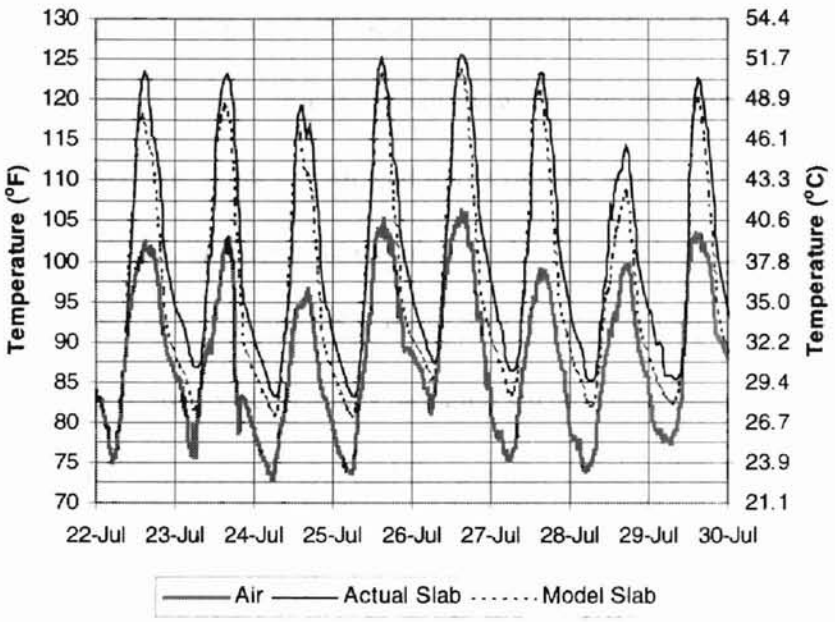

Figure 4-8. Comparison of observed and simulated slab surface temperatures for the parking lot test section with no heat rejection to the slab.

Since different parameters had been measured during the bridge deck field tests and the parking lot field tests, the model performance was evaluated accordingly. For comparison of the model results to the bridge deck field test data, the model performance was evaluated by comparing (1) the simulated to the observed bridge deck surface temperature and (2) the simulated to the observed return temperature of the heat exchange fluid. For comparison of the model results to the parking lot field test data, the

model performance was evaluated by comparing (1) the simulated to the observed return temperature of the heat exchange fluid and (2) the simulated cumulative heat rejected to the pavement slab to the measured water heating element and pump power input. These comparisons are shown in Figures 4-9 and 4-10 respectively.

A review of the plots in Figure 4-9 shows that model predicted the bridge deck surface temperature and fluid return temperature quite well. For the night of March 7-8, 1996, the average observed and modeled surface temperatures were 27.9°F (-2.27°C) and 27.2°F (-2.67°C), respectively, and the average observed and modeled fluid return temperatures were 84.8°F (29.33°C) and 85.1°F (29.50°C), respectively. For the night of March 24-25, 1996, the average observed and modeled surface temperatures were 36.9°F (2.72°C) and 36.8°F (2.67°C), respectively, and the average observed and modeled fluid return temperatures were 85.0°F (29.44°C) and 85.7°F (29.83°C), respectively. One main purpose for the bridge deck simulations was to verify the model's applicability to system performance over relatively short time periods. Another important purpose of these simulations was to verify the model's applicability to the serpentine pipe arrangement. The quantity of data was limited regarding snow and ice conditions and further experiments need to be conducted to fully evaluate the model's capability to account for snow and ice events.

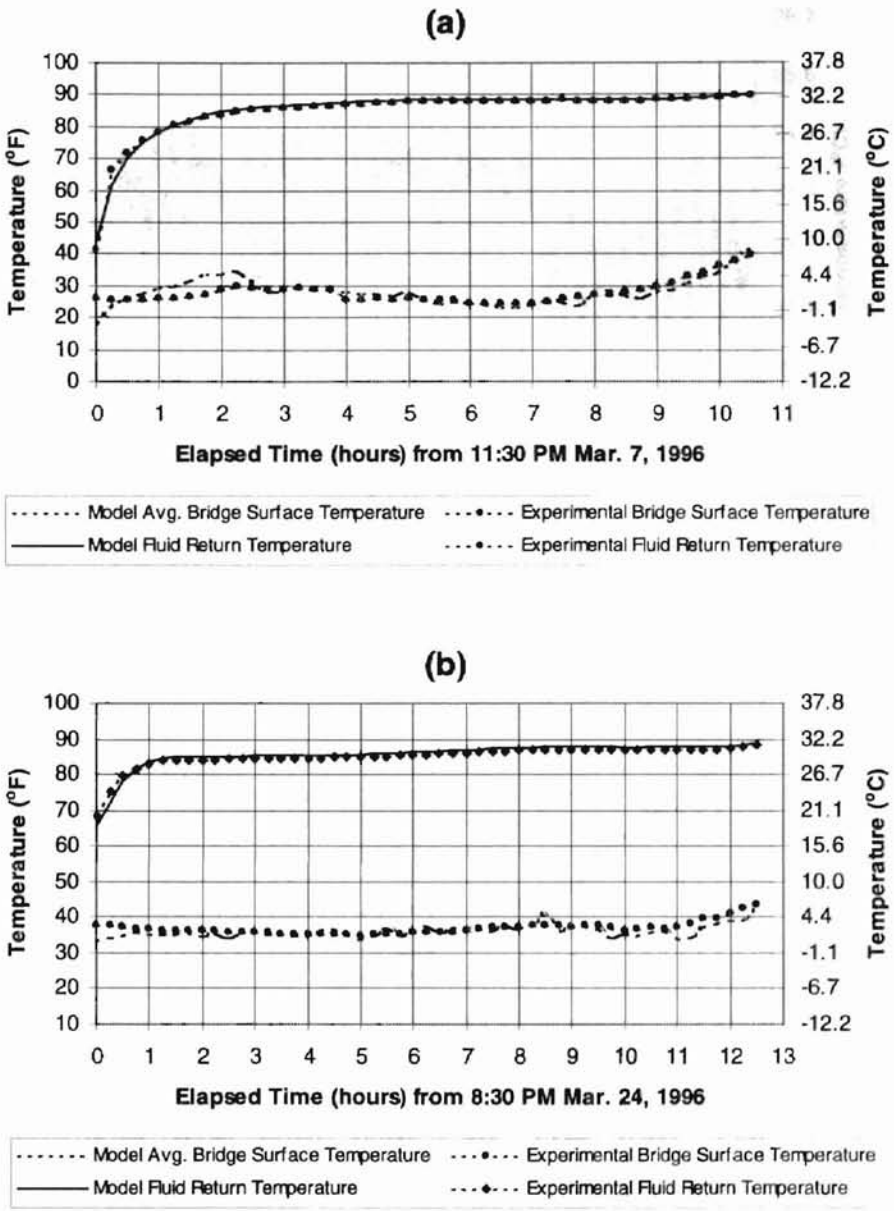

Figure 4-9. Comparison of observed and simulated slab surface temperatures and heat exchange fluid return temperatures for the bridge deck test section for the nights of **(a)** March 7-8, 1996 and **(b)** March 24-25, 1996.

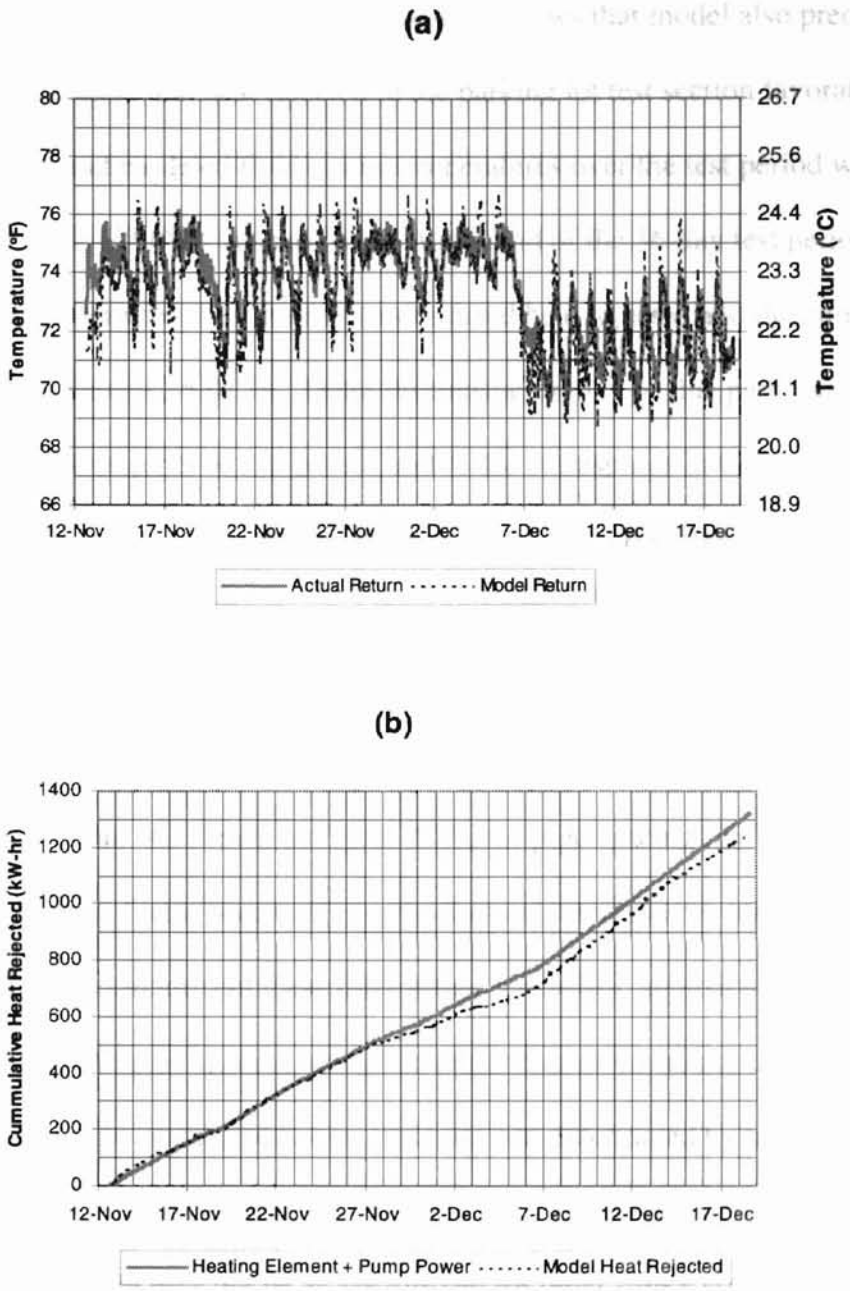

Figure 4-10. Comparison of observed and simulated **(a)** heat exchange fluid return temperatures and **(b)** heat rejected to the parking lot test section.

A review of the plots in Figure 4-10 shows that model also predicted the fluid return temperature and heat rejected to the parking lot test section favorably. The average observed and modeled fluid return temperatures over the test period were 73.1°F (22.8°C) and 73.4°F (23.0°C), respectively. At the end of the 36-day test period, the percent difference between the cumulative simulated heat rejected and the cumulative measured heat rejected is –5.01 %. These discrepancies may be due partly to heat losses from the supply/return pipes to the ground and to the atmosphere in the equipment building. A model and experimental uncertainty analysis is presented in Appendix A.

Further explanation is required regarding the parking lot test section simulations. Explicit modeling of a slinky pipe is difficult because there are no true lines of symmetry along its cross-section. As shown in Figure 4-2b, the pipe spacings are not uniform. Another complicating factor is quantifying the thermal interferences induced by overlap of the pipe coils. To circumvent these difficulties, a heuristic approach was used to determine an effective pipe spacing along the center-line of the slinky coil. For a 10-inch pitch, an effective pipe spacing of 8.4 in. (0.21 m) was determined by taking the arithmetic average of the pipe spacing at the points where the pipe coils overlap. However, this approach may not be as appropriate for other slinky configurations.

4.5.3. Model Application

To illustrate the applicability of the model as well as the viability of using pavement heating systems as supplemental heat rejecters in GSHP systems, a model of a hypothetical GSHP system was constructed in the TRNSYS modeling environment. A

simplified system schematic is shown in Figure 4-11. For this example, a pavement heating system similar to the parking lot test section described above was used. That is, a slinky coil installed at the interface of a 6-inch (0.1524 m) concrete slab and underlying sand fill material. Each of the component models is described briefly below.

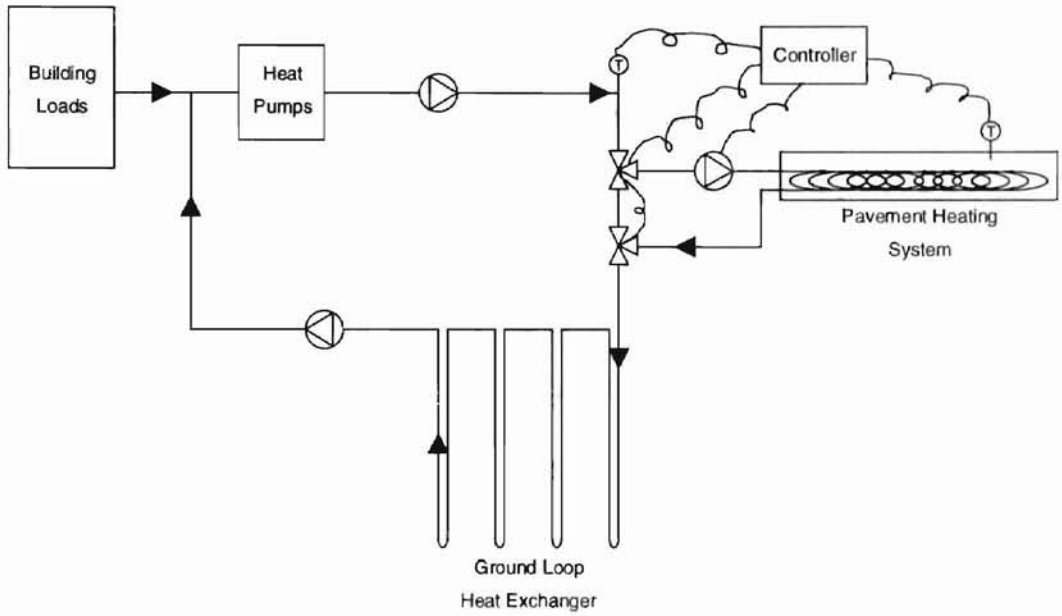

Figure 4-11. System schematic for the example model of a GSHP system with a pavement heating system supplemental heat rejecter.

The building is not modeled explicitly in this application. The hourly building thermal loads are pre-computed using a proprietary building energy analysis program and are read from a file and passed to the heat pump subroutines. The building, the same one described in Section 3.5.3, is an actual four-story, 45,000-ft^2 (4181-m^2) office building located in Tulsa, Oklahoma and is highly cooling dominated. The building thermal loads are shown in Figure 3-8.

A simple water-to-air heat pump model was developed for this and other GSHP system simulations. Inputs to the model include sensible and latent building loads, entering fluid temperature, and fluid mass flow rate. The model uses quadratic curve-fit equations to manufacturer's catalog data to compute the heat of rejection in cooling mode, heat of absorption in heating mode, and the heat pump power consumption. Outputs provided by the model include exiting fluid temperature, power consumption, and fluid mass flow rate. In this application, one heat pump component model handles the heating load and a second heat pump component model handles the cooling load.

The ground-loop heat exchanger model used in this application is that described by Yavuzturk and Spitler (1999) which is based partly on the work of Eskilson (1987) who developed "long time-step" (monthly) response factors for vertical ground-coupled U-tube heat exchangers. The model of Yavuzturk and Spitler (1999) extends the work of Eskilson (1987) to hourly or less ("short-time step") time intervals. The development of the short time-step response factors are based on an analytically validated, transient two-dimensional implicit finite volume model (Yavuzturk et al., 1999) that simulates the heat transfer over a vertical U-tube ground heat exchanger. In this application, the modeled borehole field consisted of one hundred 250-feet (76.2-m) deep boreholes arranged in a 10 by 10 square pattern. A total system flow rate of 270 gpm (61.36 m^3/hr) was assumed. Representative thermal properties of sedimentary rock were chosen.

Ancillary components such as pumps, t-pieces, flow diverters, and the differential controller are described by SEL (1997). The control strategy used to activate the circulating pump to the pavement was chosen somewhat arbitrarily by using the

temperature difference between the pavement surface and the exiting fluid temperature from the heat pumps. When this temperature difference exceeds 9°F (5°C), the circulating pump to the pavement is energized and heat will be rejected to the pavement. During these times, all flow is diverted to the pavement system. The properties of each heat exchanger coil in the example model are the same as those described in the parking lot test section experiments. Hourly input weather data for the model were taken from a typical meteorological year (TMY) record for Tulsa, Oklahoma.

The model was run for two cases for a duration of 3 years with a time step of one hour. The first case was the GSHP system with no pavement and the second case was the GSHP system with the pavement. Hourly heat pump entering water temperatures are shown in Figure 4-12 for both cases.

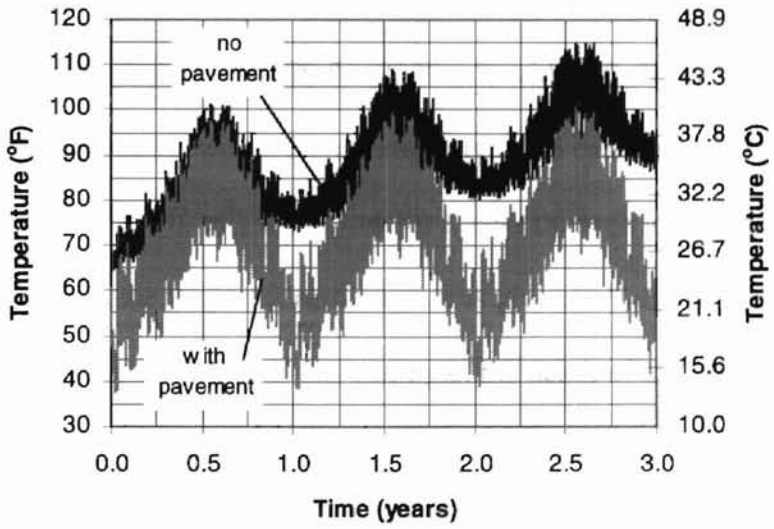

Figure 4-12. Entering heat pump water temperatures for the example GSHP system simulation with no pavement heating and with a 24,000 ft^2 (2230 m^2) parking lot with pavement heating.

A review of the data presented in Figure 4-12 shows the advantages of using a pavement heating system as a supplemental heat rejecter. Assuming that a maximum heat pump entering water temperature of 100°F (37.78°C) is desirable, the system without the pavement system would fail during the second year of operation. In fact, based on the results of a ground-loop heat exchanger sizing program (Spitler et al., 1996), the boreholes of a 10 by 10 square pattern would need to be approximately 400 feet (121.9 m) deep to accommodate the cooling dominated loads of this building for 20 years of operation. Such a system would be eliminated from consideration early on in the design phase because of excessive first cost.

Using the TRNSYS model as a design tool, the size of the pavement supplemental heat rejecter was determined under the assumption that the 10 by 10 borehole field could not be feasibly deeper than 250 feet (76.2 m). The heat pump entering water temperatures for the GSHP system with the pavement heating system shown in Figure 4-12 were produced by simulating a 24,000 ft^2 (2230 m^2) with 200 slinky heat exchanger coils. This size of a parking lot would have a capacity of 75 cars (in parking lot design, an area per car of 320 ft^2 (29.73 m^2) will allow for access through lots (Lindeburg, 1992)). A summary of the pavement system performance is given in Table 4-1. By adding the pavement supplemental heat rejecter in this example, the depth of the borehole field could be decreased by approximately 35%. A more detailed system analysis could involve system life-cycle operating cost analyses, control strategy variations, and design variable optimization.

Table 4-1. Summary of Pavement Heating System Performance for Example GSHP System Simulation

Year	Hours ON	Average Surface Temperature		Heat Pump Maximum Entering Fluid Temperature		Heat Rejected	
		(°F)	(°C)	(°F)	(°C)	(kBtu)	(MJ)
1	6245	63.65	17.58	97.71	36.51	3,418,368	3,605,695
2	6448	63.96	17.76	99.41	37.45	3,670,277	3,871,409
3	6603	64.15	17.86	100.79	38.22	3,837,759	4,048,068

4.6. Concluding Remarks and Recommendations for Future Work

A design and simulation tool for modeling the performance of a pavement heating system as a supplemental heat rejecter in ground-source heat pump systems has been developed. The model has been developed in the TRNSYS modeling environment (SEL, 1997) and can be coupled to other GSHP system component models for short-time step (hourly or minutely) system analyses. The model has been validated by comparing simulation results to experimental data.

The model accounts for several environmental heat transfer mechanisms plus convective heat transfer due to a closed-loop heat exchanger coil. The heat transfer fluid is assumed to be carried by a series of pipes in a "serpentine" configuration or a "slinky" configuration. Environmental heat transfer mechanisms that are simulated by the model include solar radiation heat gain, convection heat transfer to the atmosphere, thermal or long-wave radiation heat transfer, and sensible and latent heat and mass transfer due to rain and snow. The model uses an explicit finite-difference method to solve the transient two-dimensional heat conduction equation. Some outputs provided by the model include

the pavement surface temperature, the exiting fluid temperature, and the amount of heat rejected to the pavement slab.

An example application has been presented to demonstrate the use of the model as well as the viability of the use of pavement areas as supplemental heat rejecters in GSHP systems. Through this example, it is shown that ground-loop heat exchanger sizes can be significantly decreased by incorporating a pavement heating systems into the GSHP system.

The potential exists for significantly increasing the performance of pavement heating systems used as supplemental heat rejecters in GSHP systems. Further research is suggested in the following areas:

- Optimization of the design procedure and control strategy as described for the shallow pond supplemental heat rejecter in Section 3.6.
- Additional validation of the model, using data from a working system, would be useful.
- Additional validation of the model, using data collected under a wider range of weather conditions (i.e. rain, snow, and ice conditions), would be useful.
- The impact of the pipe configuration on the overall system performance, particularly with regard to accounting for slinky pipe spacing in models.
- Application of the model to other uses such as modeling the performance of horizontal ground-loop heat exchanger systems and snow melting systems.

5. Summary and Conclusions

Ground-source heat pump (GSHP) systems have received considerable attention in recent decades as an alternative energy source for residential and commercial space heating and cooling applications. GSHP systems offer proven advantages over conventional heating and cooling systems, specifically with respect to efficiency, maintenance costs, and overall operating costs. Depending on the configuration, a GSHP system may either use the earth, ground water, or surface water as a heat source and/or sink. Hybrid GSHP systems use combinations of these or a combination of a GSHP system with conventional equipment (i.e. a cooling tower).

This study has dealt with the modeling of vertical closed-loop and hybrid, ground-source heat pump systems. The challenges associated with the design of these systems originate from the fact that they present a unique type of heat transfer problem. First, there are inherent inabilities to make direct observations in the subsurface environment with respect to both space and time. Second, heat transfer within the subsurface environment can be highly transient. Consequently, a considerable amount of research in the past decade has been geared toward optimizing the design and performance of GSHP systems and this study is part of those efforts.

The objectives of this study were threefold: (1) to examine the effects of ground-water flow on closed-loop GSHP systems, (2) to develop a design and simulation tool for modeling the performance of a shallow pond as a supplemental heat rejecter with closed-loop GSHP systems, and (3) to develop a design and simulation tool for modeling the

performance of a hydronic pavement heating system as a supplemental heat rejecter with closed-loop GSHP systems.

Chapter 2 of this thesis has presented a preliminary assessment of the effects of ground-water flow on closed-loop ground-source heat pump systems. A compilation of "typical" hydraulic and thermal properties of soils and rocks was used in the study.

A simple but useful method of assessing the relative importance of heat conduction in the ground versus heat advection by moving ground water was demonstrated through the use of the dimensionless Peclet number.

A finite-element numerical ground-water flow and heat transport model was used to simulate and observe the effects of ground-water flow on the heat transfer from a single U-tube closed-loop ground heat exchanger in various geologic materials. From those simulations, it appears that it is only in geologic material with high hydraulic conductivities, such as coarse-grained soils (sands and gravels) and in rocks exhibiting secondary porosities such fractures and solution channels, that ground-water flow could be expected to have a significant effect on closed-loop heat exchanger performance.

The finite-element numerical ground-water flow and heat transport model was also used to examine the effect of ground-water flow on in-situ thermal conductivity test results. This was done by numerically simulating test conditions around a single borehole under different flow conditions. As expected, in all cases of ground-water flow,

these values were artificially high. Results from one week test data have been shown to be no more reliable than data from 50-hour tests when significant ground-water flow is present.

The finite-element numerical ground water flow and heat transport model was also used to simulate the 10-year performance of borehole fields designed from application of conventional design procedures using the derived thermal conductivity data. Even the presence of moderate ground-water flows had the effect of removing the year-by-year increase in ground temperature found in systems where there is no ground-water flow. The borehole fields designed using conventional methods and the derived effective thermal conductivities were generally over-designed. However, in some cases at very high ground-water flow rates, temperatures were found to rise above the design criteria.

From this preliminary assessment of the effects of ground-water flow, it appears difficult to adapt results from current design and in-situ measurement methods to fully account for ground-water flow conditions. Over the last decade, considerable progress has been made in developing both in-situ test methods and design procedures for borehole field design for situations where there is no ground-water flow. Research would be required in a number of areas before the same progress could be made to deal with the situations of ground-water flow. These include:

- Identification of suitable numerical and/or analytical models that include ground-water flow and could be used to analyze in-situ test data.

- Experimental investigation of potential in-situ test data analysis methods at sites with significant ground-water flow.
- Identification of suitable design methods, or adaptations to existing methods, that could be used for closed-loop ground heat exchanger design.
- Development of design guidelines and software tools that could be used by practicing engineers for in-situ testing and system design tasks in situations of significant ground-water flow.

Chapter 3 of this thesis has described the development and validation of a model for simulating the performance of a shallow pond as a supplemental heat rejecter with closed-loop ground-source heat pump systems. The model has been developed in the TRNSYS modeling environment and can be coupled to other GSHP system component models for short-time step (hourly or minutely) system analyses. The model has been validated by comparing simulation results to experimental data.

The model accounts for several natural heat transfer mechanisms within a surface water body plus convective heat transfer due to a closed-loop heat exchanger coil. The heat transfer fluid is assumed to be carried by a series of pipes in the form of bundle spools or "slinky" coils. Environmental heat transfer mechanisms that are simulated by the model include solar radiation heat gain, heat and mass transfer due to evaporation, convection heat transfer to the atmosphere, thermal or long-wave radiation heat transfer, conduction heat transfer to the surrounding soil or fill material, and ground water discharge contributions. The solution scheme involves a lumped-capacitance approach

and the resulting first-order differential equation describing the overall energy balance on the pond is solved numerically. Some outputs provided by the model include average pond temperature, exiting fluid temperature, and heat rejected to the pond.

An example application has been presented to demonstrate the use of the model as well as the viability of the use of shallow ponds as supplemental heat rejecters in GSHP systems. Through this example, it is shown that the size of ground-loop heat exchangers can be significantly decreased by incorporating a shallow pond into the GSHP system.

The potential exists for significantly increasing the performance of shallow ponds used as supplemental heat rejecters in GSHP systems. Further research is suggested in the following areas:

- Optimization of the design procedure and control strategy. Hybrid ground source heat pump systems have many degrees of freedom; there are tradeoffs between the reduction in size of the ground loop heat exchanger, the size of the pond, and the control strategy. To more fully understand this, additional research using the simulation techniques developed in this paper is needed. This research would also take into account the economic costs and benefits, which we have not investigated.
- Additional validation of the model, using data from a working system, would be useful.
- Extension of the model to cover deep ponds for situations where an existing pond or lake is available.

- The use of spray fountains and other aeration devices in the pond to enhance pond cooling.
- The impact of pipe configuration within the pond on the overall system performance.

Chapter 4 of this thesis has described the development and validation of a model for simulating the performance of a pavement heating system as a supplemental heat rejecter with closed-loop ground-source heat pump systems. The model has been developed in the TRNSYS modeling environment and can be coupled to other GSHP system component models for short-time step (hourly or minutely) system analyses. The model has been validated by comparing simulation results to experimental data.

The model accounts for several environmental heat transfer mechanisms plus convective heat transfer due to a closed-loop heat exchanger coil. The heat transfer fluid is assumed to be carried by a series of pipes in a "serpentine" configuration or a "slinky" configuration. Environmental heat transfer mechanisms that are simulated by the model include solar radiation heat gain, convection heat transfer to the atmosphere, thermal or long-wave radiation heat transfer, and sensible and latent heat and mass transfer due to rain and snow. The model uses the finite-difference method to solve the transient two-dimensional heat conduction equation. Some outputs provided by the model include the pavement surface temperature, the exiting fluid temperature, and the amount of heat rejected to the pavement slab.

An example application has been presented to demonstrate the use of the model as well as the viability of the use of pavement areas as supplemental heat rejecters in GSHP systems. Through this example, it is shown that ground-loop heat exchanger sizes can be significantly decreased by incorporating a pavement heating systems into the GSHP system.

The potential exists for significantly increasing the performance of pavement heating systems used as supplemental heat rejecters in GSHP systems. Further research is suggested in the following areas:

- Optimization of the design procedure and control strategy as described for the shallow pond supplemental heat rejecter.
- Additional validation of the model, using data from a working system, would be useful.
- Additional validation of the model, using data collected under a wider range of weather conditions (i.e. rain, snow, and ice conditions), would be useful.
- The impact of the pipe configuration on the overall system performance, particularly with regard to accounting for slinky pipe spacing in models.
- Application of the model to other uses such as modeling the performance of horizontal ground-loop heat exchanger systems and snow melting systems.

REFERENCES

Adlam, T.N. 1950. *Snow Melting*. The Industrial Press, New York, NY.

ASHRAE, 1995. *ASHRAE Handbook, HVAC Applications*. American Society of Heating, Refrigeration and Air-Conditioning Engineers, Inc., Atlanta, GA.

ASHRAE, 1995b. *Commercial/Institutional Ground-Source Heat Pump Engineering Manual*. American Society of Heating, Refrigeration and Air-Conditioning Engineers, Inc., Atlanta, GA.

ASHRAE, 1997. *ASHRAE Handbook, Fundamantals*. American Society of Heating, Refrigeration and Air-Conditioning Engineers, Inc., Atlanta, GA.

Austin, W.A. III, C. Yavuzturk, and J. D. Spitler. 2000. *Development of an In-Situ System for Measuring Ground Thermal Properties*. Submitted for publication to ASHRAE Transactions.

Bear, J. 1972. *Dynamics of Fluids in Porous Media*. New York: Dover Publications, Inc.

BLAST 1986. *BLAST (Building Loads and System Thermodynamics)*. Urbana-Champaign: University of Illinois, BLAST Support Office.

Bliss, R.W., 1961. Atmospheric Radiation Near the Surface of the Ground. *Solar Energy*, 5(103).

Cantrell, J.M. and W.J. Wepfer, 1984. Shallow Ponds for Dissipation of Building Heat: A Case Study. *ASHRAE Transactions* 90(1): 239-246.

Carslaw, H. S. and J. C. Jaeger. 1946. *Conduction of Heat in Solids*. Oxford, U.K.: Claremore Press.

Chapman, W.P. 1952. Design of Snow Melting Systems. *Heating and Ventilating*. April, pp. 96-102.

Chemical Rubber Company (CRC), 1980. *Handbook of Chemistry and Physics, 61st Edition*. CRC Press, Cleveland, OH.

Churchill, S.W. and H.H.S. Chu. 1975. Correlating Equations for Laminar and Turbulent Free Convection from a Horizontal Cylinder. *International Journal of Heat and Mass Transfer*, 18: 1049-1053.

Dake, J.M.K. and D.R.F. Harleman, 1969. Thermal Stratification in Lakes: Analytical and Laboratory Studies. *Water Resources Research*, 5(2): 484-495.

Domenico, P.A. and F. W. Schwartz. 1990. *Physical and Chemical Hydrogeology.* New York, Chicester, Brisbane, Toronto, Singapore: John Wiley & Sons.

Driscoll, F. G. 1986. *Groundwater and Wells.* St. Paul Minnesota: Johnson Filtration Systems, Inc.

Duffie, J.A. and W.A. Beckman, 1991. *Solar Engineering of Thermal Processes, 2nd Edition.* John Wiley and Sons.

Elliot, R.L., F.V. Brock, M.L. Stone, and S.L. Sharp. 1994. Configuration Decisions for an Automated Weather Station Network. *Applied Engineering in Agriculture*, 10(1): 45-51.

Eklof, C. and S. Gehlin. 1996. *TED – A Mobile Equipment for Thermal Response Test.* Master's Thesis 1996:198E. Lulea University of Technology, Sweden.

Eskilson, P. 1987. *Thermal Analysis of Heat Extraction Boreholes.* Doctoral Thesis, University of Lund, Department of Mathematical Physics. Lund, Sweden.

Fetter, C. W. 1988. *Applied Hydrogeology.* 2nd Edition, Columbus, Ohio: Merrill Publishing Co.

Freeze, R. A. and J. A. Cherry. 1979. *Groundwater.* Englewood Cliffs, New Jersey: Prentice Hall, Inc.

Gehlin, S. and B. Nordell. 1998. Thermal Response Tests of Boreholes – Results from In Situ Measurements. *Transaction of The Geothermal Project at Richard Stockton College Conference.* March 16-17, 1998.

Grant, M.A., I.G. Donaldson, and P.F. Bixley, 1982. *Geothermal Reservoir Engineering.* Academic Press.

Hart, D.P. and R. Couvillion, 1986. *Earth-Coupled Heat Transfer.* National Water Well Association, Dublin, OH.

Hellstrom, G. 1991. *Ground Heat Storage. Thermal Analyses of Duct Storage Systems.* Lund, Sweden: University of Lund, Department of Mathematical Physics.

Holman, J.P., 1972. *Heat Transfer, 3rd Edition.* McGraw-Hill Book Company.

Hull, J.R., K.V. Liu, W.T. Sha, J. Kamal, and C.E. Nielsen, 1984. Dependence of Ground Heat Losses Upon Solar Pond Size and Perimeter Insulation – Calculated and Experimental Results. *Solar Energy*, 33(1): 25-33.

IGSHPA. 1991. (Bose, J. E., Editor) *Design and Installations Standards.* Stillwater, Oklahoma: International Ground Source Heat Pump Association.

Incropera, F.P. and D.P. DeWitt, 1996. *Introduction to Heat Transfer, 3rd Edition.* John Wiley & Sons.

Ingersoll, L. R., O. J. Zobel, and A. C. Ingersoll. 1954. *Heat Conduction with Engineering, Geological, and Other Applications.* New York: McGraw-Hill.

Irvine, T.F. Jr. and P.E. Liley, 1984. *Steam and Gas Tables with Computer Equations.* Academic Press, Inc.

Jobson, H., 1962. The Dissipation of Excess Heat from Water Systems. *Journal of the Power Division, Proceedings of the American Society of Civil Engineers.* 99(P01), May, pp. 89-103.

Kavanaugh, S. P. 1984. *Simulation and experimental verification of vertical ground-coupled heat pump systems.* Ph.D. dissertation. Stillwater, Oklahoma: Oklahoma State University.

Kavanaugh, S.P. and K. Rafferty, 1997. *Ground-Source Heat Pumps. Design of Geothermal Systems for Commercial and Institutional Buildings.* American Society of Heating, Refrigeration and Air-Conditioning Engineers, Inc., Atlanta, GA.

Kelvin, Sir W. Thomson. 1882. *Mathematical and Physical Papers.* II, p.41 ff.

Kilkis, I.B. 1994. Design of Embedded Snow Melting Systems: Part 1, Heat Requirements – An Overall Assessment and Recommendations. *ASHRAE Transactions,* 100(1):pp. 423-433.

Kishore, V.V.N. and V. Joshi, 1984. A Practical Collector Efficiency Equation for Nonconvecting Solar Ponds. *Solar Energy.* 33(5): 391-395.

Liao, C.J. and T.D. Hogue. 1996. *Thermal Stress Predictions for Geothermally Heated Bridge Decks.* Prepared for the State of Oklahoma Department of Transportation.

Lindeburg, M.R. 1992. *Civil Engineering Reference Manual, 6th Edition.* Professional Publications, Inc., Belmont, CA.

Lindholm, G. F. and J. J. Vaccaro. 1988. (Back, W.B., J.S. Rosenshein, and P.R. Seaber, Editors) Region 2, Columbia Lava Plateau (Chapter 5). In*: The Geology of North America, Vol. O-2, Hydrogeology.* Boulder, Colorado: The Geological Society of America, Inc..

Marrero, T.R. and E.A.Mason, 1972. Gaseous Diffusion Coefficients. *Journal of Physical and Chemical Reference Data.* 1: 3-118.

McAdams, W.H., 1954. *Heat Transmission, 3rd Edition.* McGraw-Hill Book Company.

Mercer, J.W. and C.R. Faust. 1986. *Ground-Water Modeling*. National Water Well Association.

Mei, V. C. and C. J. Emerson. 1985. New Approach for Analysis of Ground-Coil Design for Applied Heat Pump Systems. *ASHRAE Transactions*. 91(2B):1216-1224.

Mills, A.F., 1995. *Basic Heat and Mass Transfer*. Prentice Hall.

Muraya, N. K., D.L. O'Neal, and W.M. Heffington, 1996. Thermal Interference of Adjacent Legs in a Vertical U-Tube Heat Exchanger for a Ground-Coupled Heat Pump. ASHRAE Transactions 102(2):12-21.

Newell, T.A., 1984. Solar Ponds – Alternate Energy Systems. *Military Engineer, Journal of the Society of American Military Engineers,* No. 492, March-April 1984: 110-113.

Pezent, M.C. and S.P. Kavanaugh, 1990. Development and Verification of a Thermal Model of Lakes Used With Water Source Heat Pumps. *ASHRAE Transactions* 96(1): 574-582.

Ramsey, J.W., M.J. Hewett, T.H. Kuehn, and S.D. Petersen. 1999. Updated Design Guidelines for Snow Melting Systems. *ASHRAE Transactions,* 105(1).

Raphael, J.M., 1962. Prediction of Temperatures in Rivers. *Journal of the Power Division, Proceedings of the American Society of Civil Engineers.* 88(P02), July, pp. 157-181.

Remund, C. 1998. Personal Communication. Northern Geothermal Support Center, South Dakota State University, Brookings, SD.

Rottmayer, S. P., W. A. Beckman, and J. W. Mitchell. 1997. Simulation of a Single Vertical U-Tube Ground Heat Exchanger in an Infinite Medium. *ASHRAE Transactions*, 103(2):651-658.

Rubin, H., B.A. Benedict, and S. Bachu, 1984. Modeling the Performance of a Solar Pond as a Source of Thermal Energy. *Solar Energy*, 32(6): 771-778.

Shonder, J. A. and J. V. Beck. 1999. Determining Effective Soil Formation Thermal Properties From Field Data Using a Parameter Estimation Technique. *ASHRAE Transactions*, 105(1).

Solar Energy Laboratory (SEL), University of Wisconsin-Madison. 1997. *TRNSYS, A Transient Systems Simulation Program, User's Manual, Version 14.2.*

Spencer, J.W., 1971. Fourier Series Representation of the Position of the Sun. *Search*, 2(5).

Spitler, J. D., C. Marshall, R. Delahoussaye, and M. Manicham. 1996. *Users Guide of GLHEPRO*, School of Mechanical and Aerospace Engineering, Oklahoma State University, Stillwater, OK.

Srinivasan, J. and A. Guha, 1987. The Effect of Reflectivity on The Performance of a Solar Pond. *Solar Energy.* 39(4): 361-367.

Stephenson, D.A., A. H. Fleming, and D. M. Mickelson. 1988. (Back, W. B., J. S. Rosenshein, and P. R. Seaber, Editors) Glacial Deposits (Chapter 35). In*: The Geology of North America, Vol. O-2, Hydrogeology*. Boulder, Colorado: The Geological Society of America, Inc..

United States Environmental Protection Agency. 1996. *BIOSCREEN. Natural Attenuation Decision Support System, User's Manual.* Cincinnati, Ohio: National Risk Management Research Laboratory, Office of Research and Development.

Vatnaskil Consulting Engineers. 1998. *AQUA3D Groundwater Flow and Contaminant Transport Model.* Reykjavik, Iceland: Vatnaskil Consulting Engineers.

Wadivkar, O., 1997. *An Experimental and Numerical Study of the Thermal Properties of a Bridge Deck De-Icing System.* Unpublished Masters Thesis, Oklahoma State University, Stillwater, OK.

Wang, H.F. and M.P. Anderson. 1982. *Introduction to Groundwater Modeling – Finite Difference and Finite Element Methods.* W.H. Freeman and Company, New York.

Weeks, J. B. and E. D. Gutentag. 1988. (Back, W. B., J. S. Rosenshein, and P. R. Seaber, Editors) Region 17, High Plains (Chapter 20). In*: The Geology of North America, Vol. O-2, Hydrogeology*. Boulder, Colorado: The Geological Society of America, Inc..

Yavuzturk, C. and J.D. Spitler. 1999. A Short Time Step Response Factor Model for Vertical Ground Loop Heat Exchangers. *ASHRAE Transactions*, 105(2).

Yavuzturk, C., J. D. Spitler, and S. J. Rees. 1999. A Transient two-dimensional Finite Volume Model for the Simulation of Vertical U-Tube Ground Heat Exchangers. *ASHRAE Transactions*, 105(2).

APPENDIX A

Model and Experimental Uncertainty Analysis

This appendix presents an analysis of parameter uncertainty and experimental uncertainty regarding the validation and application of the pond and pavement models.

Model Uncertainty

This section presents a sensitivity analysis to quantify the uncertainty in the final model results caused by uncertainties in the estimates of input and parameter values used in the models. The results of this analysis are shown in Tables A-1 and A-2 for the pond and the pavement models, respectively, and are discussed below.

The pond and pavement model uncertainty is quantified using influence coefficients as described by Spitler et al. (1989). An influence coefficient is the partial derivative of a simulation result with respect to a parameter which, for the purposes of this study, is approximated as:

$$Influence\ Coefficient = \frac{\Delta Result}{\Delta Parameter} \qquad \text{(A-1)}$$

where *Result* is the cumulative heat rejected and *Parameter* is a variable with some uncertainty. The term *Parameter* should not be confused with TRNSYS model parameters. Here, *Parameter* refers to any variable with a significant uncertainty, including TRNSYS model parameters as well as TRNSYS model inputs such as weather factors, fluid supply temperature, and fluid flow rate.

TABLE A-1

Pond Model Parameter Uncertainty Analysis

Modeled cumulative heat rejected from Nov.12, 1998 to Dec. 7, 1998:

Horizontal Slinky	**1486**	kW-hr
Vertical Slinky	**1508**	kW-hr

Item Adjusted	Value Used in Final Analysis	Uncertainty in Parameter	Perturbed Model Value	Perturbed Model Result (kW-hr)	Δ(result) / Δ(parameter)	Uncertainty in Result (kW-hr)	**Model Parameter Uncertainty (%)**
k_{pipe} (W/m-°C)							
Horizontal Slinky	0.391 (2)	0.06 (3)	0.5	1554	623.85	37.43	**2.52%**
Vertical Slinky	0.391 (2)	0.06 (3)	0.5	1578	642.20	38.53	**2.56%**
k_{soil} (W/m-°C)							
Horizontal Slinky	2.5 (4)	0.2 (1)	3.0	1520	68.00	13.60	**0.92%**
Vertical Slinky	2.5 (4)	0.2 (1)	3.0	1543	70.00	14.00	**0.93%**
Depth to constant sink (m)							
Horizontal Slinky	7.5 (4)	2.5 (4)	3.0	1510	-5.33	13.33	**0.90%**
Vertical Slinky	7.5 (4)	2.5 (4)	3.0	1535	-6.00	15.00	**0.99%**
ε of water surface (--)							
Horizontal Slinky	0.97 (5)	0.02 (1)	0.9	1473	185.71	3.71	**0.25%**
Vertical Slinky	0.97 (5)	0.02 (1)	0.9	1495	185.71	3.71	**0.25%**
Windspeed (m/s)							
Horizontal Slinky	1 (a)	0.10 (6)	2.0 (a)	1847	361.00	36.10	**2.43%**
Vertical Slinky	1 (a)	0.10 (6)	2.0 (a)	1880	372.00	37.20	**2.47%**
Solar radiation							
Horizontal Slinky	1 (a)	0.05 (6)	2.0 (a)	1242	-244.00	12.20	**0.82%**
Vertical Slinky	1 (a)	0.05 (6)	2.0 (a)	1256	-252.00	12.60	**0.84%**
Air temperature (°C)							
Horizontal Slinky	0 (b)	0.35 (6)	2.0 (b)	1284	-100.86	35.30	**2.38%**
Vertical Slinky	0 (b)	0.35 (6)	2.0 (b)	1305	-101.43	35.50	**2.35%**
Relative humidity (%)							
Horizontal Slinky	1 (a)	0.05 (6)	1.05 (a)	1452	-674.13	33.71	**2.27%**
Vertical Slinky	1 (a)	0.05 (6)	1.05 (a)	1474	-679.80	33.99	**2.25%**
Supply fluid temperature (°C)							
Horizontal Slinky	0 (b)	0.12 (7)	0.2 (b)	1400	-431.90	51.83	**3.49%**
Vertical Slinky	0 (b)	0.12 (7)	0.2 (b)	1413	-477.43	57.29	**3.80%**
Supply fluid flow rate (gpm)							
Horizontal Slinky	0 (b)	0.025 (7)	0.05 (b)	1486	6.66	0.17	**0.01%**
Vertical Slinky	0 (b)	0.025 (7)	0.05 (b)	1508	7.04	0.18	**0.01%**
Total Uncertainty in Results							
Horizontal Slinky							**6.13%**
Vertical Slinky							**6.35%**

NOTES:

(a) - a multiplication factor is used to vary the hourly input value of this item for this uncertainty analysis
(b) - an addition factor is used to vary the hourly input value of this item for this uncertainty analysis
(1) - estimated value
(2) - value given by pipe manufacturer Phillips Driscopipe
(3) - based on data given by Mills (1995)
(4) - based on in-situ thermal conductivity test data
(5) - value given by Incropera and DeWitt (1996)
(6) - measurement error given by Elliot et al. (1994)
(7) - based on standard error of calibration curves

TABLE A-2

Pavement Model Parameter Uncertainty Analysis

Modeled cummulative heat rejected from Nov.12, 1998 to Dec. 19, 1998: Horizontal Slinky **1255** kW-hr

Item Adjusted	Value Used in Final Analysis	Uncertainty in Parameter	Perturbed Model Value	Perturbed Model Result (kW-hr)	Δ(result) / Δ(parameter)	Uncertainty in Result (kW-hr)	**Model Parameter Uncertainty (%)**
k_{pipe} (W/m-°C) Slinky test section	0.391 (2)	0.06 (3)	0.5	1293	348.62	20.92	**1.67%**
$k_{concrete}$ (W/m-°C) Slinky test section	1.663 (4)	0.2 (1)	2.9	1314	47.70	9.54	**0.76%**
k_{soil} (W/m-°C) Slinky test section	0.4 (5)	0.2 (1)	1.0	1146	-181.67	36.33	**2.90%**
α of concrete (--) Slinky test section	0.4 (6)	0.1 (6)	0.6	1135	-600.00	60.00	**4.78%**
ε of concrete (--) Slinky test section	0.9 (6)	0.05 (6)	0.8	1192	630.00	31.50	**2.51%**
Windspeed (m/s) Slinky test section	1 (a)	0.10 (7)	2.0 (a)	1327	72.00	7.20	**0.57%**
Air temperature (°C) Slinky test section	0 (b)	0.35 (7)	2.0 (b)	1092	-81.26	28.44	**2.27%**
Relative humidity (%) Slinky test section	1 (a)	0.05 (7)	1.05 (a)	1250	-103.99	5.20	**0.41%**
Supply fluid temperature (°C) Slinky test section	0 (b)	0.12 (8)	0.2 (b)	1089	-831.18	99.74	**7.95%**
Supply fluid flow rate (gpm) Slinky test section	0 (b)	0.025 (8)	0.05 (b)	1256	16.48	0.41	**0.03%**
Total Uncertainty in Results Slinky test section							**10.47%**

NOTES:

(a) - a multiplication factor is used to vary the hourly input value of this item for this uncertainty analysis
(b) - an addition factor is used to vary the hourly input value of this item for this uncertainty analysis
(1) - estimated value
(2) - value given by pipe manufacturer Phillips Driscopipe
(3) - based on data given by Mills (1995)
(4) - based on data given by Tinker and Cabrera (1992)
(5) - value given by Spitler et al. (1996) for light soil
(6) - value given by ASHRAE (1997) light-colored surfaces
(7) - measurement error given by Elliot et al. (1994)
(8) - based on standard error of calibration curves

The influence coefficient for each parameter of interest is determined by running the model with a "perturbed" value of the parameter. The *Uncertainty in Result*, with respect to the parameter, is then determined by:

$$\textit{Uncertainty in Result} = (\textit{Influence Coefficient})x(\textit{Uncertainty in Parameter}) \quad \text{(A-2)}$$

where *Uncertainty in Parameter* is the estimated parameter error (for example, ± 0.5 W/m-°C). The non-dimensional *Model Parameter Uncertainty* is then determined by:

$$\textit{Model Parameter Uncertainty} = \frac{\textit{Uncertainty in Result}}{\textit{Result}} \quad \text{(A-3)}$$

The errors introduced to the model result by each parameter are assumed to be independent of each other. Therefore, the *Total Uncertainty in Result* is given by:

$$\textit{Total Uncertainty in Result} = \sqrt{\sum_{i=1}^{n} (\textit{Model Parameter Uncertainty})_i^2} \quad \text{(A-4)}$$

where n is the number of parameters considered in the analysis.

The parameters investigated in this uncertainty analysis can be divided into two groups: **(1)** TRNSYS model parameters and **(2)** TRNSYS model inputs. For the pond model, these items consisted of: **(1)** (a) pipe thermal conductivity (k_{pipe}), (b) soil thermal conductivity (k_{soil}), (c) depth to constant sink temperature, and (d) emissivity of the water

surface (ε) and **(2)** (a) wind speed, (b) solar radiation, (c) air temperature, (d) relative humidity, (e) supply fluid temperature, and (f) supply fluid flow rate. For the pavement model, these items consisted of: **(1)** (a) pipe thermal conductivity (k_{pipe}), (b) concrete thermal conductivity ($k_{concrete}$), (c) soil thermal conductivity (k_{soil}), (d) absorptivity of the concrete surface (α) and (d) emissivity of the concrete surface (ε) and **(2)** (a) wind speed, (b) air temperature, (c) relative humidity, (d) supply fluid temperature, and (e) supply fluid flow rate. The model values used in the final analysis and the uncertainty in each value were taken from the sources shown in Tables A-1 and A-2.

For the pond model, the supply fluid temperature has the greatest effect on the model uncertainty, on the order of 3.5%. Four other parameters have lesser uncertainties on the model results, on the order of 2.5%; these are k_{pipe}, wind speed, air temperature, and relative humidity. Of still lesser significance are k_{soil}, the depth to constant sink temperature, and the solar radiation, which produce model uncertainties on the order of 0.9%. The emissivity of the water surface has a relatively insignificant uncertainty of 0.25%. The fluid flow rate has an insignificant effect on the model uncertainty, contributing only 0.01% to the total.

For the pavement model, the supply fluid temperature also has the greatest effect on the model uncertainty, on the order of 8%. The absorptivity of the concrete surface possesses the next highest uncertainty, on the order of 5%. Air temperature, k_{soil}, and ε of the concrete surface all have uncertainties on the order of 2.5%. k_{pipe} has an uncertainty of 1.7% and wind speed and relative humidity have relatively low uncertainties on the

order of 0.5%. As with the pond model, the fluid flow rate has an insignificant effect on the model uncertainty, contributing only 0.03% to the total.

Based on the results shown in Table A-1, the total uncertainty in the results of the pond model are ± 6.13% for the horizontal slinky case and ± 6.35% for the vertical slinky case. Based on the results shown in Table A-2, the total uncertainty in the results of the pavement model is ± 10.47% for the slinky case.

The results of this uncertainty analysis can be used to identify items of concern to one who may use the model(s) for the purposes of GSHP system design or system simulation. For this study, estimates of the TRNSYS model parameters are likely no better than those that could be made by a typical user, and therefore, similar uncertainties can be expected for those items. However, the TRNSYS model inputs cannot be known exactly by a typical user because they consist of weather factors and system fluid temperature and flow rate.

A user performing some type of system design or simulation must use typical or synthetic weather data based on historical observations for the location of interest. The use of "typical weather data" is one inherent difficulty in building simulation studies because the it is obviously impossible to quantify uncertainties in future weather conditions. However, the longer the simulation time (10-20 years), the greater the probability is that average actual weather conditions approach the "typical weather

conditions". For shorter-term simulations (up to 5 years), the conservative user may want to use weather data with more extreme values, if available.

Other model inputs include the supply fluid temperature and flow rate which will be provided either as a constant value or by another model. From the results of this uncertainty analysis, model results are much more sensitive to the supply fluid temperature, and a user should therefore pay more attention to this item.

Experimental Uncertainty

This section presents an analysis of the experimental errors contributing to the measurement of heat rejected to the ponds and to the concrete slab. The purpose of this analysis is to quantify the error in the experimental results that were used to validate the pond and pavement models. The results of this analysis are shown in Tables A-3 and are discussed below.

The main sources of error in the measurements of heat rejection to the ponds and to the concrete slab are identified as: (1) calibration error in the watt meter used for power measurements and (2) heat losses or gains to the ground from the pipes between the heat rejecter and the instrumentation building.

Error in the watt meter measurements was determined from the calibration procedure. Heat losses/gains to the ground from the supply and return pipes were

estimated using the pavement model. The model was run from October 1, 1998 to December 19, 1998 with actual weather conditions and assuming a constant fluid supply temperature of 75°F (23.9°C) and constant fluid supply flow rate of 4 gpm (908 kg/hr). The thermal conductivity of the ground and the pipe backfill material were taken as 1.0 Btu/hr-ft-°F (1.73 W/m-°C) and the average pipe burial depth was taken as 1.5 ft (0.48 m). The model was used to determine the heat losses per foot of pipe for the period of November 12, 1998 to December 19, 1998, which is the period of interest for the model validation. The cumulative heat lost through the supply/return pipes was then estimated by considering the distances from the instrumentation building to each of the supplemental heat rejecters (62 ft (18.9 m) for the pond with the vertical slinky, 37 ft (11.3 m) for the pond with the horizontal slinky, and 12 ft (3.7 m) for the concrete slab).

TABLE A-3

Heat Rejection Experimental Uncertainty Analysis

Item	Value	Experimental Uncertainty
Error in Power Measurement (a)	--	0.50%
Estimated Cumulative Heat Losses to Ground: (b)		
Pond with horizontal slinky	20.25 kW-hr	1.36%
Pond with vertical slinky	33.83 kW-hr	2.24%
Slab with slinky	10.92 kW-hr	0.87%
Total Experimental Uncertainty		
Pond with horizontal slinky		**1.45%**
Pond with vertical slinky		**2.30%**
Slab with slinky		**1.00%**

NOTES:
(a) - based on instrument calibration precision
(b) - includes heat lost through supply and return headers, estimated using the pavement model

Based on the results shown in Table A-3, the total uncertainty in the cumulative heat rejection is 1.45% for the pond with the horizontal slinky, 2.30% for the pond with the vertical slinky, and 1.00% for the concrete slab. These errors are considered acceptable.

Summary

In summary, the experimentally-determined cumulative heat rejection and the model-predicted cumulative heat rejection for the test period are compared in Table A-4.

TABLE A-4

Summary of Experimental and Model Cumulative Heat Rejected

Test Configuration	Experimental Cumulative Heat Rejected (kW-hr)	Model Cumulative Heat Rejected (kW-hr)
Pond with horizontal slinky	1532 +/- 22.2	1486 +/- 91.1
Pond with vertical slinky	1591 +/- 36.6	1508 +/- 95.8
Slab with slinky	1321 +/- 13.2	1255 +/- 131.4

Two conclusions may be drawn from the above comparison: (1) the model predictions match the experimental results within the bands of estimated uncertainty and (2) the model predictions match the experiment better than would be expected by the uncertainty analysis. The second conclusion implies that the uncertainty prediction may be over-conservative.

APPENDIX A - REFERENCES

ASHRAE, 1997. *ASHRAE Handbook, Fundamantals*. American Society of Heating, Refrigeration and Air-Conditioning Engineers, Inc., Atlanta, GA.

Elliot, R.L., F.V. Brock, M.L. Stone, and S.L. Sharp. 1994. Configuration Decisions for an Automated Weather Station Network. *Applied Engineering in Agriculture*, 10(1): 45-51.

Incropera, F.P. and D.P. DeWitt, 1996. *Introduction to Heat Transfer, 3rd Edition*. John Wiley & Sons.

Mills, A.F., 1995. *Basic Heat and Mass Transfer*. Prentice Hall.

Spitler, J. D., C. Marshall, R. Delahoussaye, and M. Manicham. 1996. *Users Guide of GLHEPRO*, School of Mechanical and Aerospace Engineering, Oklahoma State University, Stillwater, OK.

Spitler, J.D., D.E. Fisher, and D.C. Zietlow. 1989. A Primer on the Use of Influence Coefficients in Building Simulation. *Proceedings of Building Simulation '89*, Vancouver, BC.

Tinker, J.A. and J.G. Cabrera. 1992. Modeling the Thermal Conductivity of Concrete Based on Its Measured Density and Porosity. *Proceedings of the ASHRAE/DOE/BTECC Conference*, Clearwater Beach, FL. American Society of Heating, Refrigerating and Air-Conditioning Engineers, Inc., Atlanta, GA.

VITA

Andrew David Chiasson

Candidate for the Degree of

Master of Science

Thesis: ADVANCES IN MODELING OF GROUND-SOURCE HEAT PUMP SYSTEMS

Major Field: Mechanical Engineering

Biographical:

Education: Received Bachelor of Applied Science and Master of Applied Science degrees in Geological Engineering at the University of Windsor, Ontario, Canada, in June 1989 and June 1992, respectively. Completed the requirements for Master of Science with a major in Mechanical Engineering from Oklahoma State University, Stillwater, Oklahoma, December 1999.

Experience: Employed as a Geothermal Systems Research Assistant at the School of Mechanical & Aerospace Engineering, Oklahoma State University, Stillwater, Oklahoma from August 1997 to present; Geological Engineer at EnviroSolutions, Incorporated, Dearborn Heights, Michigan from 1996 to 1997; and Geological Engineer at Dragun Corporation, Farmington Hills, Michigan from 1990 to 1996.

Professional Memberships: American Society of Heating, Refrigerating and Air-Conditioning Engineers (ASHRAE), National Ground Water Association (NGWA).